Measurement and Deduction of Emissions of Short-lived Atmospheric Organo-chlorine Compounds

by

Gary Kleiman

B. A. Physics and Mathematics
University of Colorado at Boulder, 1991

M. S. Physics and Astronomy
University of Massachusetts at Amherst, 1993

Submitted to the
Department of Earth, Atmospheric and Planetary Sciences
in partial fulfillment of the requirements
for the degree of

Doctor of Philosophy in Atmospheric Chemistry

at the

Massachusetts Institute of Technology
September, 1999

Signature of Author:_____
Department of Earth, Atmospheric, and Planetary Sciences
August 10, 1999

Certified by:_____
Ronald G. Prinn
TEPCO Professor of Atmospheric Chemistry
Supervisor

Accepted by:_____
Head, Department

)_____
d G. Prinn
y Sciences

Measurement and Deduction of Emissions of Short-lived Atmospheric Organo-chlorine Compounds

by

Gary Kleiman

Submitted to the Department of Earth, Atmospheric, and Planetary Sciences on August 10, 1999 in partial fulfillment of the requirements for the degree of Doctor of Philosophy in Atmospheric Chemistry.

ABSTRACT

Atmospheric studies of halogenated organics have centered on long lived halocarbons due to their effect on stratospheric ozone. Now that controls have been put in place to curb emissions of longer lived halocarbons through the Montreal Protocol, and speculation about the safety of many short-lived chlorinated organic molecules has been raised, there has been more consideration given to the efforts aimed at determining the levels of human exposure to all types of halogenated organics. Most previous studies of reactive chlorine compounds have focused solely on quantifying their ambient levels in urban and rural regions. However, for many of these organo-chorine molecules a detailed knowledge of emissions levels, transport, and final environmental disposition still does not exist. The present work was designed to aid in understanding the emissions patterns for several reactive halogenated organic compounds including trichloromethane (chloroform, $CHCl_3$), trichloroethene (TCE, $CHClCCl_2$), and tetrachloroethene (perchloroethylene, CCl_2CCl_2). A high temporal frequency (hourly) measurement campaign in Nahant, Massachusetts (approximately 10 km. northeast of Boston) provided automated gas-chromatographic measurements for these species as well as the somewhat more stable 1,1,1 trichloroethane (methyl chloroform, CH_3CCl_3). Cryogenic preconcentrations, daily calibrations, and weekly linearity tests insure high precision ($\leq$5%) measurements using electron capture detection. Calibration gases used for these tests, initially manufactured at MIT, have been corrected by intercomparison with gas standards used by the AGAGE program (produced at Scripps Institution of Oceanography) as well as those used at the National Center for Atmospheric Research. The absolute accuracy of our corrected MIT standard is estimated to be $\leq$10%.

Over 12,000 measurements of the selected species were made between March, 1998 and January, 1999. These data show wide variability for the shortest lived species ranging from our detection limits (4.5 ppt for trichloroethene, 4.2 ppt for tetrachloroethene, and 7.8 ppt for trichloromethane) up to several hundred ppt during periods of local pollution.

Data analysis combines the measurements with backtrajectory information obtained from the HYSPLIT4 model (HYbrid Single-Particle Lagrangian Integrated Trajectory model, NOAA Air Resources Laboratory, Silver Springs, Maryland). Using a Kalman filter inverse method and an analytical solution of the continuity equation to estimate the effect of diffusion, we calculate the surface emissions for the selected species necessary to optimally match the observations. These emissions are compared with the estimates determined by the Reactive Chlorine Emissions Inventory (RCEI) working group of the IGAC (International Global Atmospheric Chemistry Program) Global Emissions Inventory Activity (GEIA). RCEI estimates are primarily derived from point source emissions in the US Toxic Release Inventory (TRI) and population-based distribution of residual national consumption from sales records. The new emissions scenarios computed here provide an observation-based assessment for comparison with the emissions inventories produced by RCEI for the northeastern United States and southeastern Canada.

Results are statistically consistent with the RCEI estimates given the currently rough accuracy (±47-67%) achievable through this observation-based technique. We note, however, that the best estimate of corrections factors for land-based grid cells presented here indicate that the RCEI emissions for trichloroethene and tetrachloroethene need to be increased by a factor of ~2 to explain the observations. Only anthropogenic sources of trichloromethane were gridded in the initial (RCEI) inventory representing roughly 11% of estimated global emissions. We find that these emissions are, as expected, too low to explain the observations and that a land-based correction factor ~12 is required to produce emissions estimates that are consistent with natural sources (e.g. soil emissions). We also note that very large correction factors are calculated over the oceanic grid cells resulting in revised emissions estimates of the same order of magnitude as many land-based grid cells, consistent with a large oceanic source for this compound inferred from oceanic observations.

The 47-67% uncertainty in the estimates of emissions correction factors increases with distance from the observation site due to both the increase in trajectory error as a function of total trajectory length and the decrease in the number of trajectories which have passed through a particular grid cell as one moves further from the observation site. These and other sources of uncertainty can be reduced by providing a realistic weighting of each trajectory's accuracy thus minimizing the impact of the trajectories which are likely to be most inaccurate, increasing the total number of measurements so that all grid cells have greater trajectory coverage, and improving estimates of the effective mixed layer height.

Acknowledgments

I would like to thank Ron Prinn for his generous support of this research. Ron not only provided all the necessary (and sometimes expensive) equipment to insure that I could conduct the highest quality research, but he also gave willingly of his time whenever needed.

I would also like to thank Ron and the rest of my thesis committee, Mario Molina, Reggie Newell, and Rick Rosen, for their patience while I was participating in activities not directly related to my thesis but which contributed significantly to my education at MIT. The opportunities to be a student participant in the MIT Chlorine Project, the IGAC Aerosol Characterization Experiment, the Reactive Chlorine Emissions Inventory, and the Martin Society of Graduate Fellows for Sustainability, have given me a deeper appreciation for the significance of my work to society as well as a broader perspective of environmental research than that which can be obtained through a single narrowly focused thesis topic.

Thanks are also due to the many who have helped in producing the work described here. Bina Patel, Elaine Kutchka, Rusty Sammon, Dave Weaver, and Wendy Chou have been tremendous assets to the project as undergraduate (UROP) researchers. Very little of the automation would have been possible without the technical advice of Bob Boldi. Roland Draxler of the NOAA Air Resources Laboratory wrote the HYSPLIT model and helped adapt it for its use in this work. Ray Weiss and Chris Harth (Scripps Institution of Oceanography) and Eliot Atlas (National Center for Atmospheric Research) kindly provided intercomparisons which provided the basis for my calibrations. My laboratory coworkers and officemates, Jin Huang, Stephanie Shaw, John Graham, and Don Lucas kept me going with their encouragement and conversation. Jin deserves special thanks for sharing so much computer time with me at a critical stage of her own thesis work.

I can't think of an adequate way to express my thanks to my parents. Their love and support, more than anything else, has made this thesis a reality. Thank you both.

Finally I thank Barbara and Larry Nelson for not stopping at 4! Without Kristin, this work and my life would have far less meaning.

This work has been supported by the Kahn-Rassmussen Environmental Fellowship Program as well as the Alliance for Global Sustainability at MIT. Support was also received through NSF grants ATM-9216340 and ATM-9610145, NASA grants NAG-1-2152 and NAG-5-3974, and the Tokyo Electric Power Company Professorship.

Table of Contents

Chapter 1: Introduction

Preface

Chlorine and chlorine-containing compounds have been pushed to the center of environmental debate in recent years. With over 15,000 chlorinated compounds in widespread use (Hileman, 1993), chlorine-based chemistry has become a cornerstone of our economy. It is estimated that U.S. sales of products containing chlorine total $71 billion (Graff, 1995), and the United States represents just one-third of all elemental chlorine production worldwide. Some 40 million tons of chlorine is produced worldwide every year (Fauvarque, 1996). Like other members of the halogen family, chlorine is highly reactive and as the eighteenth most abundant of the 92 natural elements (Graedel and Keene, 1996), it is readily available in terrestrial salt deposits and seawater. These properties make chlorine an exceptional agent in chemical synthesis and consequently more than half the products marketed by the chemical industry and more than 85% of all pharmaceuticals are derivatives of chlorine chemistry (Fauvarque, 1996). Chlorine is used in products ranging from plastics and solvents to pesticides and bleaching agents. Free chlorine, chlorine dioxide, and chloramine are three of the most common drinking water disinfectants (Galal-Gorchev, 1996). In the United States chlorine is used to disinfect more than 98% of the publicly supplied drinking water (Graff, 1995), and in the third world, chlorine represents the only affordable means of drinking water disinfection (Galal-Gorchev, 1996).

While there are clearly many benefits brought about by chlorine chemistry, environmentalists and some health experts claim that these benefits may have societal costs. Many chlorinated organic compounds have been classified as carcinogenic or potential carcinogens and it is theorized that some chlorinated organics (e.g. several pesticides and chemical intermediaries used in plastics manufacture) may disrupt the normal action of the body's endocrine system. Some of these compounds (none of the chemicals considered in this thesis) have been correlated with documented abnormalities in both wildlife and humans (Colborn et al., 1993, Colborn et al., 1996, Ballschmiter, 1996). Faced with the uncertainty as to the extent to which chlorine chemistry affects human health and the environment, some environmental advocates are calling for a total elimination of the industrial use of chlorine and chlorine-containing compounds, and a few European nations have begun active discussion of such proposals (Hileman, 1993).

Industry associations such as the Chemical Manufacturers Association (CMA) and the Chlorine Chemistry Council (CCC) do not deny that there may be cause for banning a few particular compounds which are commercially available, but they suggest a strategy of increased testing and product stewardship on a compound by compound basis. They would like to single out just those compounds which have determined risk rather than ban all 15,000 compounds indiscriminately. Those in favor of a total chlorine ban see this as impractical, as it would take decades to subject each compound to the rigorous screening procedures necessary to demonstrate carcinogenicity or mutagenicity.

Because of the extreme difficulty in isolating environmental systems to determine precise cause-effect relationships, controversy abounds with regard to potential adverse health effects of chlorine containing-compounds. Determination of accurate methods for risk assessment remains a point of contention between environmentalists and industry representatives (Putnam and Graham, 1993). Environmental persistence, bio-accumulation, and toxicity remain the three key considerations in most risk assessment schemes, yet there is no established metric for determining what level of risk is acceptable with regard to these factors.

Given the contentious nature of the debate, the high societal dependence on chlorine chemistry, and the high degree of uncertainty regarding the links to health impacts, the future use of chlorine in the environment remains an open question. Credible scientific input is needed to help guide the reasoning of policymakers and interested stakeholders. The medical and toxicology community must explore the effects of these compounds on the human body. Political scientists and economists are necessary to predict the costs and effects of proposed regulation, and the public health and earth science communities are needed to determine human exposure and environmental disposition of these compounds.

Atmospheric Relevance and Justification

In an atmospheric context, the study of halogenated organic compounds has centered on the long-lived Chloro-FluoroCarbons (CFCs) due to their potential for stratospheric ozone depletion (Molina and Rowland, 1974). The AGAGE (Advanced Global Atmospheric Gases Experiment) network (Prinn et al., 1999a) and NOAA-CMDL (National Oceanic and Atmospheric Administration's Climate Monitoring and Diagnostics Laboratory) record (Elkins et al., 1998) have documented the increase, plateau and, in some cases, decrease of several extremely stable halogenated gases in the troposphere. With legislation in place prohibiting the manufacture and sale of many CFCs, stratospheric chlorine levels are expected to decline over the next several decades bringing gradual recovery of stratospheric ozone (Prinn et al., 1995; Montzka et al., 1996; Cunnold et al., 1997; Prinn et al., 1999a).

Those compounds with a shorter atmospheric residence time (<1 year) have been examined in an urban pollution context. As with all hydrocarbons, the breakdown of these compounds can lead to urban ozone formation (Warneck, 1988, pg. 178). Monitoring of hydrocarbons and other Volatile Organic Compounds has been ongoing for decades, but it is only recently that the relatively small fraction of halogenated hydrocarbons have been paid such close attention.

As early as 1974, tri- and tetrachloroethene were being measured in urban areas (Lillian et al., 1975). Throughout the 1980s, several investigators continued to refine analytical precision of ambient concentration measurements for all the species of interest in this work. These studies documented the presence of a host of halogenated solvents in urban areas of the US, Europe, and Japan at levels 10-100 times background concentrations (Singh et al., 1981, 1982, Hecht et al., 1987, Hartwell et al. 1987, Makide et al., 1987, Urano et al, 1988). Others focused solely on industrial areas and known

emissions sources where concentrations of halocarbon solvents were found at levels of ~0.1-10 ppb (Pellizari, 1982; Harkov et al., 1983; Kessel and Bachmann, 1991). During this time, background levels were also documented by studies in rural settings, contrasting the high levels seen in urban and industrial areas (Singh et al., 1983; Makide et al., 1987; Frank et al., 1991 a, b). Since these early studies, our understanding of the sources, ambient levels and distribution of halogenated organics has grown substantially, yet given the nature of the chlorine debate in recent years, much more research is needed. Recent studies have started to focus on the development and analysis of global and long term datasets (Wiedmann et al., 1994; Singh et al., 1996; Hurst et al., 1997; Bakwin et al., 1997). The breadth of compounds studied has also expanded to encompass nearly all sources of halogens to the atmosphere, allowing us to ask questions about the total budgets of atmospheric chlorine and bromine.

The budget of reactive chlorine in the troposphere is of interest because of its relative impact on the total halogen burden. As concentrations of long-lived halocarbons in the atmosphere come down, a detailed knowledge of the budgets of many short-lived halocarbons and the biogeochemical cycles they participate in becomes necessary to adequately assess the effectiveness of legislated restrictions (Graedel and Keene, 1996, Keene et al., 1999).

A major step forward in developing this knowledge comes in the form of the Reactive Chlorine Emissions Inventory (RCEI)(see Graedel and Keene, 1999 for an overview). While the emissions inventories produced by this project represent the latest and most detailed effort to date, emissions estimates are based on very sparse observational data, if any at all. In fact, for trichloroethene (TCE, C_2HCl_3), tetrachloroethene (perchloroethene, C_2Cl_4), and 1,1,1 trichloroethane(methyl chloroform, CH_3CCl_3) all anthropogenic emissions estimates are based on production and sales records provided by industry (McCulloch and Midgely, 1996; McCulloch et al., 1999). Trichloromethane (chloroform, $CHCl_3$) emissions estimates are based on extrapolations of industry reports(Aucott et al., 1999) and highly uncertain emission factors to calculate biomass burning emissions (Lobert et al., 1999). Additionally, trichloromethane has significant natural sources which have been estimated based on few measurements in remote regions of the world (Khalil et al., 1999). Significant uncertainty exists as to the magnitude of the global emissions of these gases, and there are virtually no estimates of uncertainty regarding the distribution patterns of many anthropogenically and naturally emitted reactive chlorine species. We aim to improve this situation by providing an observational test of current emissions inventories.

Scientific Objective

Because *emissions* cannot be measured directly, in order to achieve our goal of determining the emissions of short-lived halocarbons we must find a suitable inverse method which can be used to calculate them. The Lagrangian form of the continuity equation can provide a framework for calculating emissions for purely anthropogenic chemicals from observations of concentrations as described below.

The change in ambient mole fraction, χ, of a particular chemical species at a given time as it travels along a Lagrangian trajectory (position "0" to position "s") is given by the continuity equation as it is integrated along its path (Prinn, 1999b):

$$\chi(s,t) - \chi(0,0) = \int_0^s \frac{1}{[M]}\left(P_{net} - \nabla \cdot \varphi\right)\frac{ds'}{v} \qquad (1.1)$$

where $[M]$ represents the molar density of air, P_{net} represents net chemical production, φ represents the molar diffusive flux, and v is the instantaneous local velocity. Net chemical production is true chemical production minus true chemical loss plus chemical emissions. For the 4 species reported here (trichloromethane, 1,1,1 trichloroethane, trichloroethene, and tetrachloroethene) there is no evidence for significant natural chemical production in the atmosphere. Thus we are only concerned with chemical loss, emissions, and diffusion as an air parcel moves along a trajectory.

Chemical loss for the reactive species is achieved primarily by reaction with the hydroxyl radical (OH). Breakdown products resulting from this reaction depend on the initial halocarbon, but common products of haloalkene oxidation are phosgene, formic acid, carbon monoxide, and di- and trichloroacetyl chloride (Gay et al., 1976). The rate of reaction with OH varies for each species and in turn determines the atmospheric residence time of each molecule with respect to OH oxidation ($\tau_{OH} = 1/k\,[OH]$). The chemicals of interest, their reaction rate constants with OH (k), and the associated lifetimes with respect to typical OH levels in the extratropical Northern Hemisphere are listed in Table 1 below. Longer lived compounds (e.g. 1,1,1 trichloroethane) tend not to react as quickly with OH and have a variety of other sinks including UV radiation in the stratosphere and oceanic uptake (Keene et al., 1999) which act on time scales far greater than transport and diffusion and thus are not considered here.

Inspection of Table 1 shows that the shortest lived compound of interest is trichloroethene with a lifetime of ~10 days with respect to OH in Northern Hemisphere locations. To the extent that we are interested in transport times much less than the atmospheric residence time, we can ignore chemical destruction as a significant perturbation to the observed mole fraction.

Table 1.

Compound	$k_{OH}(278)$ (cm^3/molec·sec) [a]	τ_{OH} (yrs) [b]
Trichloromethane	7.85×10^{-14}	0.93
1,1,1 Trichloroethane	6.82×10^{-15}	10.8
Trichloroethene	2.47×10^{-12}	10.8 (days)
Tetrachloroethene	1.25×10^{-13}	0.58

[a] factors calculated from DeMore et al., 1997.

[b] [OH] = 4.3 x 10^5 radicals/cm^3 for annual average taken from Prinn et al., 1995 (Northern Hemisphere, extratropical, lower tropospheric box)

Because we do not know v at all points in space and time, we are forced to include parameterizations of unresolved motions in our model. Unresolved turbulent mixing is then a much greater influence on concentration than molecular diffusion when considering the large spatial scales of interest here. Turbulent mixing is usually approximated as a diffusive flux, φ_{eddy} ($>>\varphi$), due to eddy processes, represented as proportional to the product of an eddy diffusion coefficient matrix, **K**, and the spatial gradient vector of the mole fraction (Prinn, 1999b). After taking time and/or space averages, denoted by < >, we have a simplified form of the relevant diffusional processes:

$$\nabla \cdot \varphi_{eddy} \approx \nabla \cdot \left(- K[M]\langle \nabla \chi \rangle\right) \tag{1.2}$$

Combining these assumptions we have a revised form of the Lagrangian continuity equation showing the linear relationship between change in observed mole fraction of a compound and its emissions, E :

$$\chi(s,t) - \chi(0,0) \cong \int_0^s \left(\frac{E}{h[M]} + \frac{\nabla \cdot K[M]\langle \nabla \chi \rangle}{[M]} \right) \frac{ds'}{v} \tag{1.3}$$

where $\chi(0,0)$ is the mole fraction for the selected compound at the boundary of our study region (defined in Chapter 3). Here h is the mixed layer height. The units of E are moles per unit area per unit time. When E/h is divided by the molar density of air, [M], the first term in the integral is then the change in mole fraction per unit time. For surface emissions, equation (1.3) assumes a vertically well mixed layer (no vertical gradient in χ) and that E=0 above the mixed layer.

Thus with a set of observed mole fractions, a detailed knowledge of the resolved wind velocities and diffusion coefficients along a trajectory, and estimates of the emissions in each region passed through by that trajectory, one can, in principle, calculate an estimated ambient mole fraction to compare with observations. Using a simple inverse method to minimize the differences between estimated and weighted observed mole fraction, we can derive an optimal correction to the initial emissions estimate. Thus we can achieve our goal of testing an emissions inventory of several short-lived organochlorine compounds based on a set of observed mole fractions.

Chapter 2: Instrumentation and Observations

Instrumentation

Air monitoring was conducted in Nahant, Massachusetts at the Northeastern University Marine Science Center (MSC) (42.4° N, 70.9° W). Space was made available to MIT in the John B. Murphy bunker on the MSC campus which provided a unique location (approximately 10 km. northeast of Boston over open water) for an automated laboratory to make in-situ air measurements. This location was chosen for the variety of meteorological conditions experienced which provides the site with air masses originating in the clean marine environment, the polluted East Coast urban corridor, the polluted Mid-West, and the relatively clean northern New England and rural Canadian regions. The bunker sits at approximately ground level with a 6 meter thick concrete ceiling topped by 1.5 meters of rocks and soil. A 5 meter meteorological instrument tower sits above the bunker to which we attached our inlet. (See Appendix A for photographs of the experimental setup, inlet, and surroundings.). Air samples were brought from about 12 meter height down through ¼"OD (outer diameter) stainless steel tubing into our laboratory by means of a Metal Bellows® pump (Senior Flexonics Inc., Sharon MA) at a flow rate of approximately 14 liters/min. The majority of the air was vented to the laboratory through a two-foot 1/8"OD tube elevating the output pressure at the pump to approximately 25 psia. A smaller stream of 40 sccm was diverted from the output of the metal bellows pump through a borosilicate microfiber filter (1.6 μm. pore size, Micro Filtration Systems, Dublin CA) to remove fine particles. The stream then passes through a three-way solenoid valve which selects from two streams (ambient air or calibration gas) and passes the selected stream through a Nafion® dryer (Perma Pure Inc., Tom's River, NJ) with 60cc/minute UHP N_2 counterflow to remove excess moisture. Finally the sample is passed through a 1 meter $^1/_{50}$" ID (inner diameter) stainless steel capillary tube which is part of the cryogenic pre-concentrating collection system. Downstream of the collection system, a calibrated pressure transducer measures the loop pressure and a Tylan® mass flow controller (Millipore Corp., Bedford, MA) determines the flow rate. (See Figure 1.) The entire flow path is maintained at a positive pressure from the output of the Metal Bellows pump up to the Tylan® flow controller to insure that any undetected micro-leaks in the system would not lead to contamination of the sample stream.

The collection system used to pre-concentrate air samples consists of a stainless steel capillary tube inserted into the neck of a dewar of liquid argon. The dual chamber dewar consists of a narrow center chamber open at the bottom to a larger surrounding reservoir. The internal pressure of the dewar is kept at ~33 psig, and thus the temperature of liquid argon remains at roughly -172°C. The loop is wrapped with a 30W rope heater. An 85W cartridge heater (Omega, Stamford, CT) is located in an aluminum cylinder in contact with the bottom of the loop. The heaters boil off liquid argon in the center section of the dewar elevating the pressure and forcing down the level of cryogen in the central chamber below that of the collection loop. Omega CN2002 temperature controllers with remote setpoint option and dual output control (hot/cold) are used to control both heaters on the loop and a pressure release valve which is used to cool the loop to cryogenic temperatures.

When remote setpoints on the Omega temperature controllers are reduced to -172°C, the pressure release valve is opened, releasing excess pressure in the central chamber, allowing the cryogen level to rise until the bottom of the loop is immersed and the desired temperature is achieved. The temperature controller maintains that temperature until the remote setpoint is raised to 75°C at which time the heaters are turned on and the liquid level is forced down again as the pressure increases. The timing of the setpoint switching is programmed to correspond to valve switches on the sample line which will block off the collection loop completely during the 5 minutes required to heat the loop and re-volatilize the collected trace gases. The volatilized sample is then injected. This automation allows for the collection of trace gases contained in a large volume of ambient air by collecting only the constituents of an air sample that condense at -172°C and allowing the nitrogen and oxygen to pass through to vent. Because the flow rate is maintained at 40 ml/min by a Tylan mass flow controller, the collection volume is determined by the collection time (25 minutes = 1 liter).

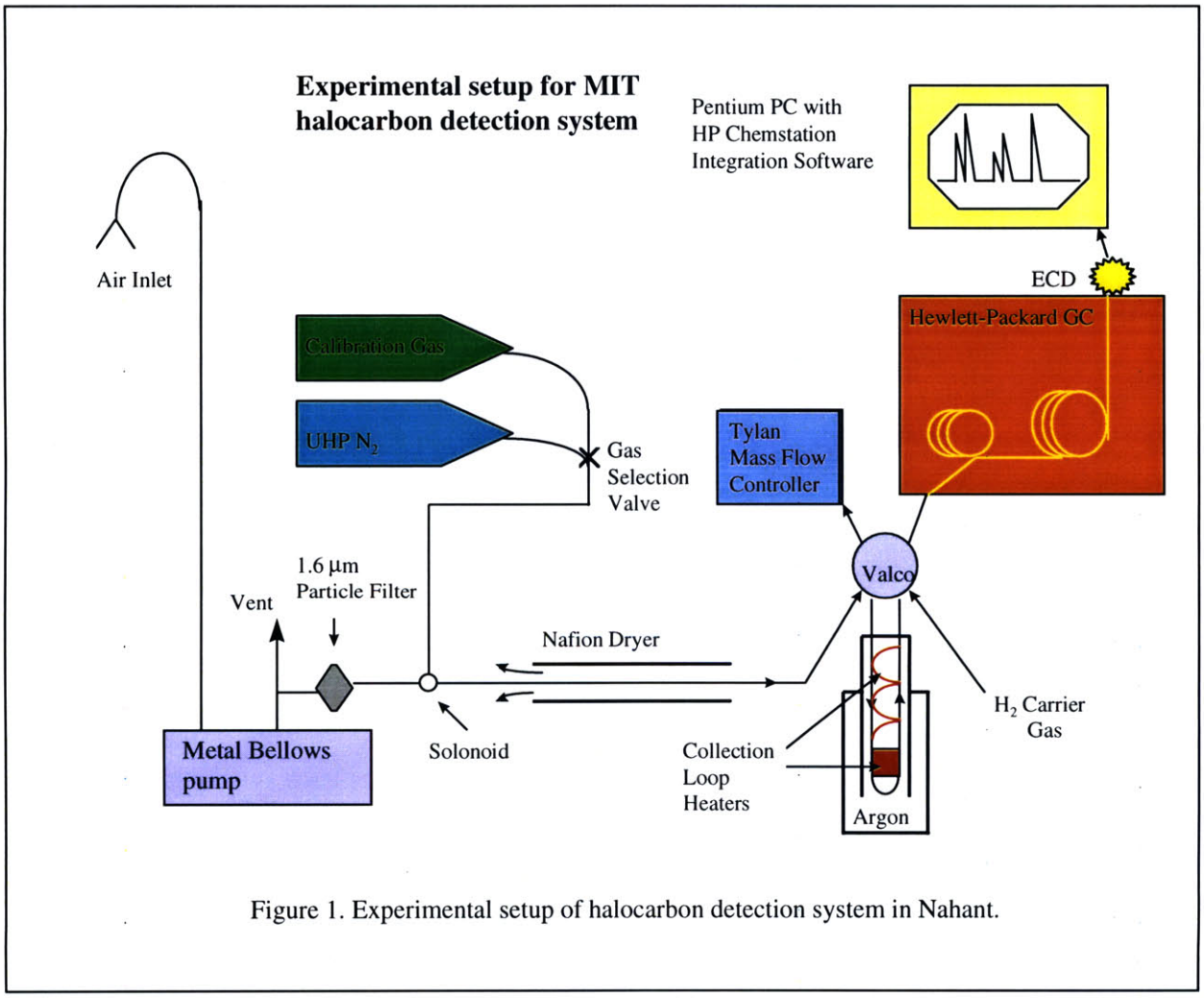

Figure 1. Experimental setup of halocarbon detection system in Nahant.

Once a sample is collected and then re-volatilized, the multiposition Valco valve (Valco Instruments, Houston, TX) is switched such that the collection loop containing the volatilized sample is in line with the H_2 carrier gas. The sample is then swept (~1.5

ml/min) into fused silica tubing (0.5mm OD, 0.32mm ID) which in turn brings it to a 5 meter fused silica capillary pre-column. The pre-column is a wide bore (0.75mm ID) column with VOCOL® stationary phase (Supelco, Bellafonte, PA) for preliminary separation. This column is connected in series (through a 2-position electrically actuated Valco valve) to a 30 meter Supelco SPB-624® capillary column (0.32mm ID).

As soon as the sample is injected into the series of columns, the GC is activated for data collection and temperature programming. The GC is kept at 35°C for 10 minutes after which it is heated at 1°/minute up to a temperature of 60°C. At this point (35 minutes) the rate of heating is increased to 4°/minute until a temperature of 100°C has been reached. The oven is held at this temperature for 5 minutes before cooling back down in preparation for the next sample injection. About 28 minutes after the sample has been injected into the GC and the temperature program has commenced, all the compounds of interest have passed through the pre-column (indeed many have eluted into the detector), and the Valco valve located between the two columns is actuated preventing heavier compounds from contaminating the main column. The flow in the pre-column is reversed, and any heavy compounds remaining in the pre-column are then backflushed out of the pre-column to vent. The pre-column remains in the backflush configuration for the remainder of the 60-minute temperature program.

The Gas Chromatograph used was a Hewlett-Packard 5890 Series II® equipped with an electron capture detector (ECD). The ECD operates by measuring the flow of electrons from a radioactive ^{63}Ni source across a chamber to an anode. As molecules pass through the chamber, they intercept some of the electrons bound for the anode. A decrease in current is observed as electrons become bound to the electron-capturing molecules and carried out of the chamber. The current signal is inverted and is proportional to the amount of a compound which has passed through the chamber. The ECD is especially sensitive to chlorine and other halogen-containing molecules due to their large electron capture cross-sections and is uniquely suited for very sensitive measurements of atmospheric halocarbons. A typical chromatogram from an air sample collected in Nahant through this system is shown in Figure 2. We note that tetrachloromethane (carbon tetrachloride) was measured along with the more reactive halocarbon species; however, we use this compound only as a reference peak to aid in the peak identification process, and due to calibration difficulties for this compound, we do not report the data here.

The GC is controlled by Hewlett-Packard Chemstation® Software on a IBM compatible personal computer (Micro X-perts, Solon, OH). The software is capable of controlling the GC, detector, and input valves. Additionally, it can provide electronic control for two external relays which have been configured to control switches used for automating other aspects of the collection process. All instrument setpoints and external controls are stored in a method file which can be tailored for different types of collections (i.e. calibration runs, Nitrogen "blank" collections, ambient air samples, etc..). The ability to program a sequence of runs using selected methods allows for continuous uninterrupted operation for up to 7 days including daily calibration runs. The only required maintenance involves refilling the cryogen and changing the borosilicate microfiber particle filter.

Daily collections of 250 ml of calibration gas allow continuous monitoring of instrument response and collection efficiency. These daily calibrations are supplemented with weekly linearity checks. Linearity is determined by a collection of 1 liter of ultra high purity (UHP) N_2, followed by 100 ml, 250 ml, and 1 liter of calibration gas. Any small amount of system contamination is thus accounted for by setting the response of the blank run (1 liter UHP N_2) into account. The response of the detector to atmospheric levels of each compound lies well below the response to the 1 liter sample of calibration gas for that compound insuring that the detector's linearity has been established over the range of

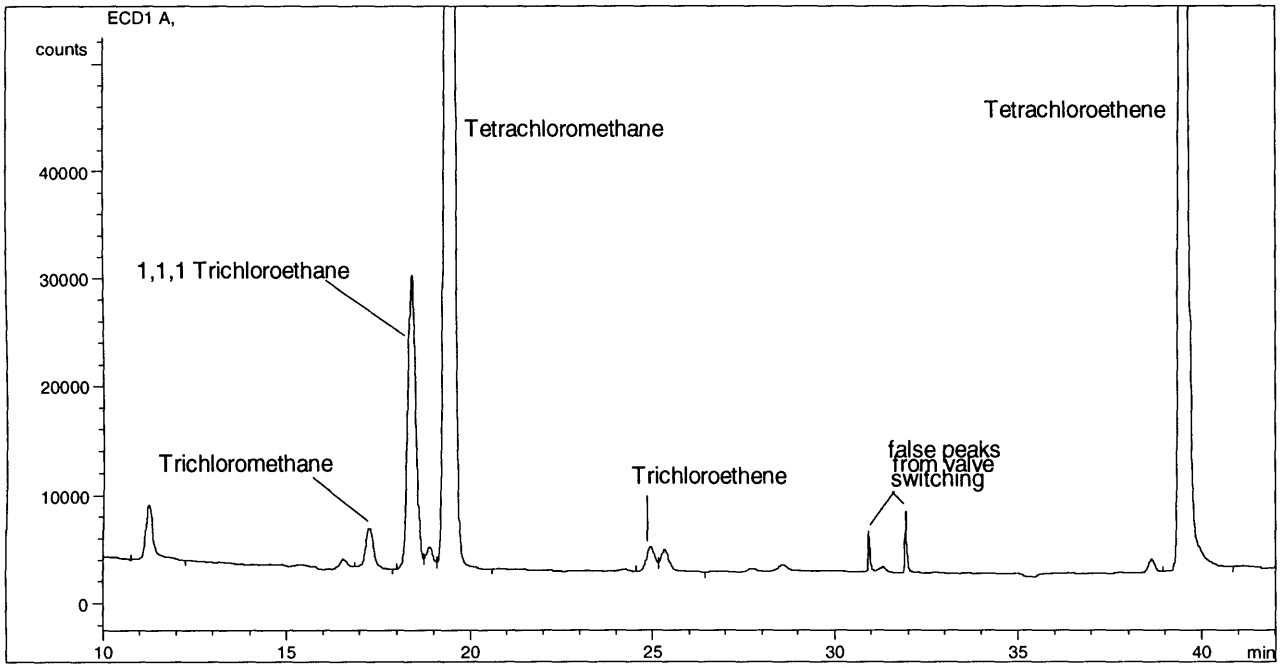

Figure 2. Typical chromatogram of a Nahant air sample.

all observations.

Data are recorded by the Chemstation® software and stored in datafiles which are then stored on 100 Mbyte zip® disks (Iomega Corp, Roy, UT). The data are transferred to a Winbook laptop computer running the analysis software. The Chemstation® software performs integration, identification, and quantification of chromatographic peaks.

Integration is carried out using the HP enhanced integrator algorithm. This new algorithm allows for several user selectable parameters such as minimum area below which a peak is rejected, minimum height below which a peak is rejected, whether to detect shoulders or not, etc.. A typical integration events table containing these parameters is shown in Table 2 along with the values used for the integration of the chromatogram shown in Figure 2.

The Hewlett-Packard identification scheme is based on a set of expected retention times which are then scaled to match the retention times of three reference peaks. A reference peak is defined as the largest peak within a specified time window. F-11, tetrachloromethane and tetrachloroethene have high responsivities and thus make excellent

candidates for reference peaks. After identifying the reference peaks within a 7% time window, the remaining retention times are interpolated between the reference peaks' retention times assuming a linear migration of retention times. Any peak found within 5% of a specific chemical's calculated retention time is associated with that compound.

Table 2.

Time (min)	Integration	Value
Initial	Slope Sensitivity	100
Initial	Peak Width	0.08
Initial	Area Reject	1000
Initial	Height Reject	1500
Initial	Shoulders	OFF
5.9	Integration	ON
23.0	Detect Shoulders	ON
27.0	Detect Shoulders	OFF
27.0	Area Reject	50000
41.0	Integration	OFF

Finally quantification is achieved by calculating a response curve for each compound based on the observed integrated areas of the four runs from the linearity check described earlier. A calibration table is created which includes (for each species) the peak name, its suggested retention time (which is used for peak identification described in the previous paragraph), peak area, known mole fraction, and the calculated response factor (ppt/area). Known mole fractions are entered by the user (their determination is discussed in the next section). Response functions for each compound, which cover the whole range of observations, are then calculated using a piecewise linear relationship between the response factors for the 4 individual calibration runs. The level 3 calibration (250 ml calibration run) is replaced when the subsequent level 3 calibration run becomes closer in time to the run being analyzed (this is approximately every 24 runs since a 250 ml calibration run was collected once per day). The appropriate response factor is applied to the integrated area (identified with a particular compound) for each air sample to calculate the mole fraction present in that sample.

Results of each sequence of collections are output as a Microsoft Excel® spreadsheet with a row for each atmospheric sample including the retention times and mole fractions (ppt) for each compound.

Calibration, Accuracy, and Precision

The calibration gases used as working standards at the field site were manufactured at MIT in the Laboratory for Atmospheric Chemistry using a dilution manifold and analytical techniques described by Sprengnether (1992, Appendix A). By following these methods, one can make a volumetric dilution of a pure compound into Ultra High Purity (UHP) N_2 at approximately the 5 ppb level. During the course of this thesis work, 5 standards were manufactured containing varying amounts of the halocarbons species of interest. These standards (identified by their respective tank serial numbers 593 and 5140) are subject to analytical errors during the manufacturing process, and thus we do not expect them to contain the exact quantities of pure compound that we theoretically calculate based on the techniques described in Sprengnether (1992). These errors stem from differences in

physical properties of the individual chemicals (e.g. different chemisorption or physical adsorption affinities) or from high analytical errors associated with measurements of very small pressure differentials necessary for production. From these two standards, several working standards or "daughters" were produced which were typically 50:1 dilutions of the originals. These standards were produced by diluting the original "mother" standards by nitrogen in passivated, humidified, stainless-steel canisters to produce working standards which contain compounds at the 100 ppt level. Standards 594 and 595 were produced from standard 593, and standard 5141 was produced from standard 5140.

During the process of manufacturing these standards, as well as during other dilution experiments, it became clear that a static dilution of a standard resulted in a new sample whose constituents had different dilution factors from one another. This counterintuitive result (most likely due to the errors mentioned previously) requires that each individual standard and/or sample produced be treated as completely independent of any other sample. Thus the "bootstrap" technique commonly used to calibrate related standards will not work for our purposes. To develop a consistent scale by which all samples can be measured, we have chosen standard 594 as the "gold standard" by which the MIT scale is defined. All values reported under the MIT scale have been calibrated against the theoretical estimates of the composition of this standard. This required an "internal" intercomparison between 594, 595, and 5141 which produced estimates (within our instrumental precision of 2%) of the composition of each standard on the MIT Scale.

To improve on absolute accuracy achieved during the production of these standards, intercomparisons have been carried out with Dr. Ray Weiss of the Scripps Institution of Oceanography (SIO) and Dr. Eliot Atlas from the National Center for Atmospheric Research (NCAR). For each of these intercomparisons, an aliquot of a working standard was diluted into UHP N_2 in stainless steel flasks to produce nearly ambient concentrations. The samples within the flasks were analyzed at MIT, against the MIT standards, before sending them to another laboratory for analysis. The contents were then re-analyzed after the participating lab had performed their own analysis and returned the cylinders to us. The individual details of each of these intercomparisons are described in the next paragraphs, and the results are shown in Tables 3 and 4.

The first intercomparison took place in April, 1998. Two 2.9 liter flasks were prepared for use by repeatedly flushing with UHP N_2, followed by evacuation to reduce potential contaminants within each canister to below 1 ppt. The flasks were then evacuated to less than 100 millitorr. Pure distilled water was then added to each tank up to a pressure of 10 torr to preferentially bind to adsorption sites inside the canister. An aliquot of working standard #594 was added to one of the evacuated, humidified flasks and pressurized up to ~65 psia (Sample 1). The Sample 1 pressure was high enough to sample the tank several times to calibrate it on the MIT scale before shipping with ~40 psia remaining. A second flask (Sample 2) was made in exactly the same manner except the working standard #594 was only used to partially pressurize the flask, and then UHP N_2 was used to complete the remaining pressurization. The flasks were shipped to SIO for calibration against the SIO-AGAGE scale, then returned to MIT. The before and after analysis at MIT show differences $\leq$5% for all cases.

Table 3.

Compound	MIT Before	SIO (ppt)	MIT After (ppt)	SIO/MIT
Sample 1	*(n=2)*	*(n=7)*	*(n=2)*	
F-11	263	350	268	1.32±0.04
Trichloromethane	149	193	141	1.33±0.07
1,1,1 Trichloroethane	374	458	371	1.23±0.03
Tetrachloromethane	342	487	348	1.41±0.04
Trichloroethene	267	--	282	--
Tetrachloroethene	103	--	102	--
Sample 2	*(n=2)*	*(n=6)*	*(n=2)*	
F-11	102	139	108	1.32±0.05
Trichloromethane	61	79	64	1.25±0.03
1,1,1 Trichloroethane	135	137	142	0.99±0.06
Tetrachloromethane	107	143	111	1.31±0.03
Trichloroethene	135		146	--
Tetrachloroethene	48		47	--

A second intercomparison was undertaken at the end of the data collection period in December, 1998. Aware of the fact that we needed an independent absolute calibration for each compound we were testing, the focus of this intercomparison was to obtain an absolute calibration for tri- and tetrachloroethene where an intercomparison was not possible with the SIO-AGAGE standards; thus NCAR was selected for this round of intercomparisons. In an attempt to minimize preferential adsorption on the inner wall of the flasks, we selected 16 liter flasks to reduce the surface area to volume ratio. Larger canisters also allow for more analyses per flask and thus more accurate determinations of their contents. Two 16 liter stainless steel flasks were sent out for electropolishing (Electromatic, Inc. Goleta, CA http://www.electromatic.com), an electrolytic process for smoothing the interior surface of the tanks, thereby minimizing adsorption sites, and passivating the surface with a chromium-rich, contaminant free coating. These tanks were then prepared by flushing with UHP N_2 several times and evacuating to <1torr. Both tanks were analyzed filled with UHP N_2 alone, so that contamination levels could be constrained

Table 4.

Compound	MIT Before (ppt)	NCAR (ppt)	MIT After (ppt)	NCAR/MIT
Tank 1	*(n=3)*		*(n=4)*	
F-11	67	92	66	1.39±0.03
Trichloromethane	39	52	38	1.35±0.06
1,1,1 Trichloroethane	99	128	94	1.33±0.03
Tetrachloromethane	99	125	99	1.26±0.02
Trichloroethene	64	98	72	1.45±0.16
Tetrachloroethene	21	41	20	1.99±0.06
Tank 2	*(n=3)*		*(n=4)*	
F-11	--	267	--	
Trichloromethane	15	16	18	0.95±0.09
1,1,1 Trichloroethane	54	67	52	1.27±0.02
Tetrachloromethane	81	101	82	1.23±0.01
Trichloroethene	12	17	16	1.22±0.18
Tetrachloroethene	31	62	31	2.00±0.05

prior to their final filling. Pure distilled water was again added to these tanks up to about 10 torr to insure complete passivation of any remaining active sites. UHP N_2 was then added to Tank 1 *before* the addition of working standard #595. In this way, the working standard was not introduced to an evacuated flask with just water, but a flask which already contained ~30 psia of UHP N_2.

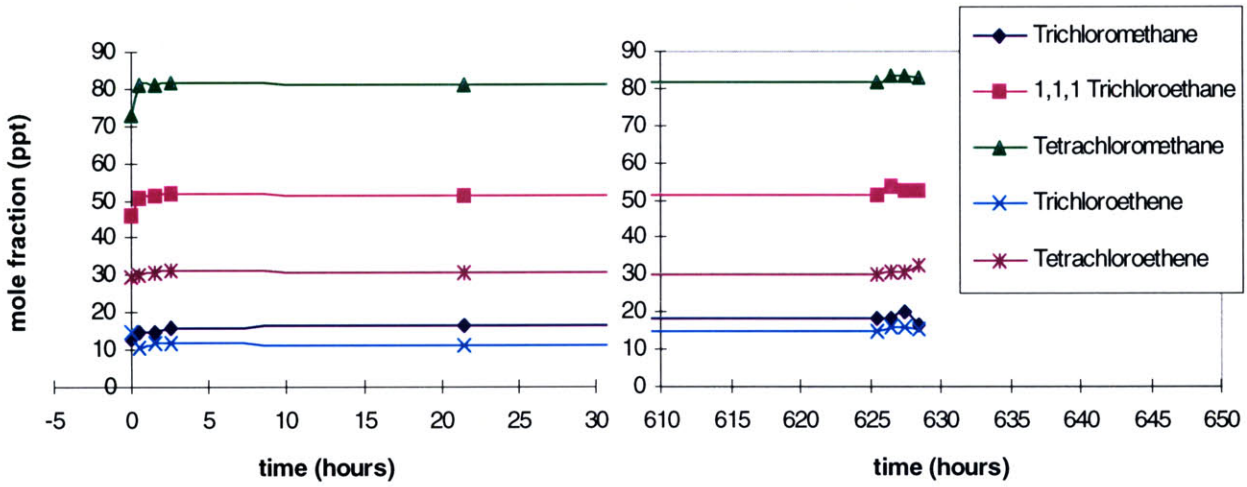

Figure 3. Measurements of Tank 2 at varying times subsequent to its collection. The value at t=0 represents a measurement of ambient air at Nahant at the time of collection.

Tank 2 was flushed with ambient air at the Nahant field site for 2-3 hours and then pressurized to ~40 psia. Ambient air was analyzed simultaneously, and then Tank 2 was analyzed at 30 minutes, 90 minutes, 2.5 hours and 20.5 hours subsequent to its collection. Both tanks were shipped to NCAR for analysis and returned to MIT to be analyzed again 26 days after they were filled. Figure 3 shows the results of these multiple analyses for Tank 2 and demonstrates the stability of whole air in these prepared flasks. Most gases are extremely stable from the outset, though some tend to increase slightly over the first few analyses. It is of some concern that trichloroethene is measured to be considerably higher in Tank 2 after the NCAR analysis, indicating that this compound is not entirely stable over long time periods. We also note that a similar phenomena occurred in Tank 1 where a higher concentration of trichloroethene is measured after the tank's return from NCAR. This trend in the mole fraction of trichloroethene was observed during the NCAR analysis as well (Eliot Atlas, personal communication); however we note that the NCAR analysis was performed very nearly halfway between our analyses. Thus if we assume a linear growth rate of the mole fraction within the tanks, an average value of the before and after analyses will still give an accurate scale adjustment factor.

The results of the second intercomparison experiment with respect to trichloromethane are shown in Table 4 and are significantly different for Tank 1 versus Tank 2. We note that Tank 2 was a sample of whole air, which raises the possibility that there may be a compound in whole air that co-elutes with trichloromethane in our analytical system. If we apply the calibration scale factor for trichloromethane derived from the Tank 1 sample (1.35) to the NCAR analysis of the Tank 2 sample (16 ppt), we find that on the MIT scale,

we would expect to observe a trichloromethane mole fraction of 11.9 ppt. We measured an average mole fraction of 16.7 ppt in the Tank 2 ambient air sample indicating that ~4.8ppt of another compound may have co-eluted with trichloromethane during this analysis. While we can still use the results of the Tank 1 analysis and the intercomparison with the AGAGE standards (both of which were manufactured samples) to calculate an accurate absolute calibration, we should be mindful of how a small amount of a co-eluting peak would affect the measurements of trichloromethane. This possible complication is discussed in Chapter 4.

The results of the four intercomparisons summarized in Tables 3 and 4 show that for all compounds our best estimate of the concentrations in the samples were approximately 30% too low for almost every compound except tetrachloroethene where a 100% difference was observed. This is not surprising given the significant difficulty involved in producing highly accurate trace gas standards for reactive and readily adsorbed chlorocarbons at the 100 ppt level as noted earlier. In fact for tetrachloroethene, for which we observe the greatest discrepancy in calibration, we have calculated what the expected uncertainty was from the manufacturing process at MIT. Due to the high sensitivity of the ECD to this compound, we attempted to make as large a dilution factor as possible during the primary and secondary dilution steps. Unfortunately this involved making measurements of pressure *differences* which were at times less than the precision of the pressure transducer, allowing >100% error at two stages of the process. When all the experimental uncertainties are accounted for, we find that the discrepancy in absolute calibration scale observed for each compound is within the expected experimental uncertainty of the standard production process.

From Table 3 and 4 the correction factors needed to put our measurements on either the SIO-AGAGE scale or NCAR scales are very close to each other, indicating they have much smaller differences in their absolute calibration scales (<10%) than with the MIT scale. Given their performance in the IGAC/NOMHALICE experiment (Prinn et al., 1999c), we have considerably greater confidence in the absolute calibration of SIO and NCAR than our own standards and have, therefore, chosen to report our data using the average absolute calibration scale of these two laboratories. All mole fractions reported in this thesis are reported on the combined NCAR/SIO scale created by averaging the SIO/MIT and NCAR/MIT scale factors reported in column 5 of Tables 3 and 4 (excluding the Tank 2 factor for trichloromethane) and assume an uncertainty in our resultant absolute accuracy of <10%.

An estimate of analytical precision can be obtained by making repeated measurements of a trace gas standard. Statistics from 15 repeated collections of Standard 595 are shown in Table 5. These measurements indicate that the measured values varied by less than 2%. An independent measure of precision can be made by looking at the daily instrumental calibrations used to determine long-term trends in the instrumental sensitivity and calibration gas stability. The measured peak areas for the 1-liter collections of calibration gas which were performed at the beginning of each sequence of ambient air measurements at Nahant have been plotted in Figure 4. These plots are consistent with the estimates of precision shown in Table 5 (<2% variability) for all compounds except

tetrachloromethane. Shortly after switching from Standard 594 to Standard 5141 we see a distinct trend in the measured mole fraction of tetrachloromethane indicating that this compound was no longer stable in the tank. Because the losses occur at a steady rate, we are still able to calibrate our measurements by calculating the trend (2.1% per week) and then multiply the calibration by a linearly scaled time factor. Subsequent measurements of Standard 594 show that the instrument response has remained constant with respect to this compound, and thus the observed decrease is not due to shifting instrument response but rather to a real loss of tetrachloromethane in Standard 5141. As mentioned previously, tetrachloromethane is used as a reference peak only, and in light of these calibration difficulties, we do not include the measurements for this compound with the data presented in Appendix B.

Table 5.

Std 595	**Mean Area** (n=15)	**Std Dev** (n=15)	**Precision (SD/Mean)**
CFC-11	8,960,000	137,000	0.015
Trichloromethane	427,000	6,400	0.015
1,1,1 Trichloroethane	351,000	51,500	0.015
Tetrachloromethane	15,000,000	276,000	0.018
Trichloroethene	965,000	13,000	0.013
Tetrachloroethene	2,260,000	41,200	0.018

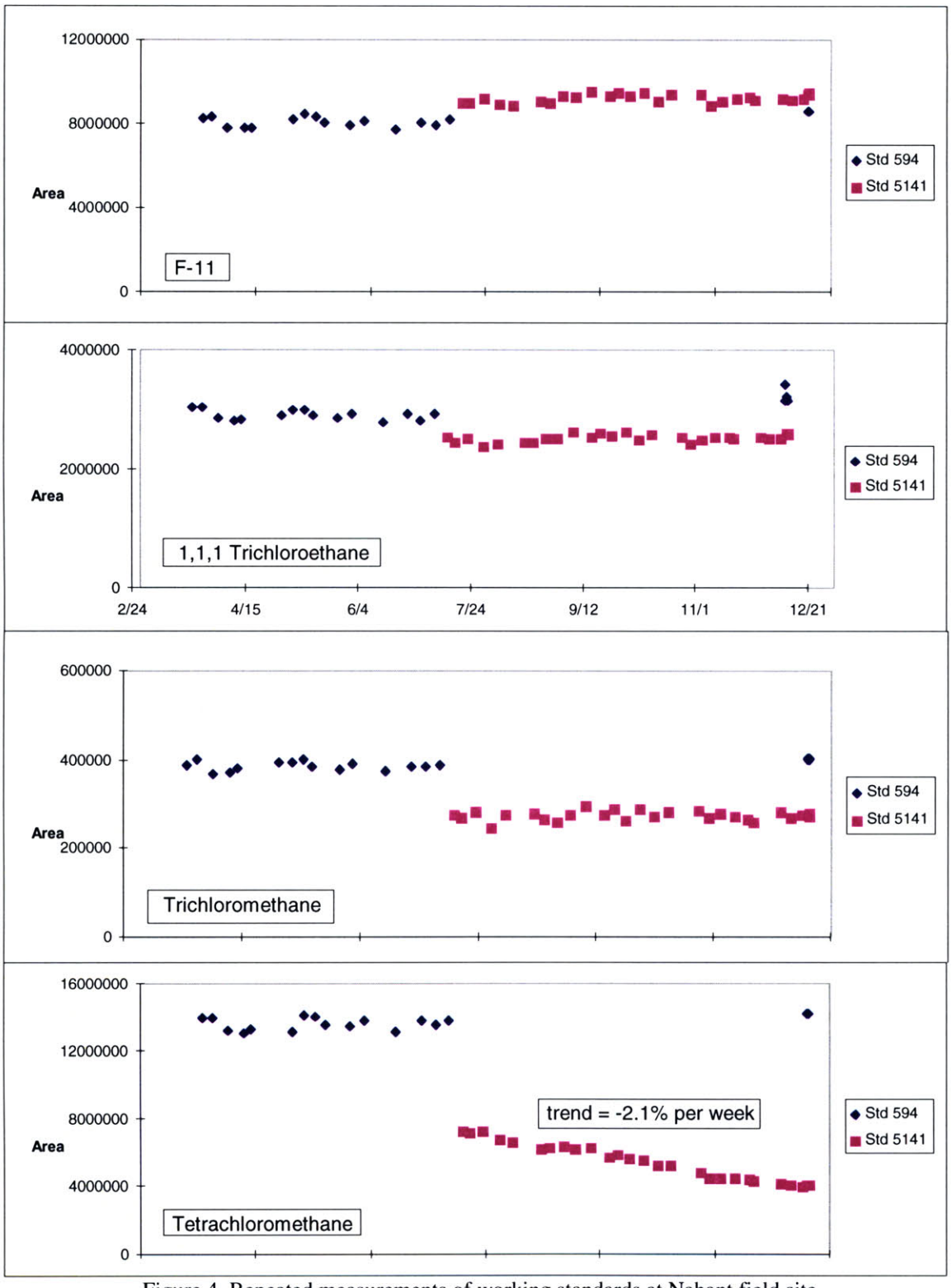

Figure 4. Repeated measurements of working standards at Nahant field site.

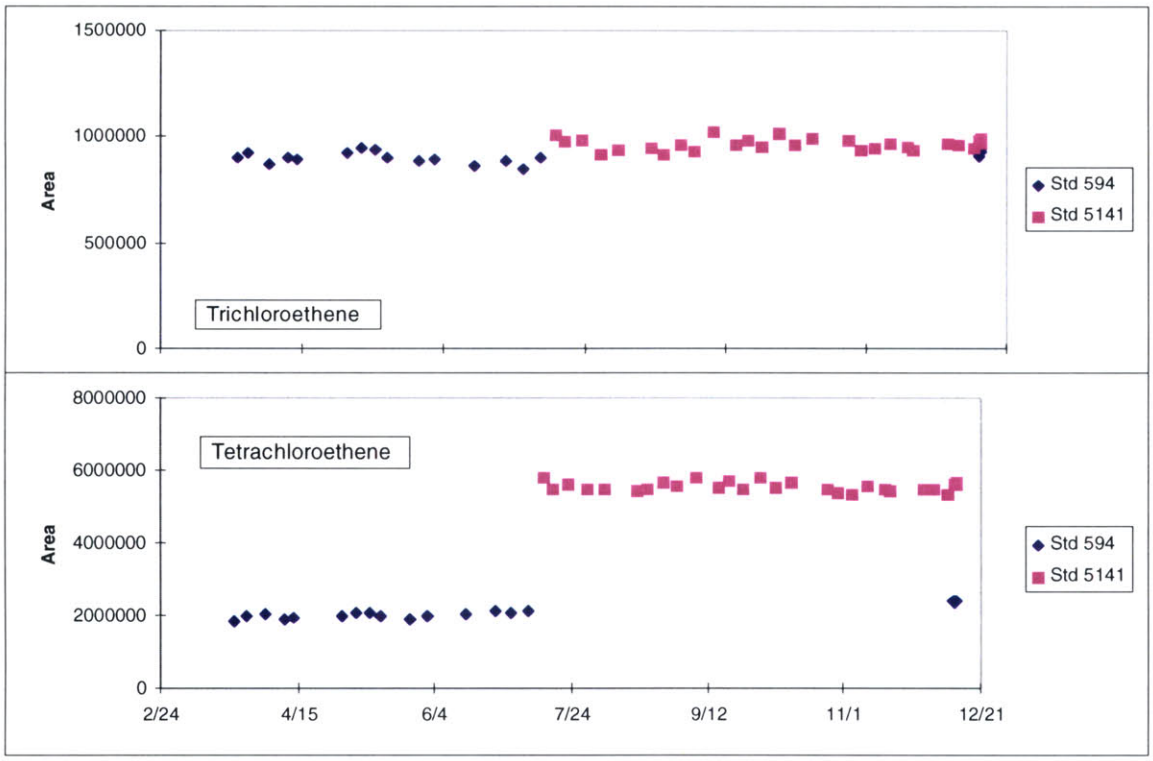

Figure 4. (Continued)

Detection limits were calculated following the method of Currie (1968) (as described by Kirchmer, 1988) and are shown in Table 6. This technique is a statistical method for establishing detection limits based on the standard deviation of blank responses. The criteria of detection establishes the limit at which we can be confident that a detection has occurred and that the signal is statistically different from the response of a blank. The limit of detection establishes the level at which one can quantitatively determine the signal level and calibrate the measurement. Thus we have reported all measurements between the criteria of detection (L_C) and the limit of detection (L_D) as being $<L_D$, and those measurements which were beneath L_C are reported as a non-detections.

Table 6 - Detection Limits for MIT Halocarbon Detection System

Compound	Criteria of Detection (ppt)	Limit of Detection (ppt)
trichloromethane	3.9	7.8
1,1,1 trichloroethane	2.3	4.6
tetrachloromethane	0.2	0.3
trichloroethene	2.3	4.5
tetrachloroethene	2.1	4.2

Measurement Data

Data collection began in December of 1997; however, changes in temperature programming in mid-March 1998 significantly improved the chromatographic separation, and thus only data obtained after March 23, 1998 are presented here. A sample of hourly measurement data from one week in September 1998 are presented in Figure 5. The entire set of hourly measurements between March 23, 1998 and January 12, 1999 are presented in Appendix B as a series of monthly plots for each compound. Note that all data are presented in units of mole fraction (ppt) and are presented on the NCAR/SIO absolute calibration scale as described in the previous section.

As Figure 5 shows, there are clear differences in observed mole fraction over the course of a week. For shorter lived compounds such as trichloroethene and tetrachloroethene, we see large spikes corresponding to pollution events where a backtrajectory would presumably show a path over high emissions regions. There are also several stable periods of time such as the afternoon of September 23rd when the short-lived compounds have observed mole fractions very close to their background values. Longer lived compounds, such as tetrachloromethane, have hardly any variation at all, indicating a lack of local sources and a rather uniformly distributed atmospheric burden.

Our analysis of these data discussed in the following chapters draws upon the sensitivity of the measured mole fractions to the past history of the air mass being sampled and to the subsequent large difference between mole fractions in polluted air and relatively clean air.

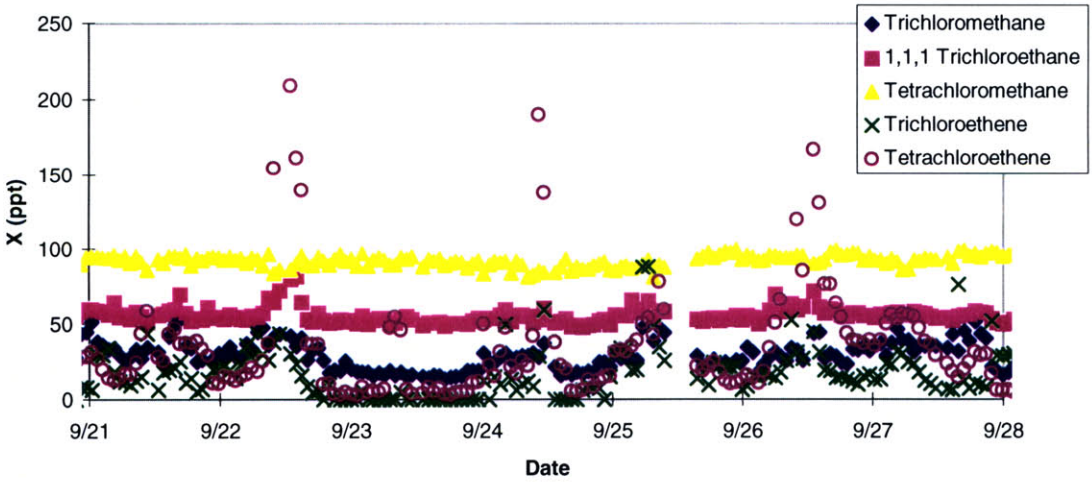

Figure 5. Time series of halocarbon mole fractions from September 21-28, 1998 at the Nahant site.

Chapter 3: Inverse Method - Theory

The development of the inverse methods that we will employ here are found in Gelb (1994) and Prinn (1999b). Inverse methods have provided a powerful means of using observed atmospheric mole fractions to deduce emissions on a global scale (Cunnold et al., 1994; Hartley and Prinn, 1993; Mahowald et al., 1997). The extension of these techniques for regional emissions estimates does not differ on a theoretical level, and the development presented here is primarily intended to give a consistent set of notation for describing the model used in this work.

Measurement Equation

If our chemical-transport model is exact, then the observed mole fraction (χ_{obs}) can be expressed as the sum of the model-estimated mole fraction and the error (ε) in χ_{obs}. Using the continuity equation from Chapter 1 (equation 1.3), χ_{obs} can be expressed in time coordinates as:

$$\chi^{*}_{obs}(s,t) = \chi_{obs}(s,t) - \chi(0,0) = \int_0^t \left(\frac{E}{h[M]} + \frac{\nabla \cdot K[M]\langle \nabla \chi \rangle}{[M]} \right) dt' + \varepsilon(s,t) \quad (3.1)$$

If we assume $\mathbf{K}$ = diag[K^{Hor}, K^{Hor}, K^{Vert}], the trajectory is confined to the mixed layer ($Z<h$), and that the gradient of χ is zero in the vertical direction (we assume a well-mixed layer), then we can define the convergence, C, in equation 3.1 in cylindrical coordinates (r,ϕ) as:

$$\begin{aligned} C &= \left(\nabla \cdot \left[K[M]\langle \nabla \chi \rangle \right] \right) / [M] \\ &= K^{Hor} \nabla_h \cdot \left(\nabla_h \chi \right) \\ &= K^{Hor} \left(\frac{1}{r} \frac{\partial}{\partial r} r \frac{\partial \chi}{\partial r} + \frac{1}{r} \frac{\partial^2 \chi}{\partial \phi^2} \right) \end{aligned} \quad (3.2)$$

To transform our continuity equation into a more useful form, we (1) use (3.2) to define the convergence, (2) discretize the integral over time, (3) let $z_k^{obs} = \chi^{*}_{obs}(s,t)$ where s is the observing site and the observing time, t, is represented by index k, and (4) express the emissions from region j as x_j in units of mole fraction/time ($x = E/(h[M])$). The resulting equation is:

$$z_k^{obs} = \alpha_k \sum_j x_{jk} \tau_{jk} + \sum_j C_{jk} \tau_{jk} + \varepsilon_k \quad (3.3)$$

where j is an index that runs over just the regions in the mixed layer that the kth trajectory passes through (i.e. not every trajectory passes through every region).

τ_{jk} represents the amount of time spent in region j during the kth trajectory, and α_k is a correction factor which is applied to the initial estimate of emissions, x, for each region passed over by trajectory k. This correction factor is the quantity we seek, and equation (3.3) is known as the measurement equation.

We note that the unknown state parameter α is a correction factor for x rather than the RCEI emissions, E. This implies that our choice of mixed layer height, h, and our resultant choice of average molar density, $[M]$, will play a role in determining what the resultant correction to the RCEI emissions are. If one assumes a mixed layer height or a molar density different than the standard values used here (h_s=1500m and $[M]_s$=38 moles/m^3), then although the correction factor for the quotient ($E/(h[M])$) will be the same, the correction factor that should be applied to E alone, which we will call α^*, must be scaled as shown:

$$\alpha^* = \alpha\left(\frac{h[M]}{h_s[M]_s}\right) \tag{3.4}$$

The molar density is a function of the mixed layer height, and we take $[M]$ to be defined as in equation 3.5:

$$[M] = [M]_0 e^{-z/H} \approx [M]_0\left(1 - z/H\right) \tag{3.5}$$

where $[M]_0$ is the molar density of air at STP (41 moles/m^3) and H is the scale height of the atmosphere (≈8km). Using a truncated Taylor expansion for the exponential and taking the mean density of our mixed layer to be the value at the midpoint ($Z=h_s/2$), we have a new expression for α^*, which is a function only of mixed layer height:

$$\alpha^* = \alpha\left(\frac{h - h^2/2H}{h_s - h_s^2/2H}\right) \tag{3.6}$$

Boundary Conditions

The background mole fraction, $\chi(0,0)$, is needed to define z_k^{obs} and will vary depending upon the origin of the air mass. When the wind direction is bringing an air mass from due west across the continent and regions of high emissions, we expect the background mole fraction at the domain boundary to be much higher than when the wind direction is bringing an air mass from due east across the ocean. To provide estimates of $\chi(0,0)$ we have paired each set of observations with an angle corresponding to the compass direction relative to Boston of the first trajectory record that lies within our domain (e.g. a trajectory that starts in Chicago, Illinois would have a trajectory angle of 269°). By plotting each measured mole fraction against its calculated initial trajectory

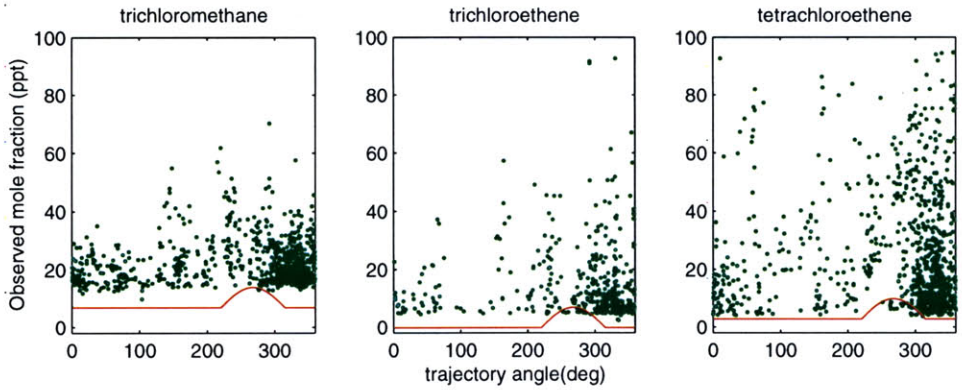

Figure 6. Observed mole fractions of trichloromethane, trichloroethene and tetrachloroethene as a function of wind angle relative to Boston. The red curves represent the functional form of background mole fraction adopted for each compound.

angle (see Figure 6), we can see the minimum observed value from each direction. In many directions, we observe values right down to our stated detection limits. In these cases, we have an upper limit on what $\chi(0,0)$ could be. At other angles the lowest observed concentrations are above the detection limits, giving us an idea of the functional form of $\chi(0,0)$. Our assumed value of $\chi(0,0)$ is shown in Figure 6 as the red curve plotted with the data. The hump in the curve for tri- and tetrachloroethene represents the angular location of North American continental emissions as shown in Figures 7-8. Trichloromethane has significant ocean emissions, but we still expect the background mole fraction to be higher over continental regions than over the ocean.

Convergence

The convergence (C) is approximately estimated using equation (3.2) and the steady state analytical solution to the continuity equation presented by Fay and Rosensweig (1980) which allows us to calculate expected observed mole fractions for point source emissions under a prescribed set of meteorological conditions. They found that the steady state continuity equation in cylindrical coordinates for a vertically well-mixed layer has the following solution:

$$\chi = \frac{x\,A}{\pi\, v\, l}\exp\left(r\cos\phi/l\right)\kappa_0\left(r\eta/l\right) \tag{3.7}$$

where $x=E/(h[M])$, v represents horizontal wind speed, A is the surface area of the emitting region, r and ϕ are the usual cylindrical coordinates, and κ_0 is the 0^{th} order modified Bessel function. (We have substituted the product of emissions per unit surface area times surface area for point source emissions which were used by Fay and Rosenzweig.) We estimate the horizontal mixing length $l=2K^{Hor}/v$ using the HYSPLIT model definition of horizontal subgrid scale diffusivity (Smagorinsky, 1963):

$$K^{Hor} = \frac{1}{\sqrt{2}}(cX)^2\,\xi \tag{3.8}$$

where c is an empirical constant (0.14), X is the grid size, and ξ is the horizontal deformation defined by:

$$\xi = \left[\left(\partial v_x / \partial y + \partial v_y / \partial x \right)^2 + \left(\partial v_x / \partial y - \partial v_y / \partial x \right)^2 \right]^{1/2} \tag{3.9}$$

Here, however, we are trying to obtain an estimate for diffusion on trajectory length scales, not subgrid scale. To obtain realistic estimates, we use the horizontal wind speed, v, and the horizontal deformation, ξ, from HYSPLIT to scale l:

$$l = l_0 \cdot \frac{v_0}{v} \cdot \frac{\xi}{\xi_0} \tag{3.10}$$

where l_0 = 1.0 x 10^6 m is based on the empirical value of K^{Hor} used by Fay and Rosenzweig for long-range trajectories (10^6 - 10^7 m^2/s, Fay and Rosenzweig, 1980). Estimated average horizontal wind speed at 500 meters altitude, v_0, is taken to be 10 m/s and ξ_0 is taken to be 0.01 s^{-1} (obtained by averaging horizontal velocities from the HYSPLIT trajectories).

The parameter η in equation 3.7 is defined by $\eta = (1+2l/vt_{atm})^{1/2}$, where $2l/v$ represents the mixing time, which is much less than t_{atm}, the atmospheric lifetime (thus $\eta \approx 1$).

This solution (equation 3.7) can be used in (3.2) to provide an estimate of convergence along a particular trajectory. Because the solution provides the perturbation mole fraction due to a point source emission, we simply sum the contribution from each grid cell in the domain to obtain the total convergence estimate at a point along a trajectory as shown:

$$C_{jk} = K^{Hor} \sum_i \nabla^2 \chi^i_{jk} \tag{3.11}$$

where χ^i_{jk} represents the contribution of the i^{th} grid cell's emissions to the total mole fraction estimated at a given point (j) and trajectory (k). Thus i is an index that runs over every grid cell in the domain, whether a trajectory passes through it or not. This notation is necessary to correctly calculate the convergence since, through the derivatives of χ, it is dependent on emissions from all regions (x_i), not just those which are along the k^{th} trajectory path.

Kalman Filter

The Kalman filter is a linear estimator which recursively provides the optimal estimate of a quantity at a given time based on all previous measurements. It has the advantage of

providing estimates with errors after the use of each observation, thus providing a measure of the usefulness of each observation. We use the Kalman filter in a simplified form equivalent to recursive weighted least-squares to find the optimal estimate of the correction factor, α, that minimizes the differences between estimated mole fractions and the weighted observations.

The first two terms of the right-hand side of the measurement equation (3.3) provide a means of estimating a mole fraction for comparison with the k^{th} observed value. To calculate this mole fraction we need: (1) an initial estimate of emissions over the entire geographical domain, and (2) a backtrajectory so that we know which emitting regions to integrate over and for how long. Both the RCEI emissions and the trajectory model used for this work are described in greater detail in the following sections of this chapter.

For each trajectory, we assume a single correction factor, α_k, is applied to the emissions from each region crossed in order to match observations. Because the same factor is applied to all of the regions crossed on a particular trajectory, this approach may be inappropriate for some of the emitting regions crossed by any one particular trajectory, as α is calculated to correct the *integrated* emissions along the entire trajectory and not a grid cell's individual emissions. This approach is appropriate if the errors in RCEI emissions are systematically too high or too low over the whole region, but inappropriate if the RCEI errors are purely random from one grid point to the next. Given the way the RCEI emissions are calculated we do expect systematic errors resulting from the use of population density to allocate emissions. A better approach requiring much more data than we have available would be to estimate a separate α value for each of the 900 grid cells in the region we are studying.

Table 7. Governing equations for the Kalman recursive linear filter.

Measurement Equation	$z_k^{obs} = \sum_j \alpha_{k-1} x_{jk} t_{jk} + \sum_j C_{jk} t_{jk} + \varepsilon_k$ $= z_k^{est} + \varepsilon_k$	(3.3)
Partial Derivative Equation	$p_k = \partial z_k^{est} / \partial \alpha_{k-1} = \sum_j x_{jk} t_{jk}$	(3.12)
State Update Equation	$\alpha_k = \alpha_{k-1} + g_k \left(z_k^{obs} - z_k^{est} \right)$	(3.13)
Kalman Gain Scalar	$g_k = \sigma^2_{\alpha\, k-1} p_k \left[p_k^2 \sigma^2_{\alpha\, k-1} + \sigma^2_{z_k} \right]^{-1}$	(3.14)
Error Update Equation	$\sigma^2_{\alpha\, k} = \sigma^2_{\alpha\, k-1} \left[1 - \{ p_k g_k \} \right]$	(3.15)

Note that each emitting region will contribute to the estimated mole fraction in proportion to its (RCEI) emission rate. Hence the most active emitting regions have the

greatest influence on the estimation of α. Also, in our case, each trajectory is weighted equally although there is no doubt that some trajectories are more accurate than others. However, the greater the number of trajectories that cross a grid cell, the less effect any one (possibly erroneous) trajectory will have on the final result. For each grid cell, we will obviously use only the trajectories which cross that cell. The Kalman filter adds each new piece of data sequentially to update the estimate of α and its uncertainty, σ_α, according to equations 3.12 through 3.15 which are shown in Table 7. These filter equations are normally written in matrix notation; however, because our implementation has only a single observing site and a single correction factor for each trajectory, they have been reduced to a set of scalar equations.

The Kalman filter starts with an initial estimate of the emissions correction factor, $\alpha_0=1.0$, and an estimate of uncertainty associated with that parameter, $\sigma_{\alpha 0}$. The correction factor is then updated and the estimate of uncertainty is reduced as each new measurement is used to improve our estimates. The Kalman gain scalar, calculated in equation 3.14, is sensitive to a balance between the error in the measurements and the error in our estimated quantity. This gain scalar is multiplied by the model residual (the difference between estimated and observed mole fraction) to determine the amount by which each new observation adjusts the correction factor, α, and reduces the error, σ_α. If there is too much error in the measurement, σ_z, then the Kalman gain scalar is small and the solution will not be adjusted very much based on this poor observation. Conversely, if the measurement is very precise, then the Kalman gain scalar is close to the maximum ($1/p$). A very small uncertainty in the measurement, coupled with the Kalman filter's explicit assumption of a perfect model (i.e. exact g value), means that the solution will be allowed to adjust completely to ensure that the estimate, z^{est}, is very close to our very accurate observation, z^{obs}.

Similarly, in equation 3.15, we are reducing the error estimate in our state parameter based on the error in each measurement through the Kalman gain scalar. If we have poor measurements, then $pg<<1$, and each new observation doesn't do much to reduce the uncertainty in our estimated quantity, while if we have near perfect measurements then $pg\rightarrow 1$, and with only a few observations we should be able to determine our estimated quantity very precisely. What these equations (and thus the resulting estimates of uncertainty) do not take into account are model errors. The Kalman filter assumes a perfect model and thus is not obviously equipped to deal with the inevitable errors which exist in all models. There are however methods to include model error indirectly. A discussion of these errors follows in the section entitled *Error Analysis*.

When we have used all the data, we will arrive at the optimal estimate for α which minimizes the difference between estimate and observation in a weighted "least squares" sense for every measurement, each of which corresponds to a backtrajectory that has crossed a particular set of grid cells. We then multiply the initial (RCEI) emissions for each grid cell by the appropriate α to produce a revised emissions field. We iterate this procedure 10 times to insure that the entire domain has a chance to adjust to each successive correction.

RCEI

The model described in this thesis addresses the area between 30° and 60° North latitude and 60°and 90° West longitude. This covers the area, roughly speaking, from New Orleans to Bermuda, up to Labrador and over to Hudson Bay. A crucial part of our methodology relies on having estimates of the emissions of the observed species over the entire region. The Reactive Chlorine Emissions Inventory (RCEI) (Keene et al., 1999) was recently published and provides just such an inventory for the entire globe with 1 degree horizontal resolution.

Reactive atmospheric chlorine has significant consequences for tropospheric and ocean surface chemistry (Graedel and Keene, 1999), and its quantification is essential to establishing accurate budgets and cycles for modelling purposes. RCEI considered four major source types: oceanic and terrestrial biogenic emissions, sea-salt production and dechlorination, biomass burning, and anthropogenic emissions. Only anthropogenic industrial emissions are relevant to the budget of tri- and tetrachloroethene. Industrial and biomass burning emissions are considered for trichloromethane.

We expect the distribution pattern, in general, to be very similar for tri- and tetrachloroethene since the majority of both solvents was distributed by population. In RCEI, the U.S. and Canadian Toxic Release Inventories were used to distribute the large industrial sources of both compounds (McCulloch, Aucott, Graedel, Kleiman, Midgely, and Li, 1999).

While the RCEI estimates a large oceanic source for trichloromethane (Khalil et al., 1999) it is pointed out (Keene et al., 1999, Figure 3) that this is at odds with the observed distribution of atmospheric trichloromethane with its large NH/SH gradient. Without a clear distribution pattern for the natural sources of trichloromethane, we have chosen to use the distributed emissions of trichloromethane due to biomass burning (Lobert et al., 1999) and industrial processes (Aucott, McCulloch, Graedel, Kleiman, Midgley, and Li, 1999) only for our initial guess. This represents only 11% of the RCEI estimated total, and thus we look to the Kalman filter and observations to correct for the absence of natural sources. Starting with only these anthropogenic emissions, we would expect a median correction factor of ~9 for this compound if the RCEI estimates are correct and that the relative contributions of each source type within our study region scale to the global values. We have converted the RCEI units to part-per-trillion per hour (ppt/h) as explained in the definition of the variable x. These units represent the impact that the estimated emissions would have on the mole fraction of a parcel of air which was uniformly mixed up to 1500m altitude.

Maps of the RCEI 1990 estimated trichloroethene and tetrachloroethene emissions for each grid cell in our study region are shown in Figures 7 and 8. The estimated trichloromethane emissions due to biomass burning and industrial emissions only are shown in Figure 9.

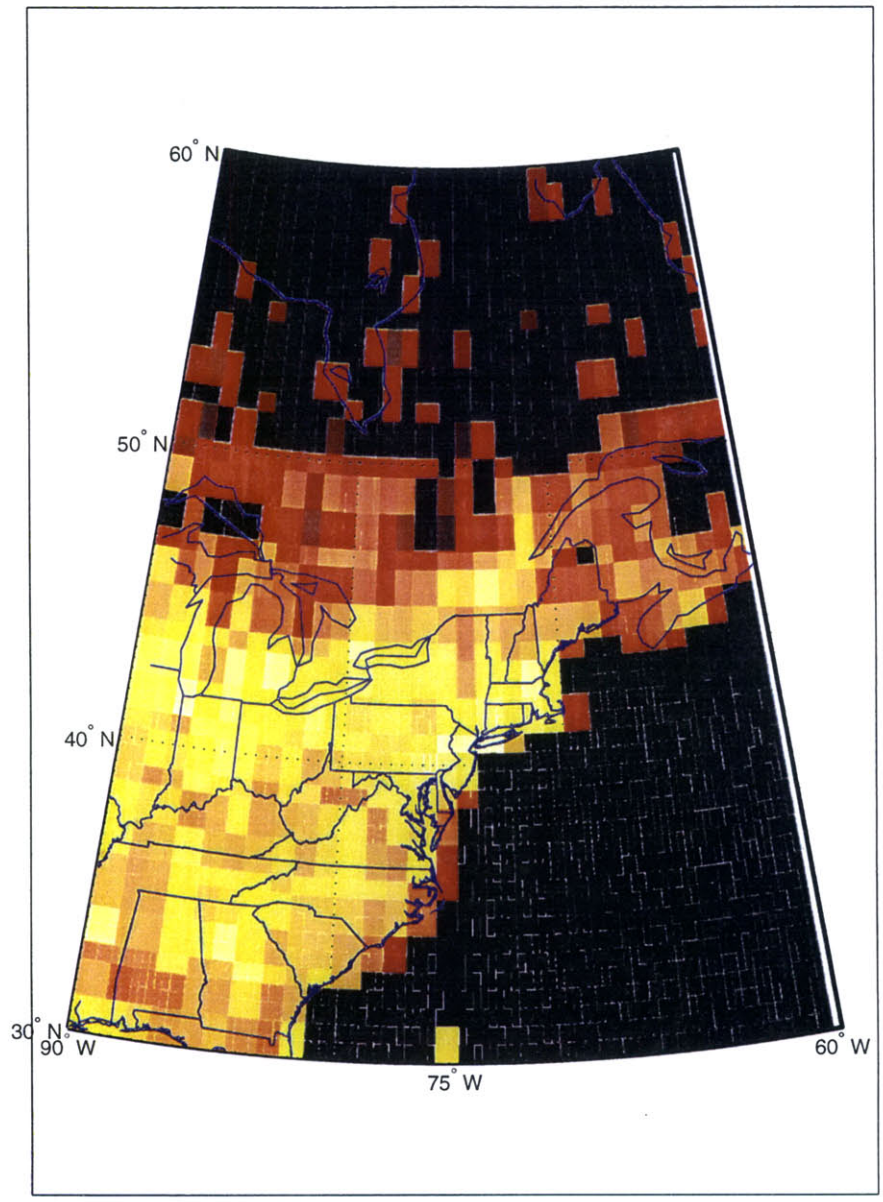

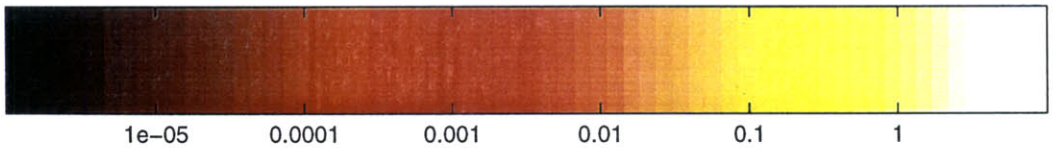

Figure7. Reactive Chlorine Emissions Inventory estimated 1990 emissions of trichloroethene for 1°x1° grid cells in the Eastern USA and Southeastern Canada. Emissions are shown in units of ppt/hr. These units assume a uniform mixed layer height of 1500 m and uniform molar density of air (38.0 moles/m^3).

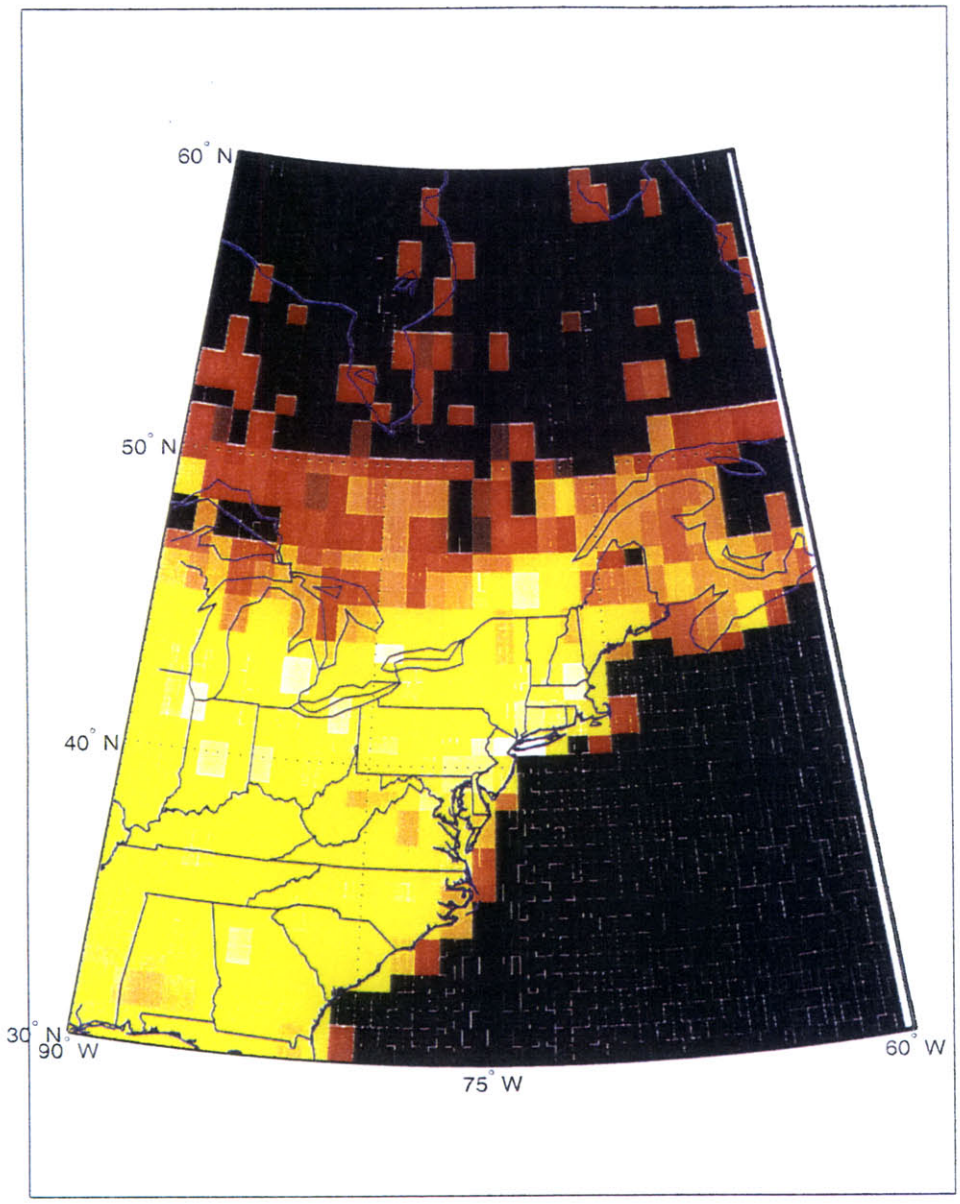

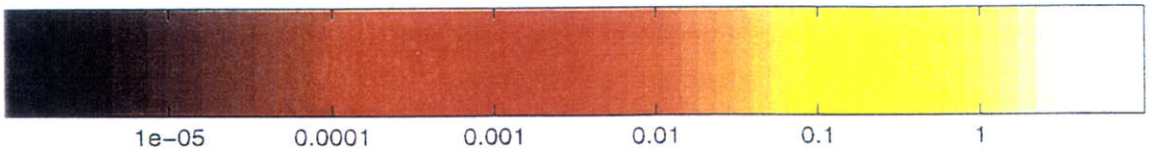

Figure 8. Reactive Chlorine Emissions Inventory estimated 1990 emissions of tetrachloroethene for 1°x1° grid cells in the Eastern USA and Southeastern Canada. Emissions are shown in units of ppt/hr. These units assume a uniform mixed layer height of 1500 m and uniform molar density of air (38.0 moles/m^3).

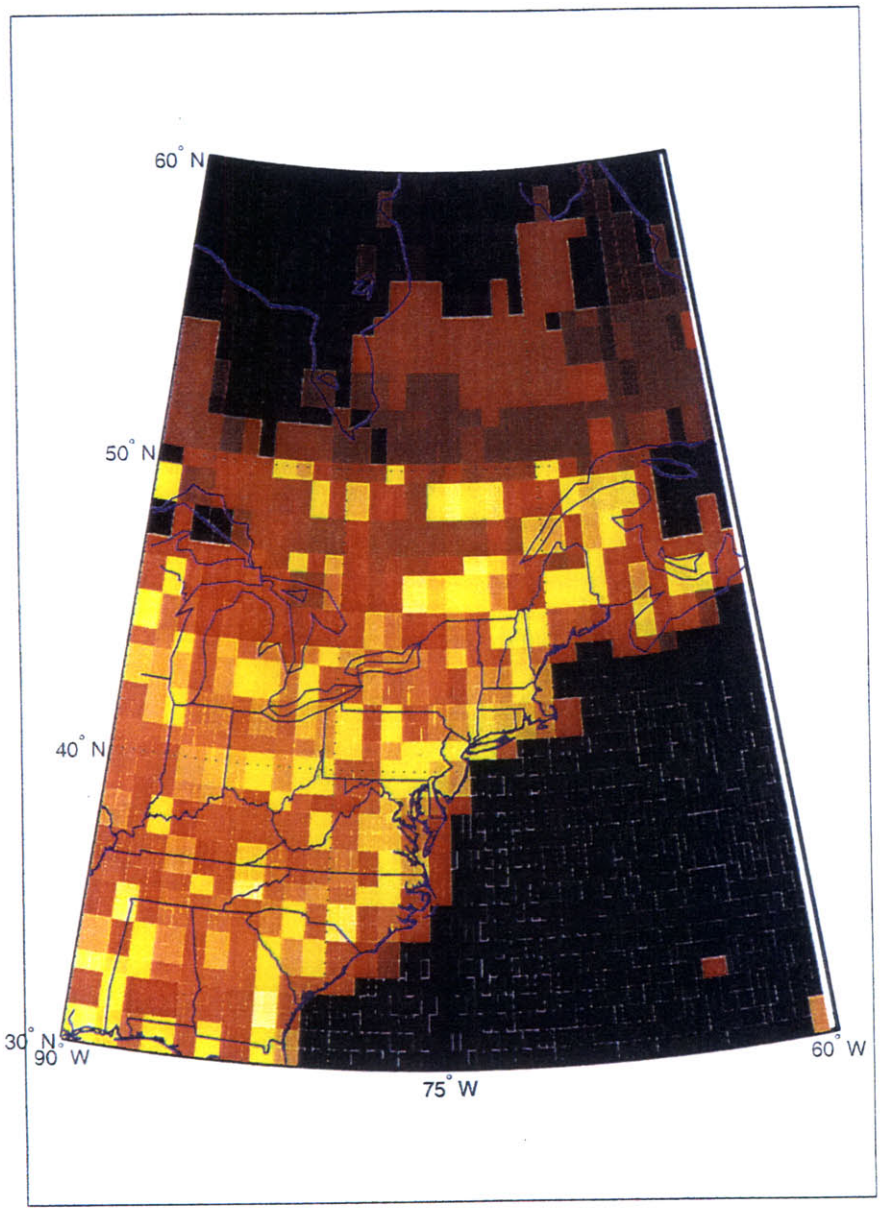

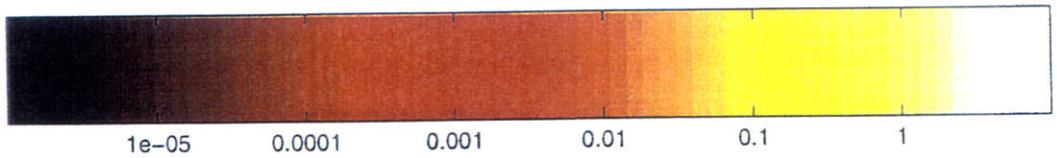

Figure 9. Reactive Chlorine Emissions Inventory estimated 1990 emissions of trichloromethane due to biomass burning and anthropogenic process emissions (including paper and pulp bleaching, water treatment, and industrial usage) for 1°x1° grid cells in the Eastern USA and Southeastern Canada. Emissions are shown in units of ppt/hr. These units assume a uniform mixed layer height of 1500 m and uniform molar density of air (38.0 moles/m^3).

HYSPLIT

The HYbrid Single-Particle Lagrangian Integrated Trajectory (HYSPLIT-4) model developed by Roland Draxler at the NOAA Air Resources Laboratory (ARL)(Draxler and Hess, 1997, 1998) is used for calculating Lagrangian trajectories from archived analyzed observed wind fields from the National Centers for Environmental Prediction (NCEP). The model has been modified to include the diffusivity parameter and horizontal deformation needed to estimate convergence (see Chapter 3) with standard trajectory output available on the world wide web (http://www.arl.noaa.gov/ready.html). Sample trajectories ending at three pressure levels above our Nahant observing site are shown in Figure 10.

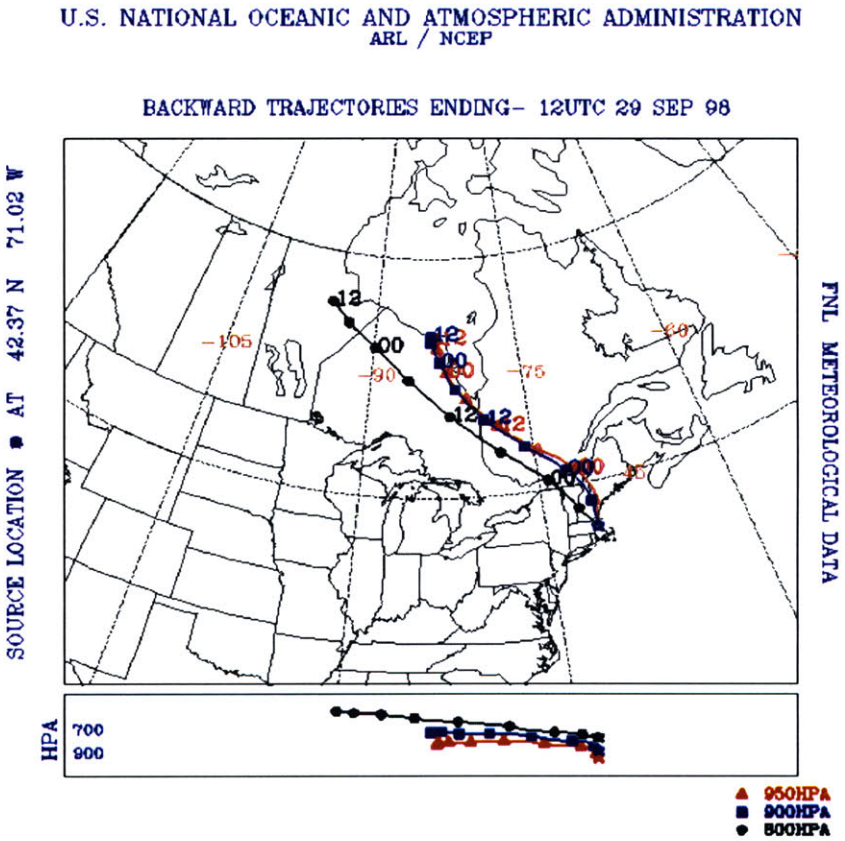

Figure 10. Backtrajectory for September 29, 1998 12:00 UTC. Trajectories are calculated for 48 hours prior to arriving over Boston. Pressure levels are indicated in red, blue and black.

In this latest version of the HYSPLIT model, a time interpolation feature is directly incorporated into the advection scheme. Thus a first guess at a particle's position, s, is given by:

$$s'(t+\Delta t) = s(t) + v(s,t)\Delta t \tag{3.16}$$

and the final estimated position is given by:

$$s(t+\Delta t) = s(t) + 0.5\{v(s,t) + v(s',t+\Delta t)\}\Delta t \,. \tag{3.17}$$

Accuracy of the trajectories is obviously affected by the temporal and spatial resolution of the input meteorological data. NOAA ARL archives analyzed meteorological products for use with the HYSPLIT model including global grids from the final (FNL) operational run of the National Centers for Environmental Prediction's Global Data Assimilation System (NCEP's GDAS) with a 191 km grid resolution and 6 hourly forecast time resolution and the Eta Data Assimilation System (EDAS) wind fields, which only cover North America but have an 80 km resolution based on 3-hourly variational analyses. For all the work described in this thesis, the EDAS data were used to reduce trajectory uncertainty as much as possible.

Using typical spatial and temporal resolutions as described above, the HYSPLIT model has been shown to have a trajectory accuracy of 10-20% of the total transport distance (Draxler, 1996, 1991). Case studies (Draxler and Hess, 1998) have also shown that due to large variations of wind speed and direction near the ground relative to higher altitudes, it is essential that the atmosphere's vertical structure be well represented by the input data. It is estimated that the HYSPLIT forecast trajectories have one-third of the relative trajectory error during low shear conditions than during high shear conditions (Stunder, 1996). It is reasonable to assume that these meteorological conditions would have a similar effect on our backtrajectories.

Backtrajectories, such as those shown in Figure 10, were calculated once each hour for the entire period of data collection. We use the backtrajectories from the point 500 m (~950 hPa) above the Nahant observing site for all modelling work, although the ability to calculate multiple trajectories is useful for examining the vertical wind structure and air mass dispersion characteristics for complicated meteorological situations. Periods of high shear could not be totally avoided and thus some trajectories do have significantly more error than others as discussed in Chapter 4. Because each measurement is equally weighted, if we experience low-shear, laminar flow conditions in the lower atmosphere for a majority of the backtrajectories, and only a few backtrajectories are subject to high shear or unstable conditions, we are likely to have average backtrajectory accuracies of 10-20% of transport distance, which translates to an estimated 20-25% error in our estimates of mole fraction as calculated by the measurement equation. However the converse is also true, and trajectory error could be significantly higher if we do not experience stable conditions for a majority of the time. Thus a careful analysis of errors in relation to the prevalent meteorological conditions is warranted in assessing the overall uncertainty of our emissions estimates.

A simple test of the HYSPLIT model can be obtained by examining the trajectories which are correlated with high values of mole fraction to ensure that they spent large fractions of their time over high emissions regions. Similarly, the trajectories associated with low values of mole fraction should show little time spent over high emissions regions. Figure 11 shows a set of trajectories (in red) which are associated with observed high

values of tetrachloroethene mole fraction during the Fall of 1998. All of these trajectories can be seen to pass directly over the high emissions regions of greater Montreal or the East Coast urban corridor prior to their arrival in Nahant. The figure also shows the trajectories associated with observations of low mole fraction during fall (in green). During these times, we see that the corresponding trajectories passed over regions not associated with high emissions and thus the associated air mass would not be expected to contain high mole fractions. With few exceptions all of the backtrajectories were qualitatively consistent with the measured mole fractions.

Error Analysis

In our use of the Kalman filter, the primary sources of model error will stem from three main sources: (1) error in the trajectory model which we can estimate, (2) the effects of local pollution events which we can eliminate, and (3) the assumption that emissions are time invariant which we can do nothing about. With the exception of trichloromethane, which has significant natural sources, we do not expect very large time variations in emissions as the industrial sales (and presumably emissions) do not vary substantially throughout the year. Releases of these compounds over shorter time periods are treated as the appropriate fraction of annual emissions; however, the uncertainty increases inversely to the size of that fraction (McCulloch et al., 1999).

As mentioned previously, HYSPLIT can have relative trajectory errors up to 20% of total trajectory distance on a routine basis. Thus for any particular trajectory/observation we may be estimating the correction factor for the emissions from a given grid cell based on a trajectory that is in error (see Figure 12). The resultant error in z^{est} can be considered as pseudo-error in z^{obs} (see equation 3.13), and this pseudo-error can be incorporated into the Kalman filter's σ_z^2 term. The rough magnitude of this error has been numerically estimated using a Monte Carlo technique. The distribution of estimated concentrations of 100 trajectories which have been offset from one original trajectory gives a sense of how much error will be incurred by estimating a mole fraction using a trajectory that strays from the actual path taken by the observed air mass. The set of start points shown in Figure 13 are normally distributed (with a standard deviation of displacement of 15% of total trajectory length) about the original start point of the straight line trajectory shown. The resulting distribution of estimated mole fraction which would be observed at the end

of these altered trajectories indicates that this error is of the order of 10 ppt. This error has been included with the error due to instrumental precision (σ_z^2 in equation 3.15), and the Kalman filter incorporates this pseudo-loss of "measurement" precision due to model error accordingly.

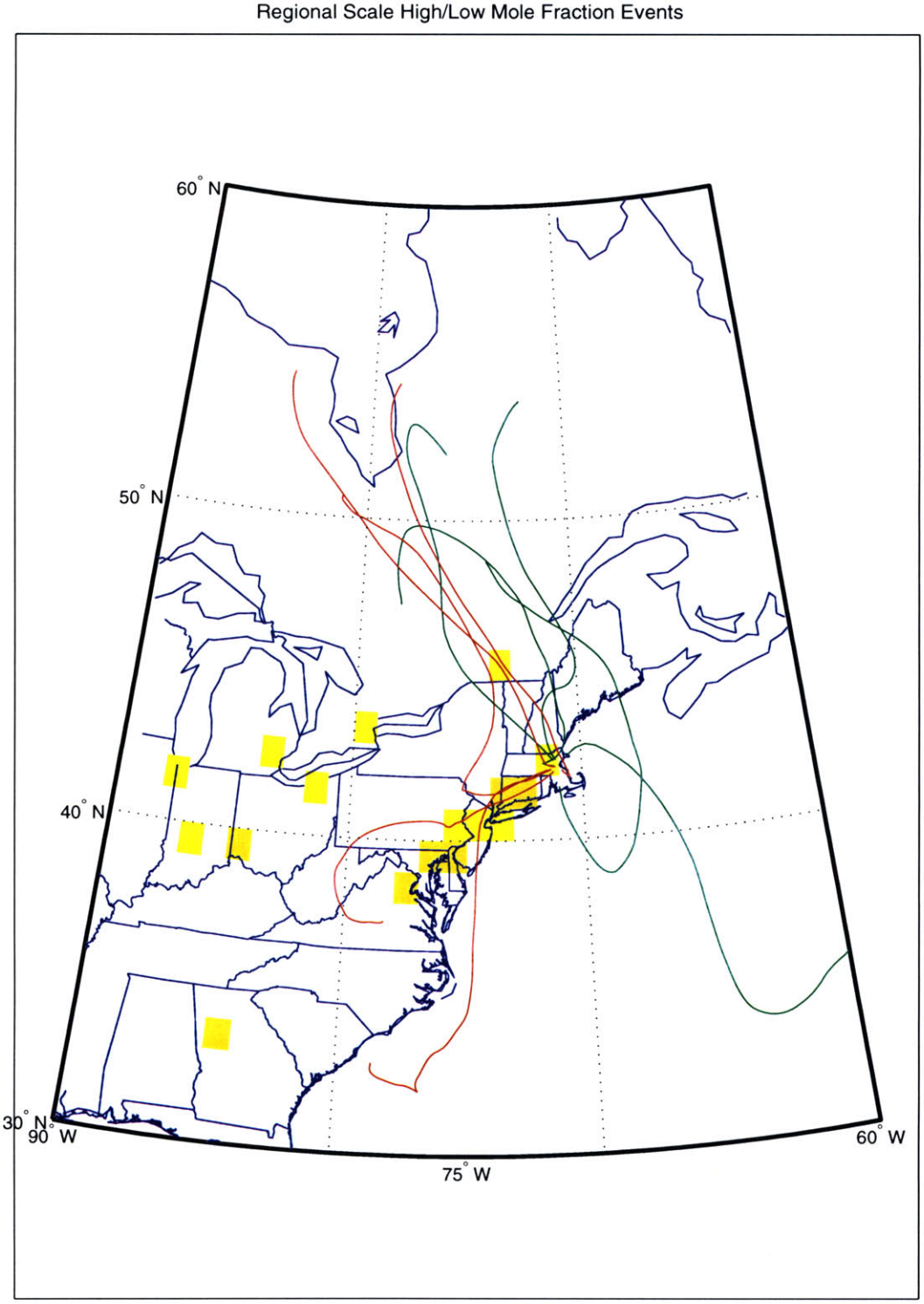

Figure 11. Backtrajectories starting 500 m above Nahant corresponding to observations of high values of ambient mole fraction for tetrachloroethene (in red) measured during Fall, 1998. Also shown are 500 m backtrajectories corresponding to low values measured during the Fall (in green). Underlying regions of high emissions (>1ppt/hr) are represented by yellow shading.

Local Pollution

Strong sources very near to our observing site can produce "local pollution events" which are not adequately represented by the 1°×1° average used in our measurement equation. These errors can not be dealt with in an entirely satisfactory way as we do not have a more accurate spatial or temporal accounting of local emissions. We can, however, make the assumption that *regional scale* emissions from high emissions regions, such as Montreal or New York, would be significantly mixed with surrounding less-polluted air after transport over several hundred kilometers from these source regions to the observing site. Thus measurements of very high mole fraction over very short time periods of the chemical of interest, preceded by and followed by significantly lower values of ambient mole fraction are very likely to be due to a nearby local source which is not accurately simulated by our 1°×1° model. A reasonable solution to this problem is to reject measurements that are consistent with a local pollution event of the above type and to base our emissions correction factor estimates only on the remaining data. If we do not

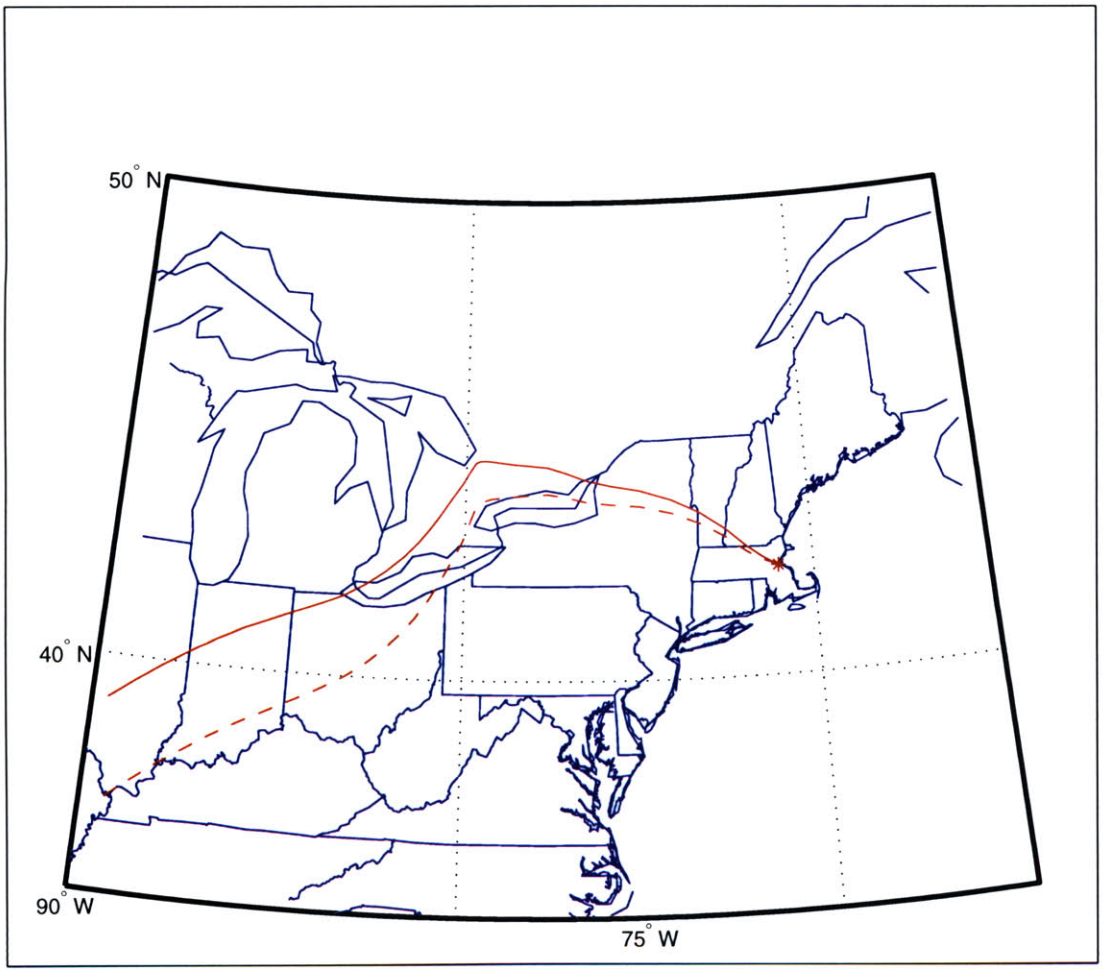

Figure 12. A given backtrajectory as calculated by HYSPLIT (red) may be in error by 10-20% of trajectory distance. The true path an air parcel which is sampled in Boston may have taken a path such as that shown by the dashed red line. The computed difference in ambient concentration between the air masses represented by the red and the dashed red lines can be thought of as either a random model error or a random measurement error without affecting the difference z^{obs}-z^{est} in equation 3.13.

eliminate these local pollution events, the resulting emissions correction factors can be seen to increase suddenly and drastically when these observations are introduced, often jumping outside of the uncertainty bounds established based on instrumental precision and measurement error from the trajectory model.

The problem of determining what constitutes a local pollution event is not trivial and is inevitably subjective. We have chosen as our criteria to reject any observations higher than 100 ppt, 30 ppt, and 40 ppt for tetrachloroethene, trichloroethene, and trichloromethane which are part of a pollution event lasting less than 6 hours. If one considers regional emissions capable of creating an air mass with several hundred ppt of tetrachloroethene which then is subject to dispersive processes resulting in a 100 ppt or greater measurement in the observed sample, then one would expect to see somewhat lower but still elevated mole fractions prior to or subsequent to that high measurement on time scales consistent with regional transport. If you have three or four measurements in a row which are very

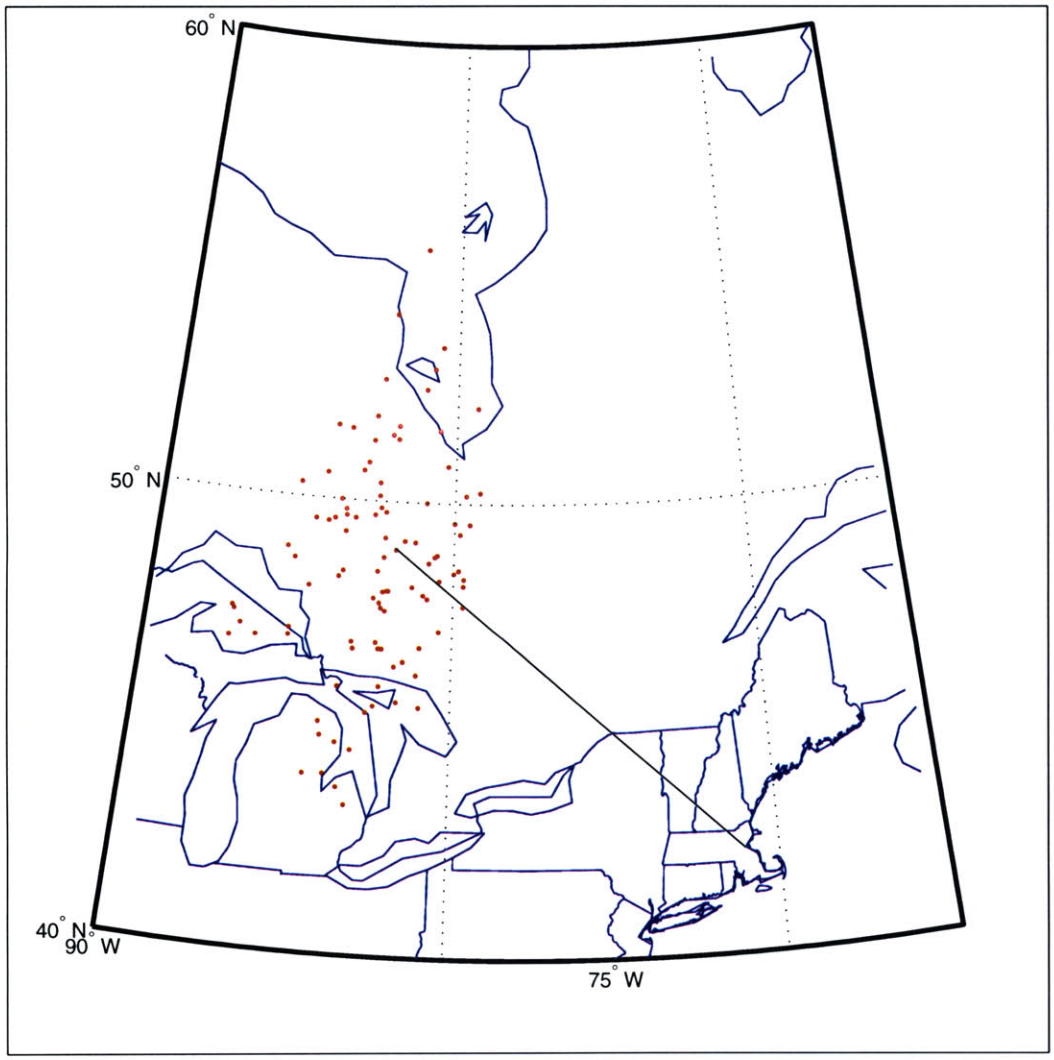

Figure 13. Straight line backtrajectory with the startpoints of 100 pseudo-trajectories normally distributed about the central startpoint corresponding to 15% relative trajectory error.

high and then concentrations drop rapidly to background levels, this indicates that a very local source is most likely responsible for the high values. Appendix B shows all data considered to be part of a local pollution event plotted in red to indicate that these data were not included in the Kalman filter runs used to estimate emissions corrections factors. Only a small fraction of the total data are polluted in this sense.

It seems likely that some high values observed directly before or directly after a pollution event may be the result of the same pollution source and may perhaps be improperly leading the filter away from the true correction factor. We consider it more cautious to reject only those data which could not, based on physical arguments, have been due to regional scale pollution. Thus we have kept all other measurements in the analysis.

In reality, at the scale of individual buildings and factories the temporal release of these chemicals are not completely uniform, but rather quite random as various industrial processes require. These variations in release time will be reflected in the observations (albeit in a diluted manner), and our model will not be able to simulate these events accurately. In addition spatial and temporal averaging errors result from the $1°\times1°$ spatial resolution underlying our model and the assumption that the emissions are constant in time. For regional emissions sources and synoptic timescales, this assumption of temporal invariance is adequate.

Chapter 4: Emissions Estimates and Discussion

In the observational program, 588 measurements of tri- and tetrachloroethene were obtained during the spring, and 289, 1,086, and 434 measurements of trichloroethene, tetrachloroethene, and trichloromethane were obtained respectively during the summer, fall and winter at times when a coincident backtrajectory could be calculated. Using only those measurements for each chemical species above the detection limits (See Chapter 2, Table 6) for which we had an associated backtrajectory, we were able to produce emissions estimates for each season using the Kalman filter.

Tetrachloroethene

For each species, we use the Kalman filter to provide successive estimates of α using each of the trajectories that had passed through a particular grid cell within the domain of our study region (30-60N, 60-90W) and the corresponding measurement of ambient mole fraction associated with each trajectory. It is assumed that each trajectory is confined to the mixed layer ($z \leq h$) and that emissions are well mixed in this layer. The results of the first iteration of the tetrachloroethene run for the grid cell containing Montreal, Canada are shown in Figure 14. You can see that our initial estimate of the correction factor (1.0) is very quickly revised upward based on the trajectories and associated measurements

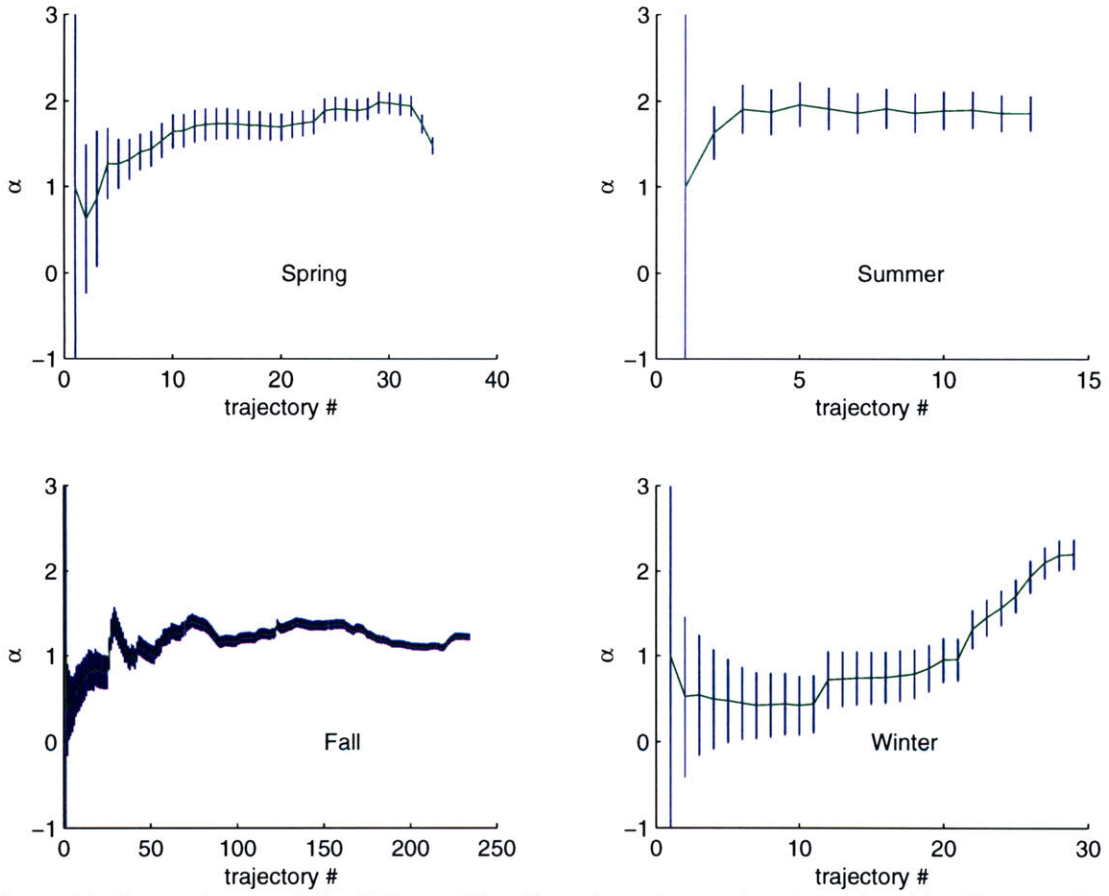

Figure 14. Seasonal runs of the Kalman filter for trajectories passing through grid cell centered at 45.5N, 73.5W (Montreal).

from spring and summer. While the early fall and early winter data tend to reduce the Montreal emissions correction factor, later trajectories, in both seasons, cause this estimate to increase. The final result is that all four seasons suggest that after the first model iteration, the tetrachloroethene emissions from this grid cell need to be increased by a factor of 1.2 to 2.1 depending on season. We can compare this to the results shown in Figure 15 which are from the same model runs, but for the grid cell containing central Vermont. This grid cell is passed through by many of the same trajectories that passed through the Montreal area, but also was passed through by several other trajectories that did not pass through the grid cell containing Montreal. The results show that on average, the emissions inventories need less adjustment for this grid cell.

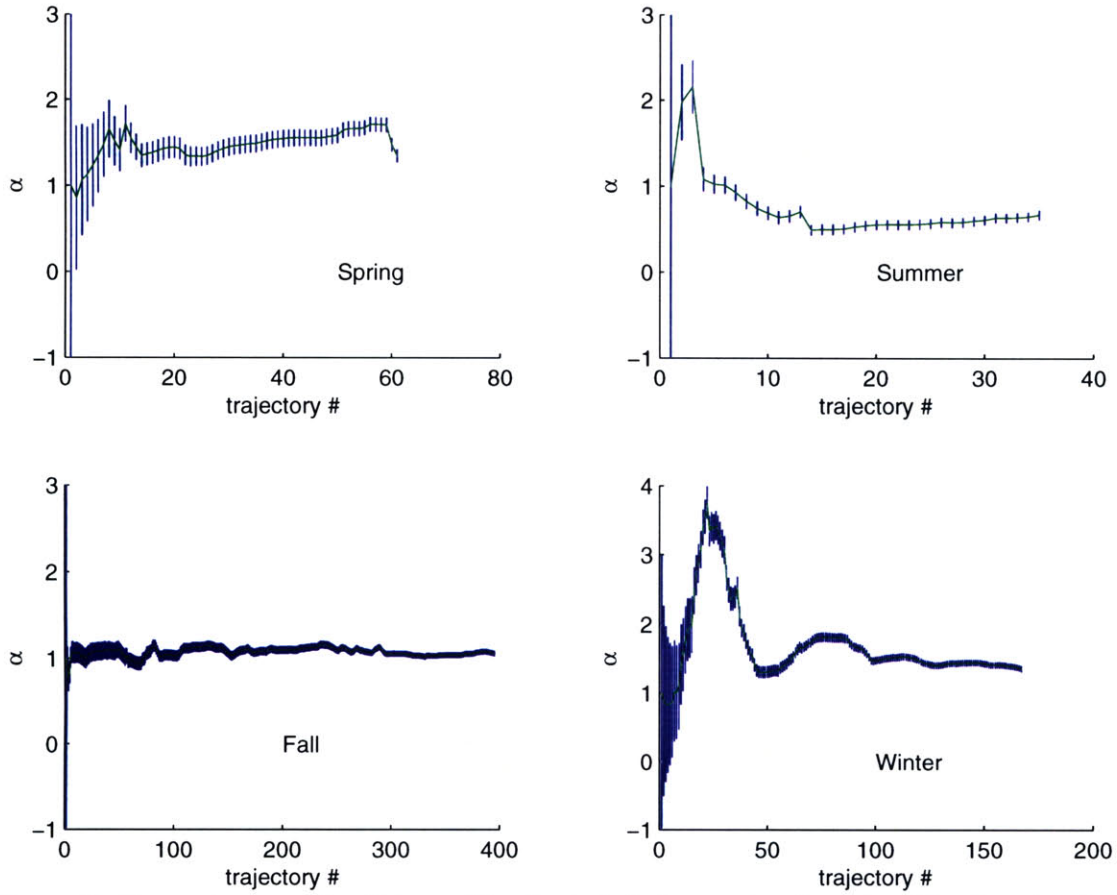

Figure 15. Seasonal runs of the Kalman filter for trajectories passing through grid cell centered at 43.5N, 72.5W (central Vermont).

The fact that Montreal's emissions need to be increased is likely to have an effect on the correction factor that we have just calculated for central Vermont, perhaps resulting in a different correction factor for that grid cell. Had the emissions for Montreal been twice as high when the filter was run for central Vermont, those trajectories in either run which passed through both grid cells would not have produced estimates quite as far off from the observations, and thus the correction factor calculated for each grid cell would have been reduced. In fact, the new emissions estimates for each grid cell have a direct effect on the z^{est} and hence α estimate for every other grid cell connected by even a single trajectory. In

addition, the convergence term, C, when recalculated using the updated emissions, will affect z^{est} and hence α.Thus we must iterate the above procedures using the corrected emissions estimates as the input to the next iteration. Figure 16 shows the results of the Kalman filter run for the Montreal grid cell on the 10th iteration. One can see that given a corrected emissions inventory, the filter now calculates a correction factor close to 1.0 for each season (relative to the emissions resulting from the previous iteration) indicating the solution converges.

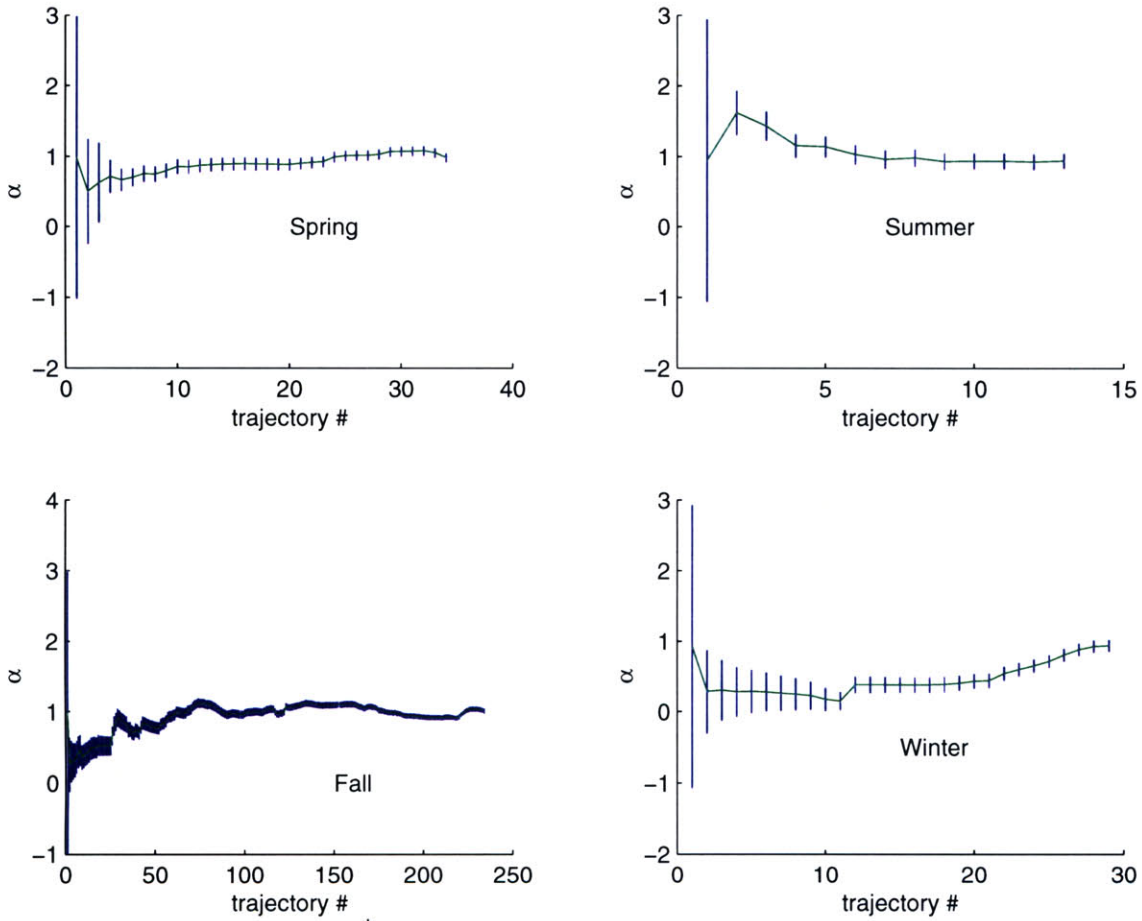

Figure16. Seasonal runs of the 10th iteration of the Kalman filter for trajectories passing through grid cell centered at 45.5N, 73.5W (Montreal).

As was noted earlier, if σ_z^2 encompassed all errors including model errors, then any particular estimate during a run of the Kalman filter should lie within the uncertainty range of all previous estimates from that run. Clearly this is not the case for these runs of the filter (e.g. see Figure 14), and one is reminded that only part of the model error (that dealing with error in the trajectory model) is accounted for in σ_z^2. Variation of the emissions over time and unusually inaccurate trajectories (e.g. due to strong unresolved vertical motions) are most likely responsible for the sudden changes in the estimates of α. The removal of the local pollution events has significantly improved the situation, (See Figure 17 for a comparison of Kalman filter runs with and without local pollution events included).

This above iterative process is carried out for each 1°×1° grid cell between 30°-60°N latitude and 60°-90° W longitude which had at least 10 trajectories pass through it during a given season. Figures 18-21 show maps of the resulting cumulative correction factors (i.e. the product of the correction factors for each of 10 iterations) for tetrachloroethene emissions during Spring, Summer, Fall, and Winter respectively. When these factors are applied to the original tetrachloroethene emissions distribution shown in Figure 8, the seasonal distributions that result are shown in Figures 22-25.

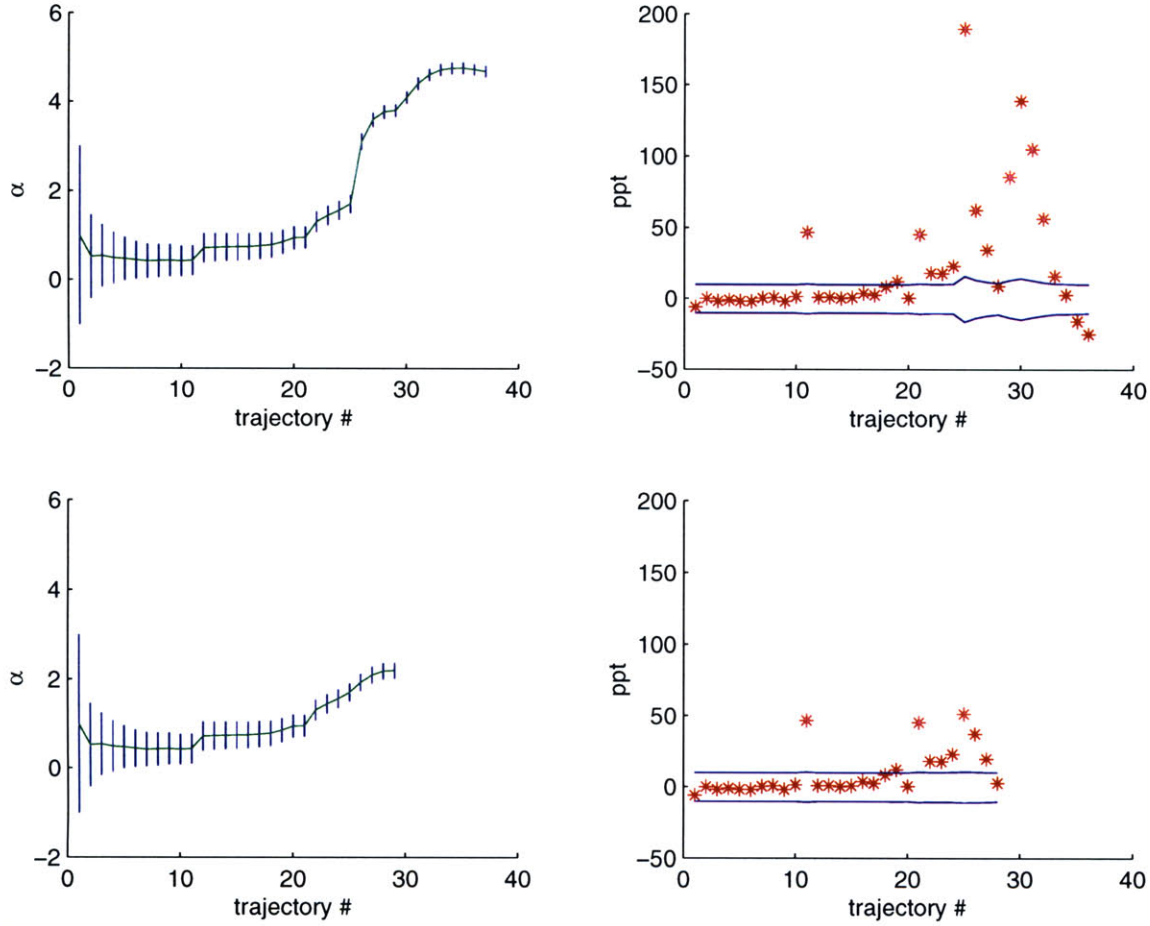

Figure 17. (a) Kalman filter estimates of emissions correction factor for the grid cell centered on Montreal, Canada during Winter based on all measurements. (b) model residual for the data plotted in (a). (c) Kalman filter estimates of emissions correction factor for the grid cell centered on Montreal during Winter after rejecting measurements associated with local pollution events. (d) model residual for the data plotted in (c). Blue error bars in (b) and (d) represent the combined uncertainty due to measurement precision and estimated trajectory model error.

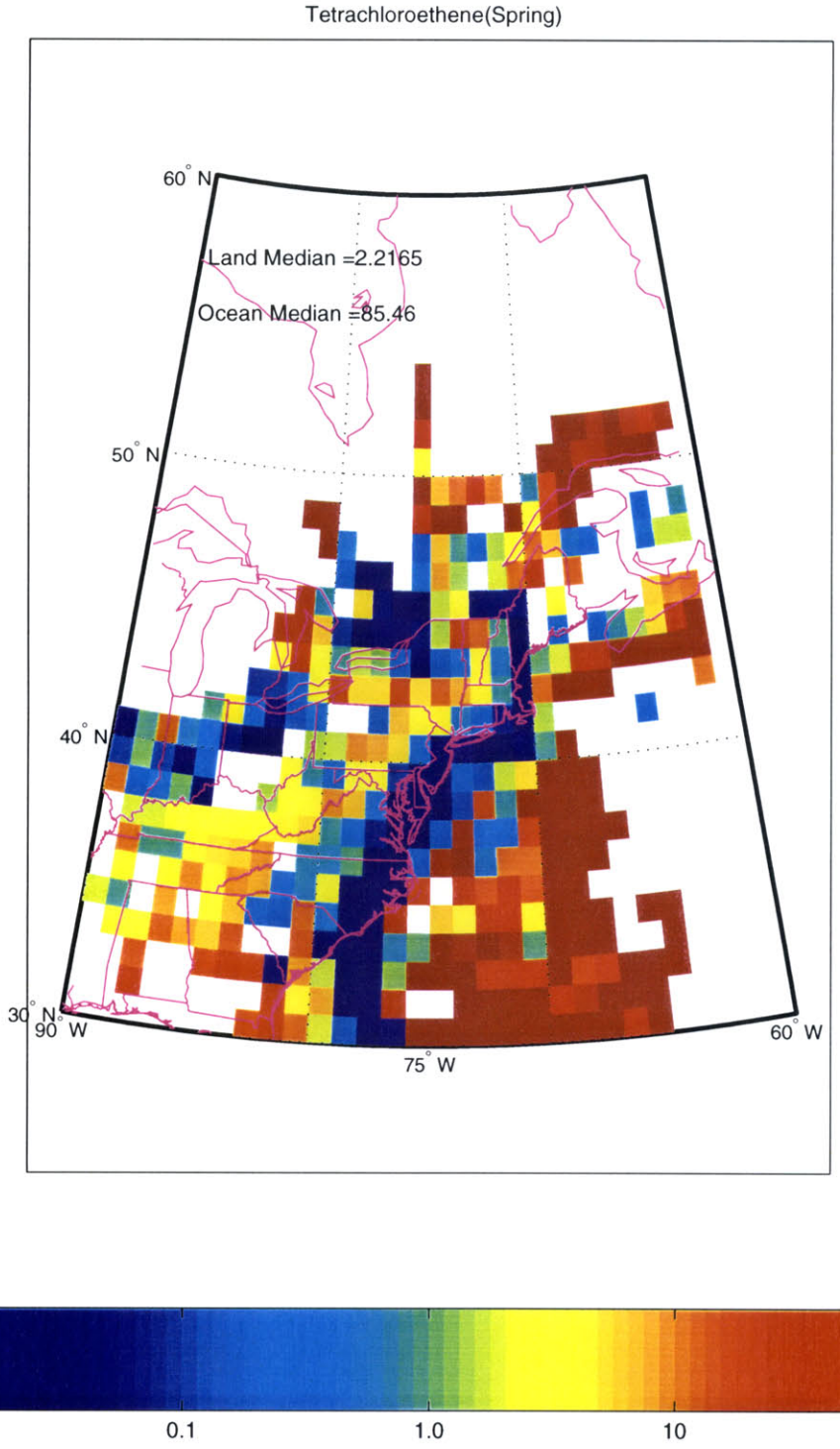

Figure 18. Tetrachloroethene emissions correction factors for each grid cell within the domain (30-60N, 60-90W) which had at least 10 trajectories with corresponding observations pass through during Spring, 1998 (March - May).

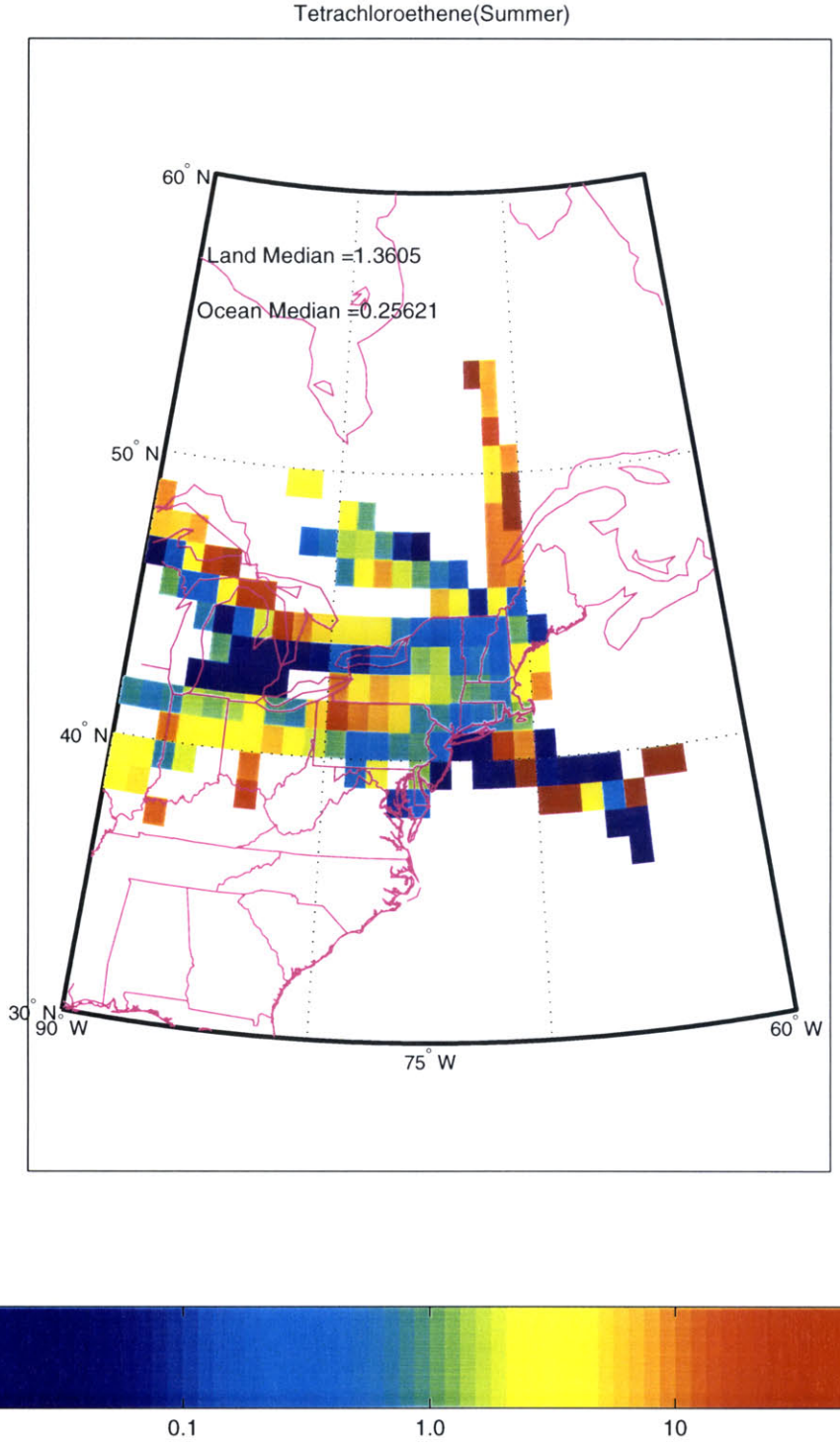

Figure 19. Tetrachloroethene emissions correction factors for each grid cell within the domain (30-60N, 60-90W) which had at least 10 trajectories with corresponding observations pass through during Summer, 1998 (July or August).

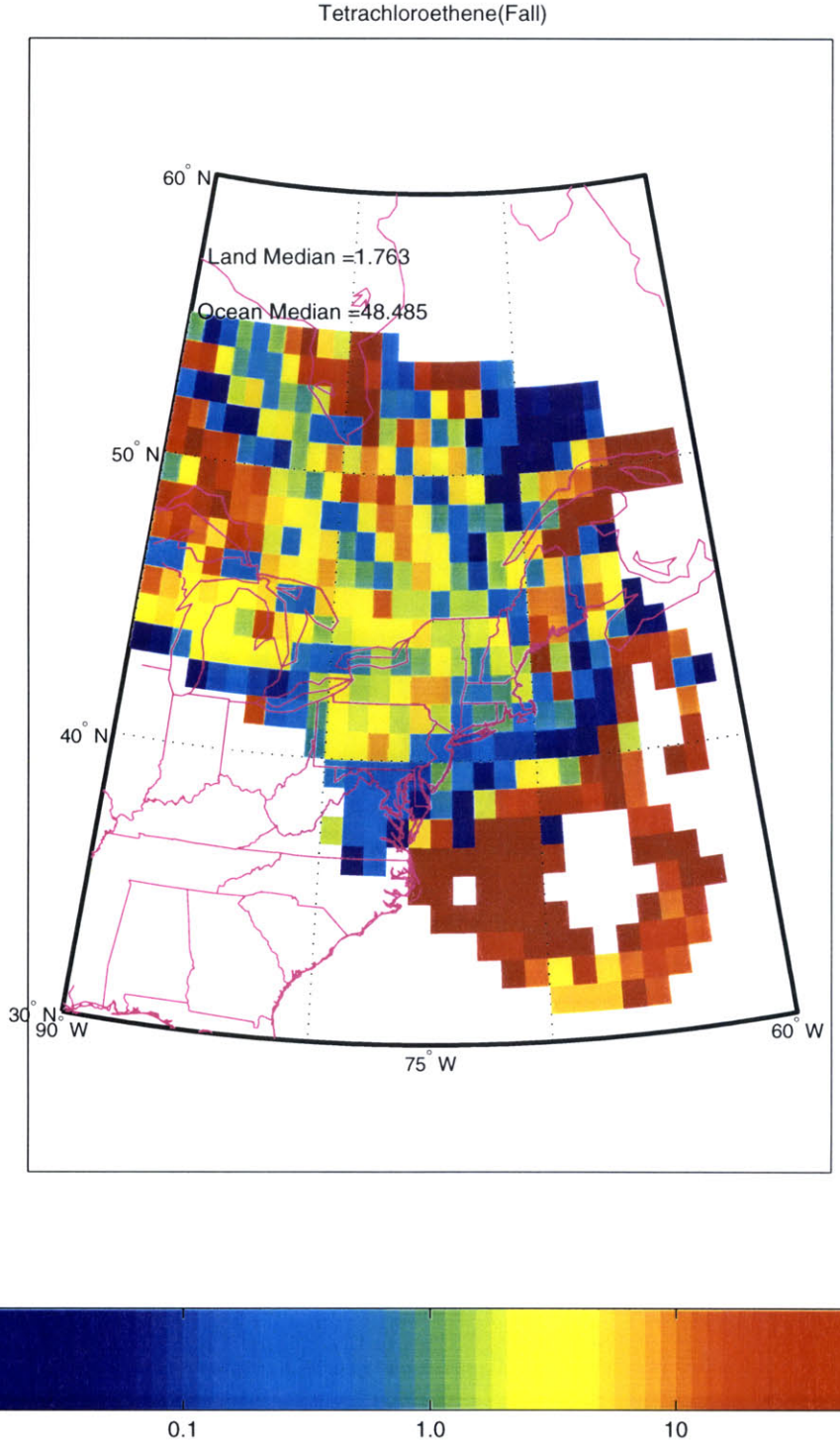

Figure 20. Tetrachloroethene emissions correction factors for each grid cell within the domain (30-60N, 60-90W) which had at least 10 trajectories with corresponding observations pass through them during Fall, 1998 (September-November).

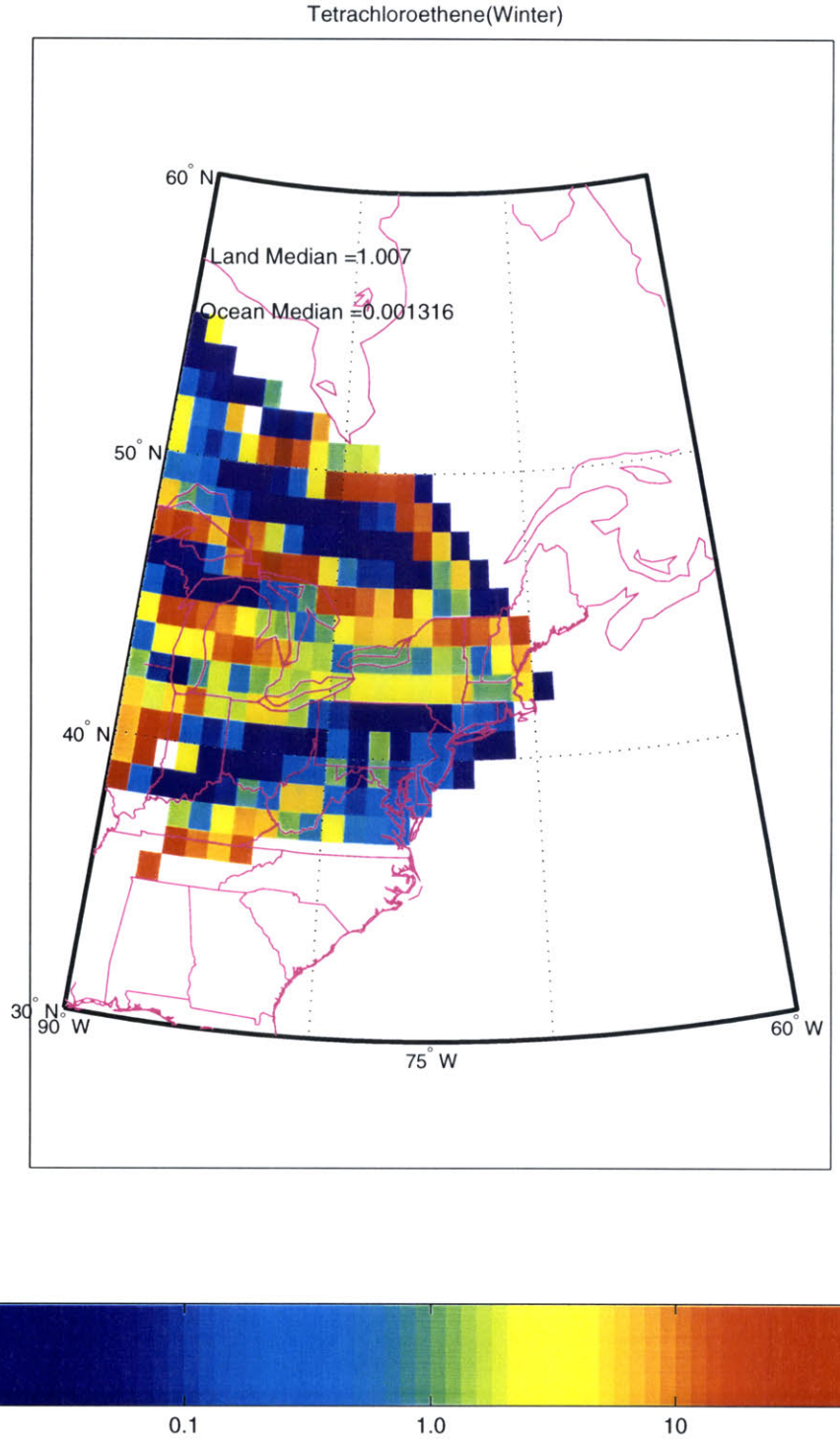

Figure 21. Tetrachloroethene emissions correction factors for each grid cell within the domain (30-60N, 60-90W) which had at least 10 trajectories with corresponding observations pass through them during Winter, 1998-99 (December-January).

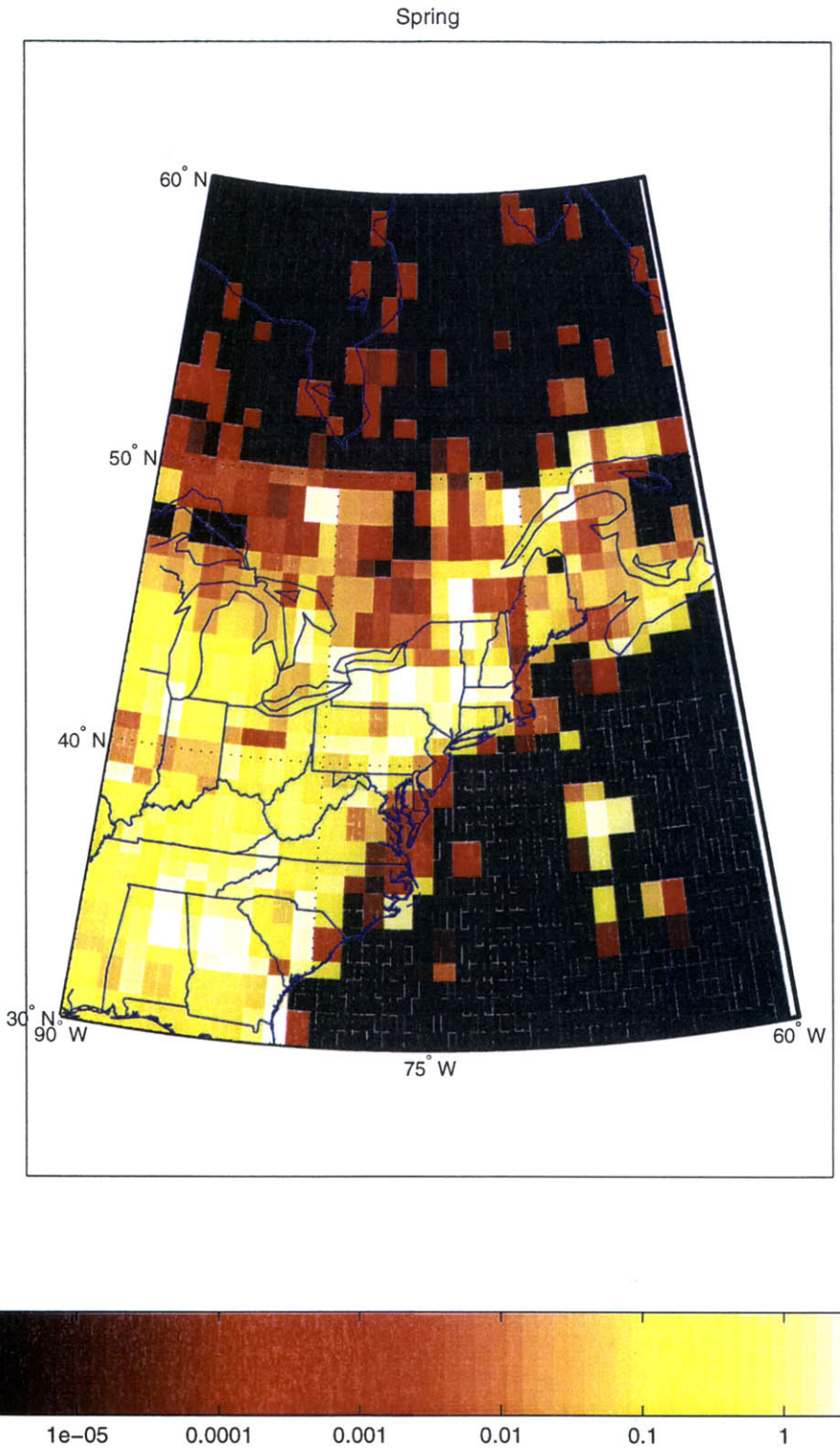

Figure 22. Distribution of Springtime tetrachloroethene emissions based on corrections to the Reactive Chlorine Emissions Inventory estimates shown in Figure 8. Units are ppt/hr as described in the caption for Figure 8. If fewer than 10 trajectories passed over a grid cell, no correction was calculated and the RCEI estimate was left unchanged.

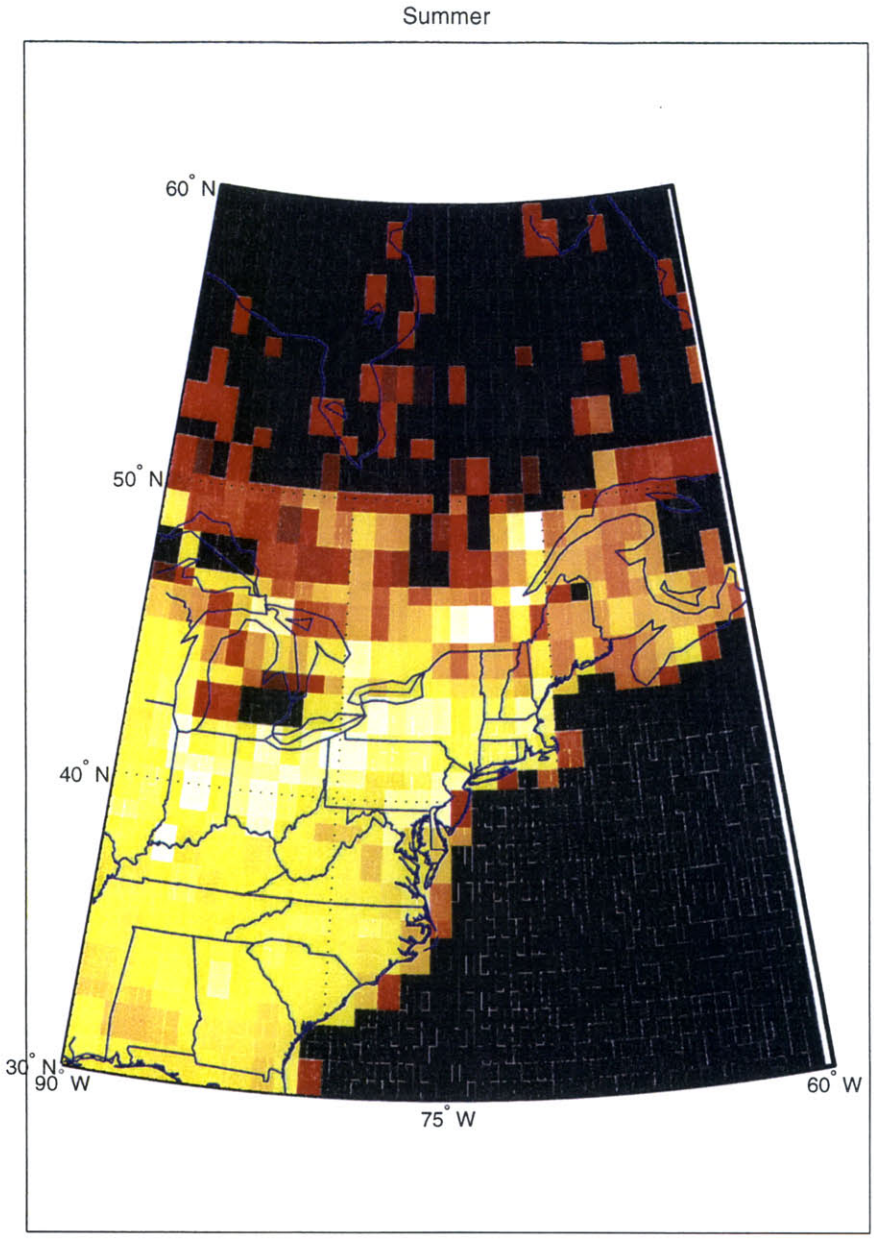

Figure 23. Distribution of Summer tetrachloroethene emissions based on corrections to the Reactive Chlorine Emissions Inventory estimates shown in Figure 8. Units are ppt/hr as described in the caption for Figure 8. If fewer than 10 trajectories passed over a grid cell, no correction was calculated and the RCEI estimate was left unchanged.

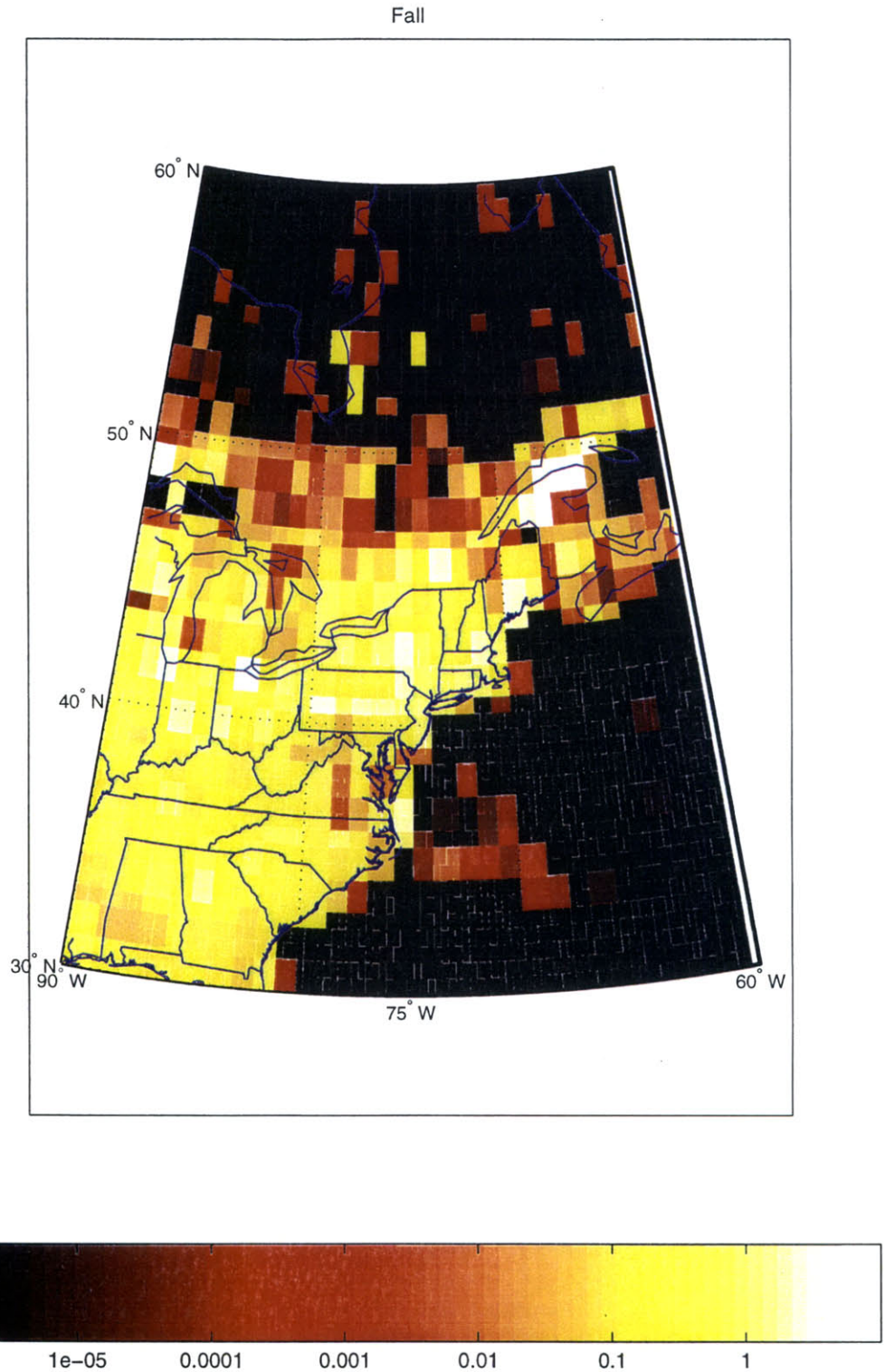

Figure 24. Distribution of Fall tetrachloroethene emissions based on corrections to the Reactive Chlorine Emissions Inventory estimates shown in Figure 8. Units are ppt/hr as described in the caption for Figure 8. If fewer than 10 trajectories passed over a grid cell, no correction was calculated and the RCEI estimate was left unchanged.

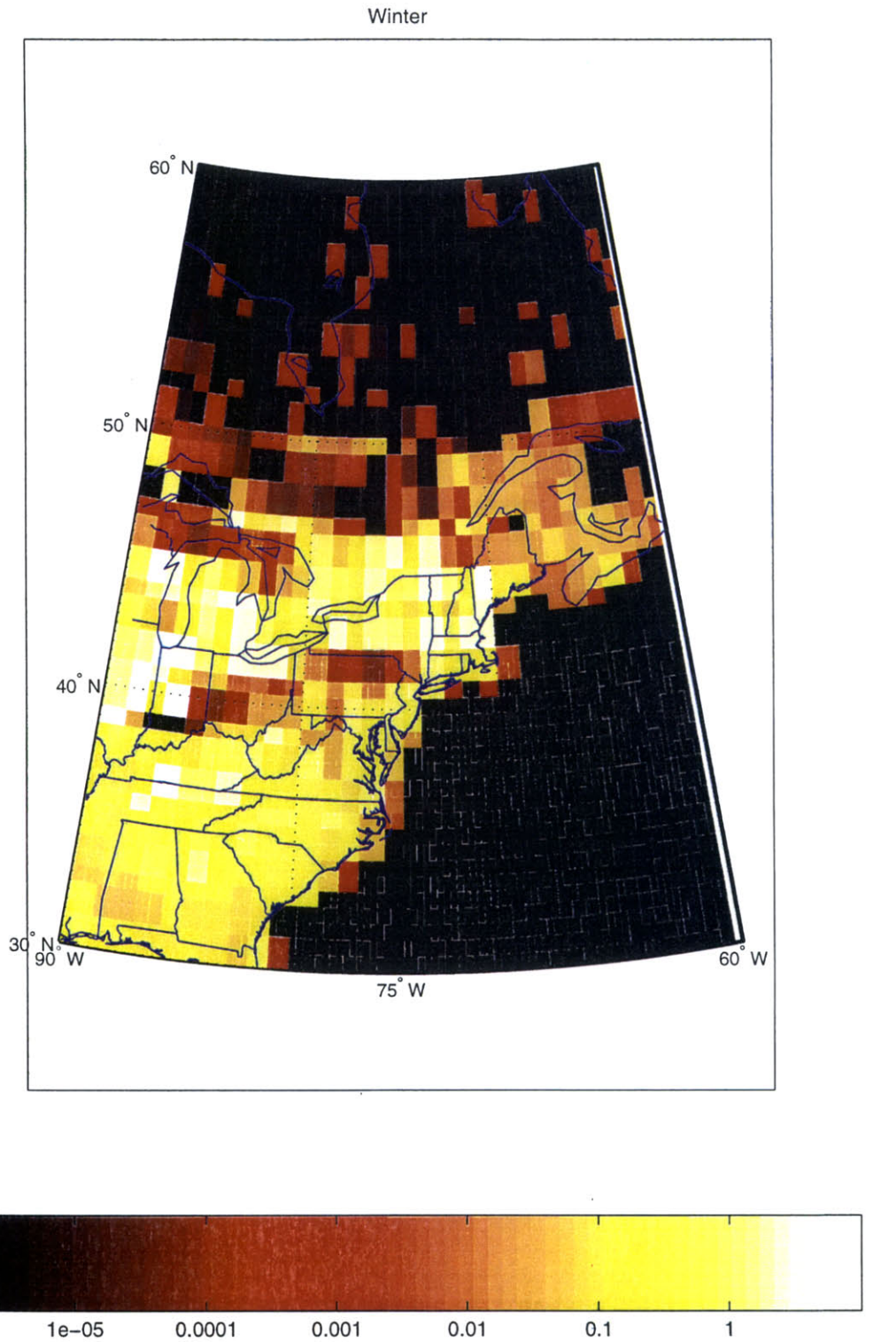

Figure 25. Distribution of Winter tetrachloroethene emissions based on corrections to the Reactive Chlorine Emissions Inventory estimates shown in Figure 8. Units are ppt/hr as described in the caption for Figure 8. If fewer than 10 trajectories passed over a grid cell, no correction was calculated and the RCEI estimate was left unchanged.

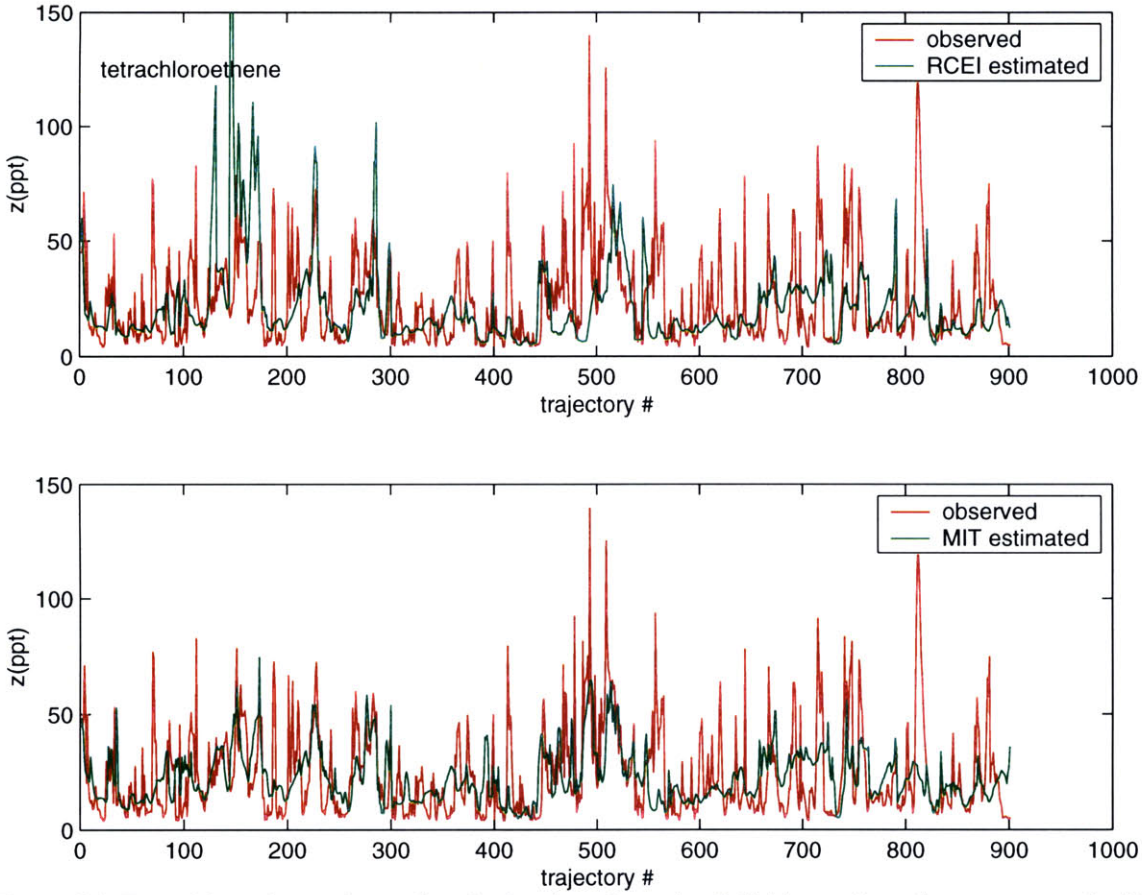

Figure 26. Tetrachloroethene observed mole fractions from the Fall (shown in red) are compared with estimated values (shown in green) calculated using trajectories associated with each observation and the emissions from RCEI (upper graph) and from the procedures used in this thesis (lower graph). Statistics for these curves (mean and standard deviations) are presented in Table 8.

In theory, the emissions distributions shown in Figures 22-25 are the set that minimizes the model residual in a least squares sense. We can check this qualitatively by examining the observations along with their estimated values based on the emissions inventory provided by RCEI and on our new emissions distributions computed here. These curves are plotted for tetrachloroethene in Figure 26. Clearly the new distribution is better able to simulate the observations, for example between trajectory 125 and 175 and between trajectory 450 and 525. We also note better agreement overall as shown in the statistical analysis of the residuals (z^{obs} -z^{est}) derived from these curves, as well as those for other seasons, shown in Table 8. The mean residual is brought closer to zero (perfect agreement on average) for all 4 seasons indicating that beneficial changes have resulted in the emissions inventory from the filtering process.

Additional information regarding the success of this estimation technique can be found in characteristics of the distributions themselves. For example, if one pays attention to the oceanic grid cells in Figure 20, we see that the filter is estimating the emissions correction factor to be greater than 100 over the oceans. In fact, while not evident on this scale,

several of these factors are estimated at ~10^7. The original RCEI-based distribution had near zero oceanic emissions, however, and thus the resulting emissions distribution obtained by multiplying by correction factors of 10^7 still show near zero oceanic emissions. In practice we set the emissions for each assumed non-emitting grid cell equal to 10^{-10} ppt/hr rather than to zero. In this way, we allow a grid cell that may have been estimated at zero emissions to grow if the observations indicate that they should. We see that the resulting tetrachloroethene Fall emissions distribution in Figure 24 shows small oceanic emissions of the order 10^{-3} ppt/hr. This level of emissions is consistent with estimates of a small oceanic source of tetrachloroethene at ~5% of the global budget (Keene et al., 1999). This consistency provides a qualitative endorsement of our estimation procedure.

Table 8. - Statistics of Model Residuals: RCEI vs. MIT(est)

Tetrachloroethene (ppt)	Mean Residual (z^{obs}-z^{RCEI})	Standard Deviation	Mean Residual (z^{obs}-z^{est})	Standard Deviation
Spring	4.4	25.4	1.6	15.0
Summer	-4.2	28.5	0.4	19.1
Fall	2.4	24.0	1.4	18.6
Winter	5.7	34.5	-0.8	25.2

This consistency is in contrast, however, to the somewhat larger oceanic emissions estimated for tetrachloroethene in the spring. In Figure 22, we notice high emissions out in the oceans and very low emissions along the east coast. To understand these results we must examine Figure 27, which shows the first of the ten filter iterations and corresponding residuals for the grid cell out in the ocean centered at 37.5N and 67.5W. The 15 trajectories which were used by the filter to produce Figure 27 all come from three synoptic events. All trajectories are similar in nature, and a representative trajectory is shown in Figure 28. These steady winds out of the southeast had mole fractions which were consistently underestimated by the model. This is not surprising since most of these trajectories' time is spent over open ocean with negligible emissions. The resulting correction factor from the first iteration should properly attempt to increase the emissions from this grid cell as well as all others that this set of trajectories pass through. In this case, that includes the grid cell centered at 41.5N, 70.5W (Cape Cod). If the Cape Cod emissions had been increased by the same factor of 4 that the model produced for the grid cell in the ocean, then on the next iteration, the same trajectories would no longer produce an underestimated mole fraction, and subsequent correction factors for this grid cell would be of the order 1.0 and the oceanic emissions would remain negligible as other oceanic grid cells do.

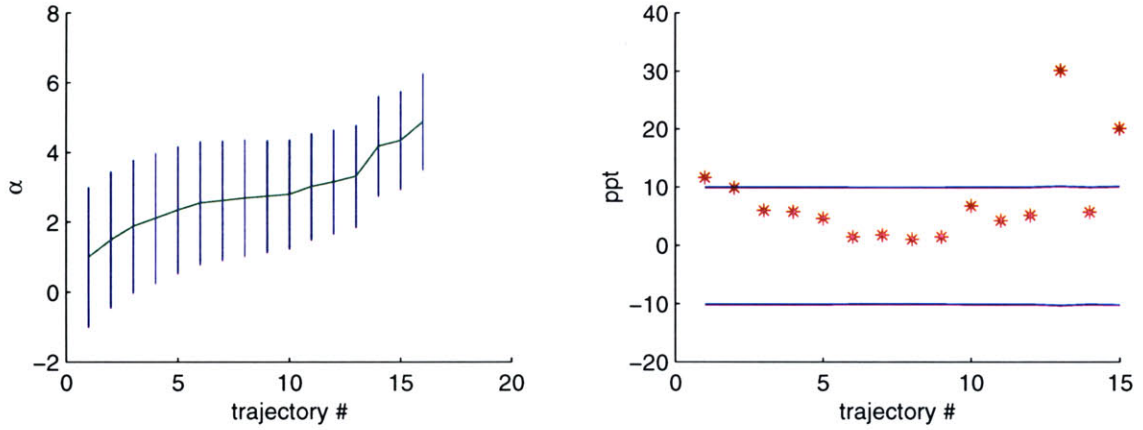

Figure 27. (a) Kalman filter estimates of emissions correction factor for the grid cell centered at 37.5N, 67.5W during Spring. (b) model residual for the data plotted in (a).

To understand where the estimation method went wrong, we must look at the Kalman filter run from the grid cell centered on Cape Cod. Figure 29 shows the first filter run and residuals for this grid cell during Spring. It is apparent that this grid cell had significantly more trajectories pass over it than our oceanic grid cell. Of the 120 trajectories that passed over it, 9 are among the trajectories that also passed over the oceanic grid cell centered at 37.5N, 67.5W. While these 9 trajectories do result in underestimated mole fractions (tending to move the filter estimate of α upwards) we see that the majority of the remaining 111 trajectories tend to bring the filter estimates of α down. Specifically the 100-110th trajectories tend to bring the filter estimate down dramatically. With the Kalman filter estimating a lowering of the emissions from the Cape Cod grid cell on subsequent iterations, the estimation method had no choice for the oceanic grid cell at 37.5N, 67.5W but to raise its estimated emissions such that the integrated emissions from the 15 trajectories which crossed it matched the observations, in a process which is repeated on all subsequent iterations.

The 100-110th trajectories to cross Cape Cod in the Spring were from a single synoptic event which occurred on May 8th and 9th GMT. A trajectory from this time period is shown in Figure 30. This trajectory spent significant time over the Cape Cod area and thus the model would have estimated a significant accumulation of trichloroethene by the time the air mass was measured in Nahant. The observations (shown in Appendix B) indicate that no such accumulation took place. The reasons for this are not entirely clear, but at least two possible explanations are presented. First, we note the first half of May was marked by several severe rain storms bringing consistently clean marine air to the Boston area. This may have played a role in preventing an accumulation of tetrachloroethene which would have occurred during drier times. Secondly, we note that the trajectory in Figure 30 is marked by significant vertical shear and that as noted earlier HYSPLIT errors can be significantly greater during high vertical shear conditions. The air mass that was measured may have spent less time over Cape Cod, or been diluted by vertical convective mixing, or come from farther east and not passed over the same regions that the model had assumed.

This example demonstrates two hurdles to be overcome in the future to significantly improve the accuracy of this technique for estimating regional emissions. Despite the removal of trajectories that are likely to have been influenced by local pollution events, many trajectories remain that are subject to either high vertical shear or significant horizontal dispersion. Both of these conditions are ill suited to producing accurate Lagrangian trajectories consistent with our estimates of trajectory error. The trajectory error (which was included with our measurement error) was estimated for straightline trajectories with 15% relative trajectory error, and is not appropriate for some of these trajectories which may have significantly higher error. A realistic weighting scheme would substantially improve the accuracy of the emissions estimates by reducing the importance of trajectories that are likely to have higher uncertainty than that which is accounted for in

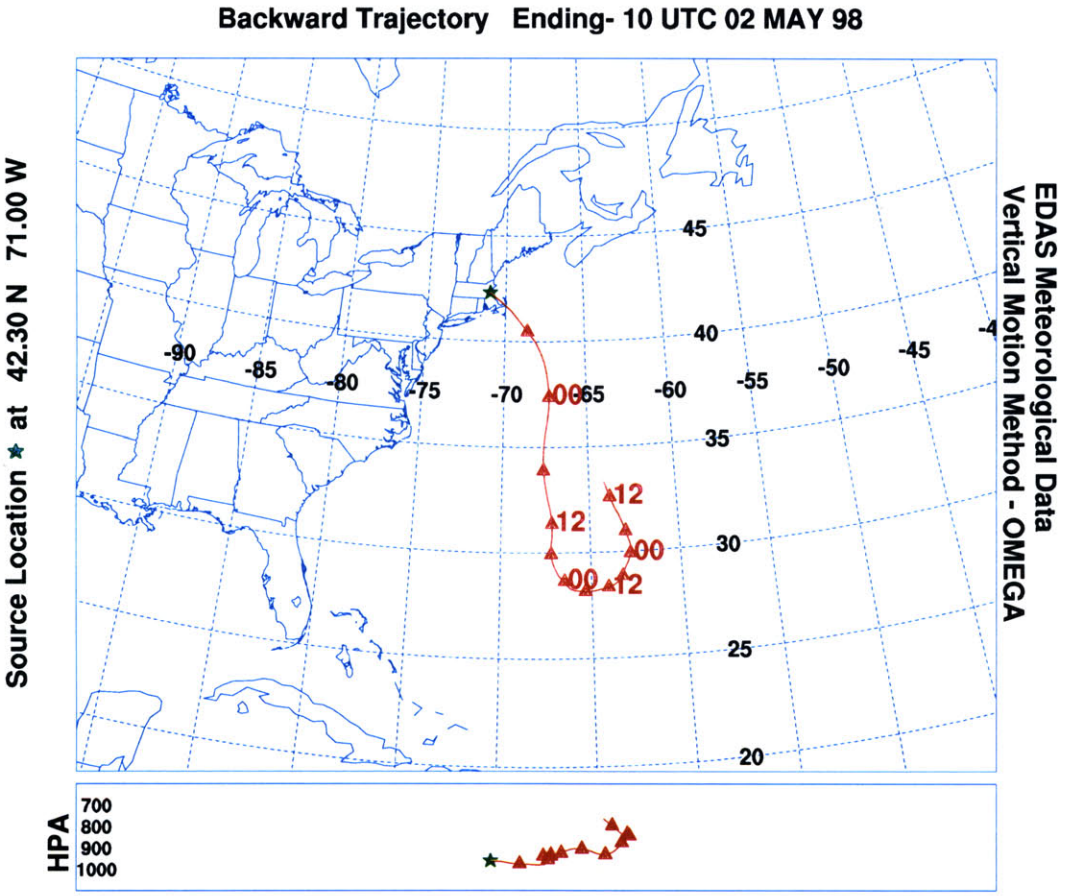

Figure 28. HYSPLIT generated backtrajectory originating in Boston on May 02,1998 10:00 GMT.

our filter equations. In addition we saw that the emissions estimates for the oceanic grid cell at 37.5N, 67.5W are heavily influenced by estimates of Cape Cod emissions. The fact that we are not producing independent emissions estimates for each grid cell requires that we have enough measurements for each region, such that no one region can unduly influence another. Thus estimates from the Fall, when we obtained substantially more measurements than during other season, are likely to be most accurate.

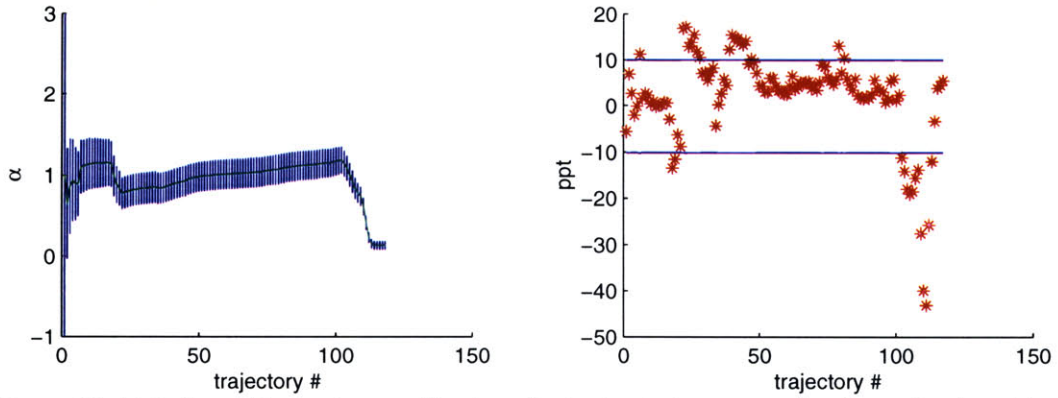

Figure 29. (a) Kalman filter estimates (first iteration) of emissions correction factor for the grid cell centered over Cape Cod during Spring. (b) model residual for the data plotted in (a).

Trichloroethene

Our use of the Kalman filter for trichloroethene was very similar to that of tetrachloroethene. Both solvents have similar uses in industry and similar RCEI distribution patterns as shown earlier in Figure 7 and 8. With a significantly shorter atmospheric residence time, background levels of trichloroethene are much lower than tetrachloroethene, and thus we consistently measured lower mole fractions for this compound (See Appendix B). To accommodate this difference we have lowered the value

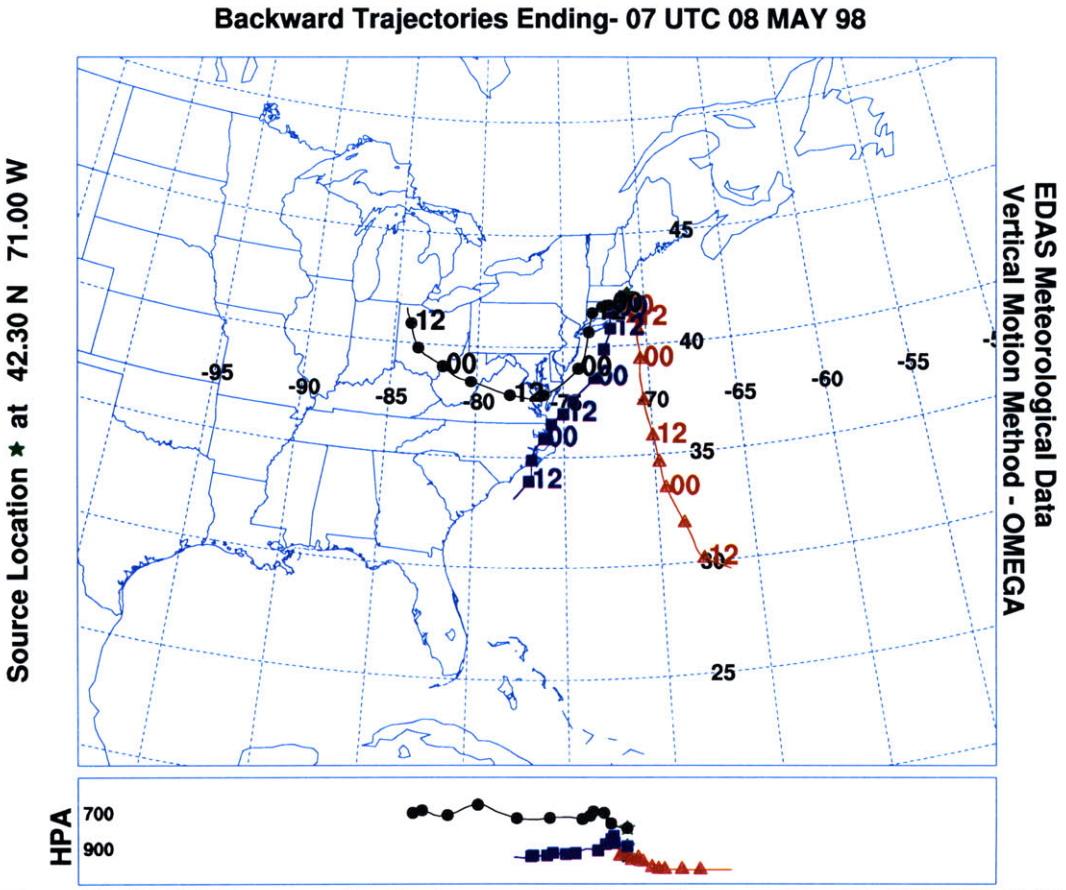

Figure 30. HYSPLIT generated backtrajectory originating in Boston on May 08, 1998 7:00 GMT.

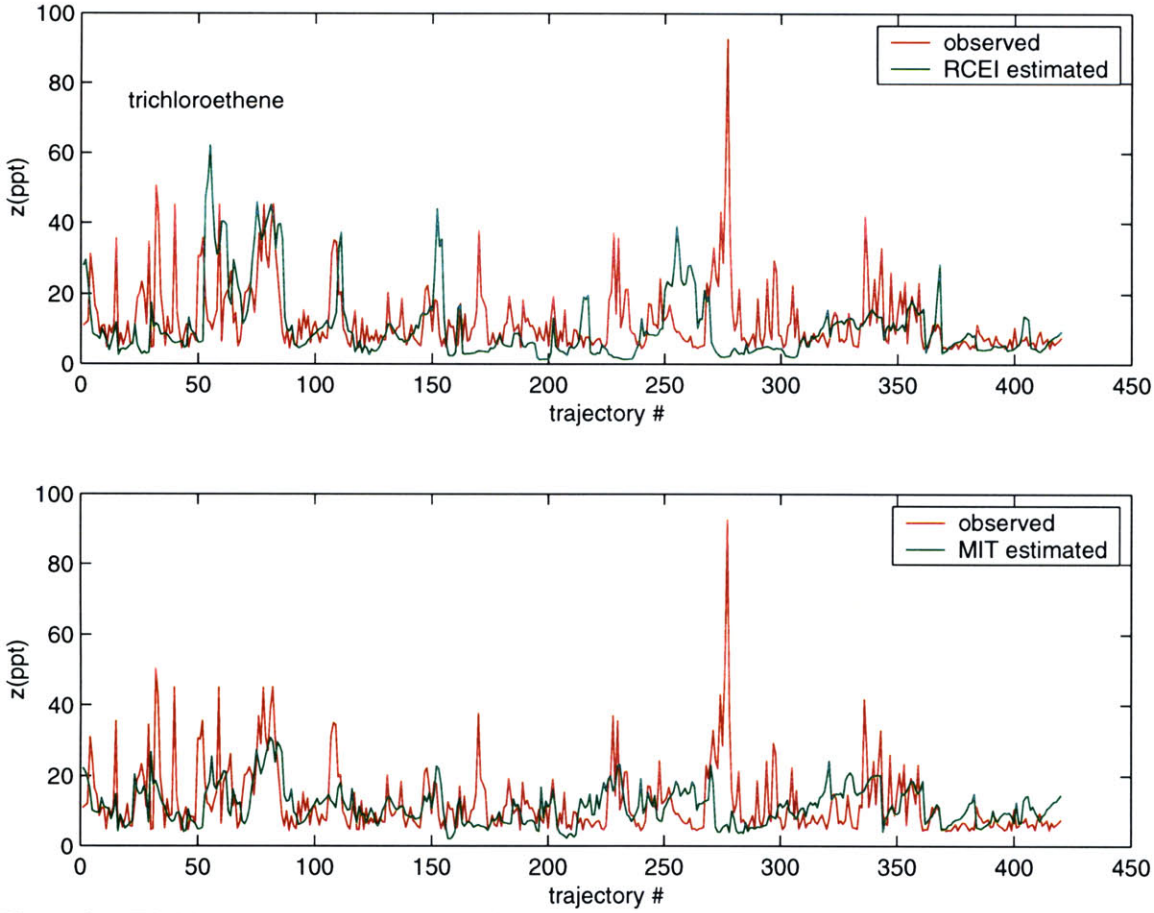

Figure 31. Trichloroethene observed mole fractions from the Fall (shown in red) are compared with estimated values (shown in green) calculated using trajectories associated with each observation and the emissions from RCEI (upper graph) and from the procedures used in this thesis (lower graph). Statistics for these curves (mean and standard deviations) are presented in Table 9.

of the assumed boundary value $\chi(0,0)$ (which is needed to compute z in the measurement equation (3.3)) for each trajectory by 3ppt relative to the tetrachloroethene values. Thus the variation of $\chi(0,0)$ with angle from the observing site remains the same, just at a lower value as shown earlier in Figure 6.

Figure 31 shows the model estimated mole fractions for the Fall based on both RCEI and our emissions inventories and the observations for comparison. As was the case for tetrachloroethene we see a significant decrease in the magnitude of the model residual in all four seasons. A summary of the residual statistics for each season is shown in Table 9. The emissions correction factors and resulting estimated emissions from the Kalman filter runs of trichloroethene for each season are shown at the end of this section in Figures 32-35 and 36-39 respectively. The new trichloroethene distributions shown in Figures 36-39 produce better agreement with observations relative to the original RCEI inventory shown in Figure 7.

Using our standard assumption of a 1500 meter mixed layer height, the RCEI estimate of trichloroethene emissions are consistently overestimated in the Great Lakes/upper mid-west region and along the Atlantic coast, resulting in emissions correction factors of 10^{-1}

to 10^{-2} in these areas. Also noticeable during fall and winter, when winds frequently came from the northwest, is that central Canadian emissions are underestimated. We do not expect natural sources of trichloroethene over land, although there may be some small oceanic source of this compound, similar to tetrachloroethene.

Table 9. - Statistics of Model Residual: RCEI vs. MIT(est)

Trichloroethene (ppt)	Mean Residual (z^{obs}-z^{RCEI})	Standard Deviation	Mean Residual (z^{obs}-z^{est})	Standard Deviation
Spring	5.6	12.5	1.1	9.4
Summer	-4.2	14.5	0.5	7.6
Fall	2.0	12.6	1.2	10.0
Winter	1.1	12.4	-.6	8.7

The same factors which affect the uncertainty of emissions estimates which were discussed above in the case of tetrachloroethene apply also to trichloroethene (as well as to trichloromethane discussed next) so the discussion is not repeated here, except to point out once again that some individual grid cells have incurred significant error due to the equal weighting of trajectories and the interdependence of emissions estimates for neighboring grid cells.

Trichloromethane

Trichloromethane has notable differences from tri- and tetrachloroethene in its emissions patterns and its behavior. This chemical has significant uses in the paper and pulp manufacturing industry as well as in the water and sewerage treatment process (Aucott, 1999). This compound also has significant anthropogenic emissions due to biomass burning (Lobert, 1999) and large natural sources which are not well understood (Khalil et al., 1999; Keene et al., 1999). The distribution of the natural sources is poorly known since observations are severely limited in their temporal and spatial coverage. Available estimates suggest that natural emissions, particularly from the oceans and soils, represent over 88% of the total trichloromethane emissions. However, with no clear means by which the emissions can be spatially distributed, this contribution has not been included in the initial emissions estimate we use for this work (See Figure 9). The estimated 64 Gg/year emissions of reactive chlorine in the form of trichloromethane resulting from industrial processes and biomass burning has been spatially distributed and serves as the basis for our initial estimate. We therefore expect to see large emissions correction factors (with a median ~$O(10)$ and largest values over the ocean and remote land areas) resulting from our runs of the Kalman filter if the speculation about large natural trichloromethane emissions is correct.

Given trichloromethane's long lifetime relative to the other compounds considered here, the background level observed is significantly higher with mole fractions rarely measured below 15 ppt. Thus background levels for this compound are set at the boundary to be 7-14 ppt as shown in Figure 6. Although this compound has significant continental and oceanic sources, we still expect the boundary level to be somewhat higher over continental regions.

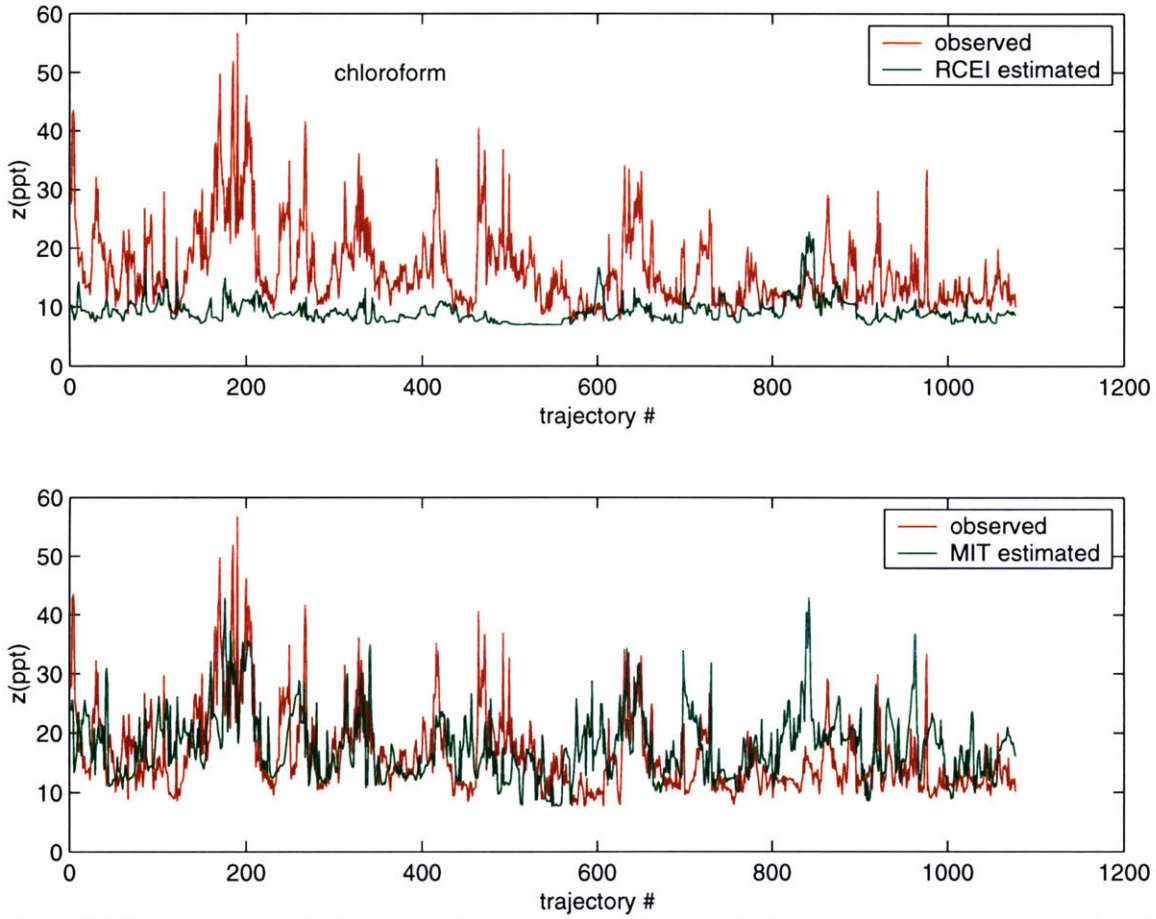

Figure 40. Observed mole fractions for trichloromethane from the Fall (shown in red) are compared with estimated values (shown in green) calculated using trajectories associated with each observation and the emissions from RCEI (upper graph) and from the procedures used in this thesis (lower graph). Statistics for these curves (mean and standard deviations) are presented in Table 10

We note that there is a possibility, as was pointed out in Chapter 2, that another peak may co-elute with the trichloromethane peak on the analytical system used to obtain the measurements at the Nahant field site. To understand the effect of such a co-elution on the emissions estimates deduced following the methods described in this thesis, we have performed two separate runs of the Kalman filter for trichloromethane. First we incorporated the observed mole fractions from Appendix B as we measured them. We then compare those results to a similar run subtracting 5 ppt from each measured mole fraction to account for a possible co-elution of this magnitude. The results are similar and the uncertainty introduced is small (about 15%) relative to the significantly larger uncertainties associated with our final emissions correction factors, α. The results of both

these runs, as well as those of tri- and tetrachloroethene are found in Chapter 5 (Table 11).

As opposed to tri- and tetrachloroethene, the initial gridded RCEI trichloromethane inventory which we chose to start with (shown in Figure 9) was quite incomplete. Thus as expected, the comparison between observations and estimated mole fraction using RCEI emissions estimates is quite poor (Figure 40). Despite the poor initial (RCEI) emissions estimates, we see that using the Fall observations the Kalman filter has been able to adjust the emissions such that our new distributions give much better agreement significantly reducing the mean model residuals. Figure 40 shows the comparison of model estimated and observed mole fractions for the Fall using our Kalman filter estimates of emissions. Table 10 summarizes the statistics of the model residual for both the gridded subset of the RCEI emissions as well as the new Kalman filter derived emissions. Note that the improvement in the Kalman filter estimates compared to the RCEI estimates is evident largely in the mean residual and not the standard deviation.

Table 10. - Statistics of Model Residual: RCEI vs. MIT(est)

Trichloromethane (ppt)	Mean Residual (z^{obs}-z^{RCEI})	Standard Deviation	Mean Residual (z^{obs}-z^{est})	Standard Deviation
Summer	20.6	12.5	0.1	12.9
Fall	7.2	7.1	-1.3	7.3
Winter	6.3	5.3	0.1	5.7

Figures 41-43 (at the end of this section) show the cumulative trichloromethane emissions correction factor after 10 iterations of the Kalman filter through the full set of observations and trajectories for each grid cell. As before, we only estimate α for grid cells that were passed through by at least 10 trajectories during a season. Trichloromethane measurements were not obtained during the Spring. Following our expectations, these figures indeed show that significant increases in the estimated emissions from biomass burning and industrial emissions alone are necessary to match the observed mole fractions. These large correction factors are particularly noticeable in the central Canadian forest lands and over the oceans where we had very low emissions initially due to our lack of inclusion of soil and oceanic sources. This is consistent with the aforementioned natural sources of trichloromethane emissions in the soil and surface layers of the ocean which provides another qualitative endorsement of our estimation procedures. The final estimated emissions distributions are shown in Figures 44-46.

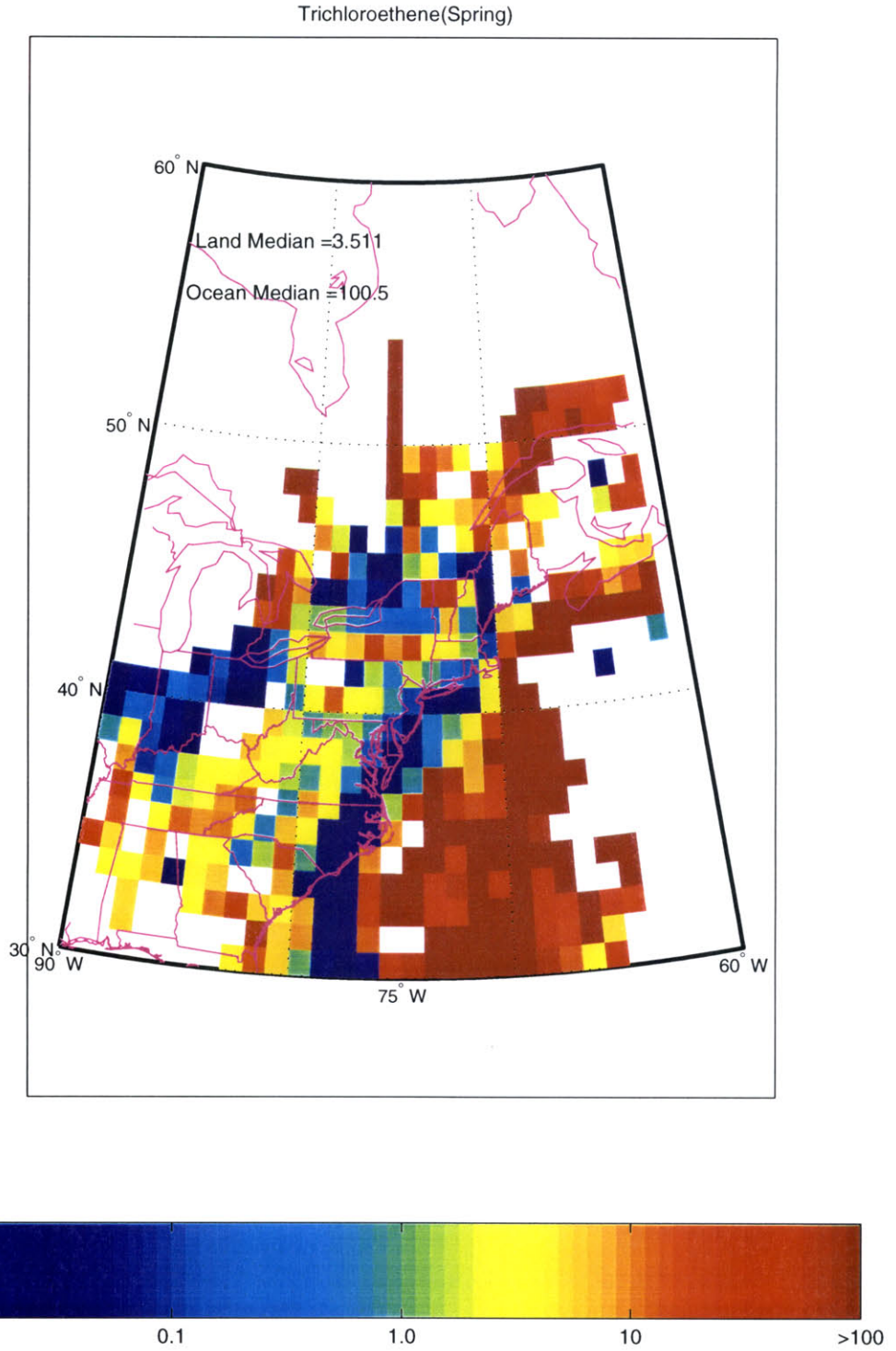

Figure 32. Trichloroethene correction factors α obtained after the tenth iteration of the Kalman filter for each grid cell within the domain (30-60N, 60-90W) which had at least 10 trajectories pass through them during Spring, 1998 (March-May).

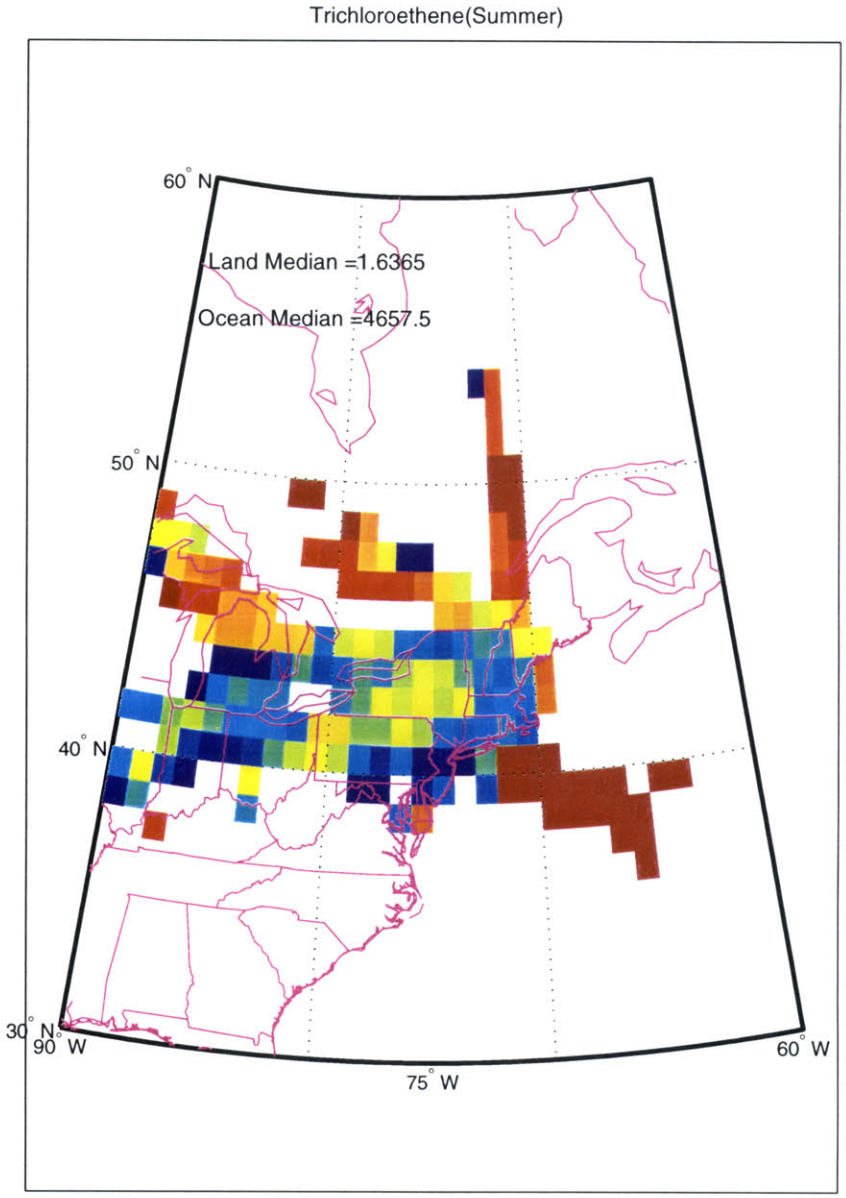

Figure 33. Trichloroethene correction factors α obtained after the tenth iteration of the Kalman filter for each grid cell within the domain (30-60N, 60-90W) which had at least 10 trajectories pass through them during Summer, 1998 (July-August).

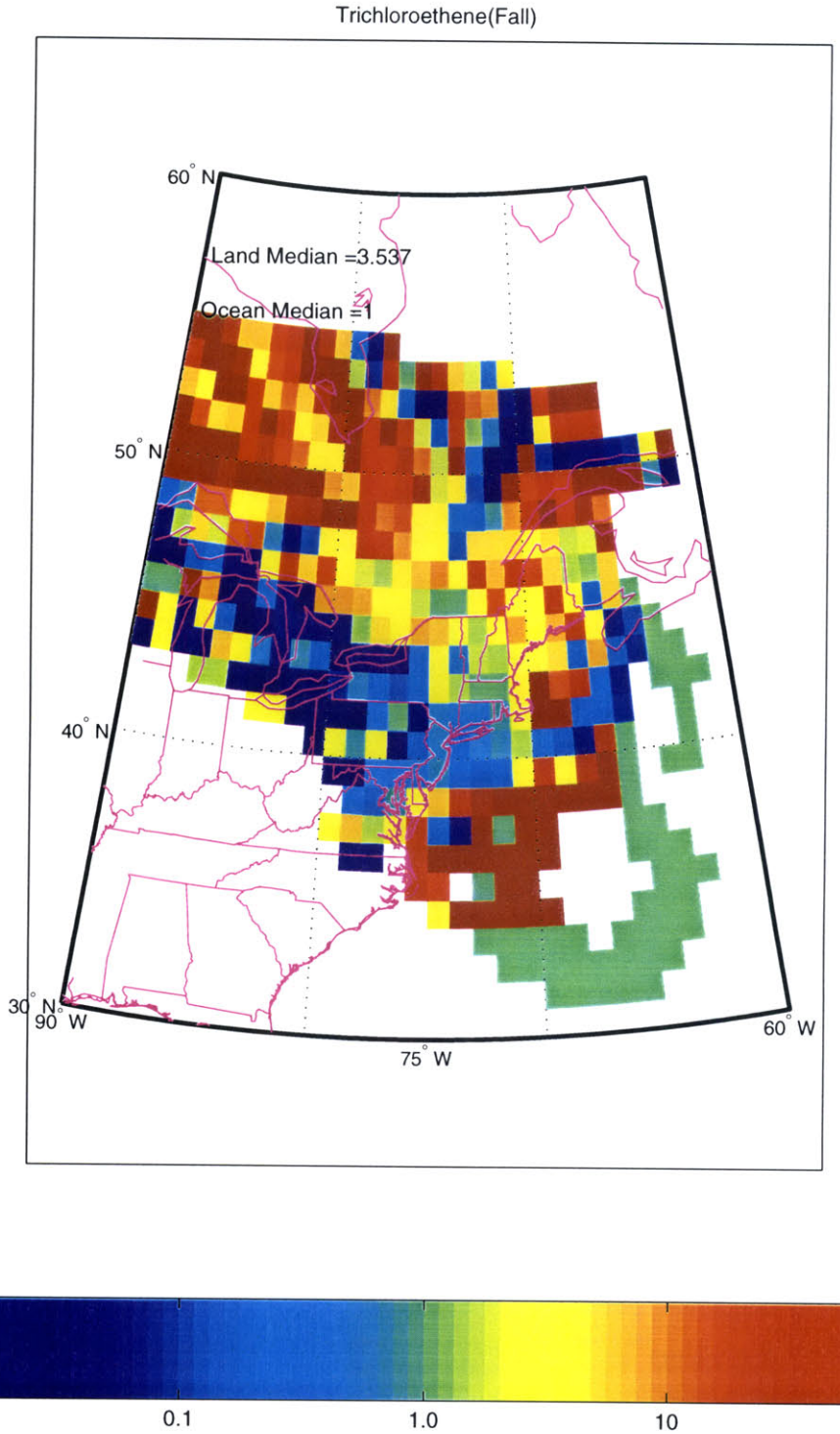

Figure 34. Trichloroethene correction factors α obtained after the tenth iteration of the Kalman filter for each grid cell within the domain (30-60N, 60-90W) which had at least 10 trajectories pass through them during Fall, 1998 (September-November).

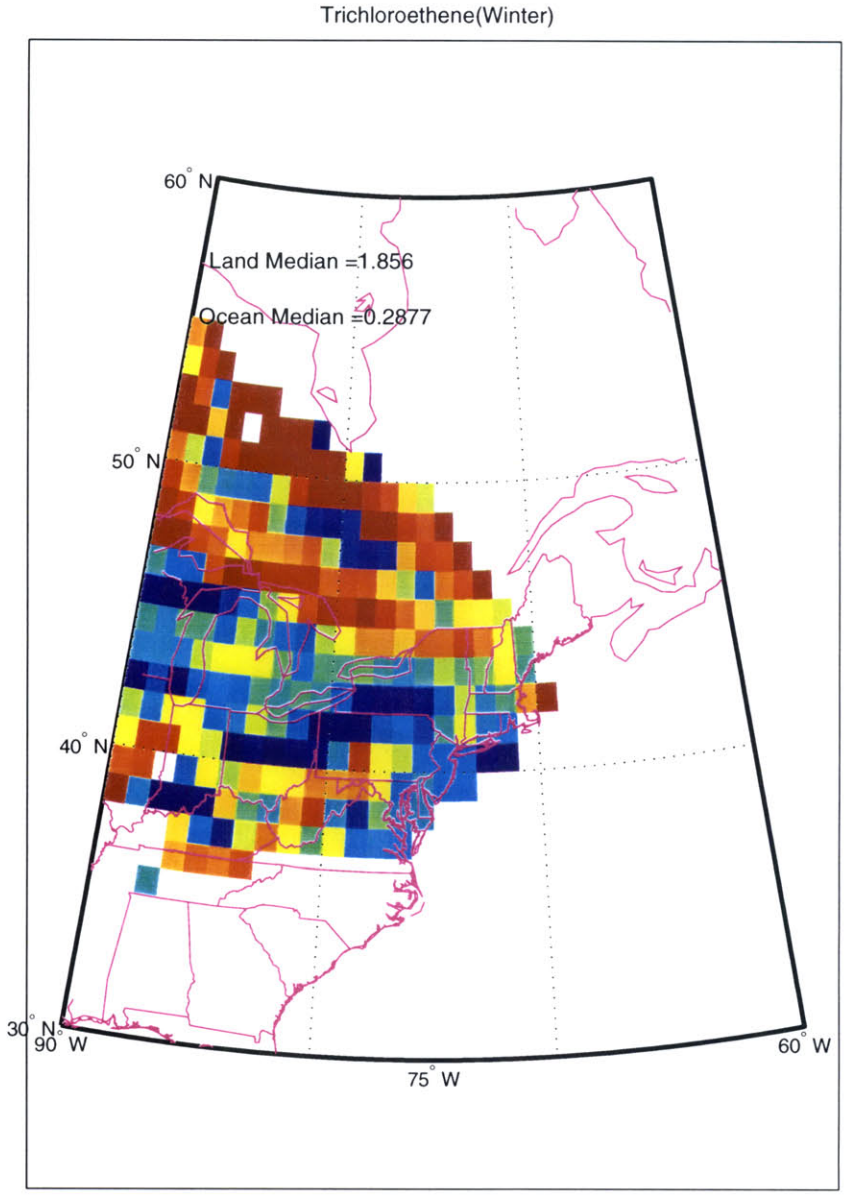

Figure 35. Trichloroethene correction factors α obtained after the tenth iteration of the Kalman filter for each grid cell within the domain (30-60N, 60-90W) which had at least 10 trajectories pass through them during Winter, 1998-99 (December-January).

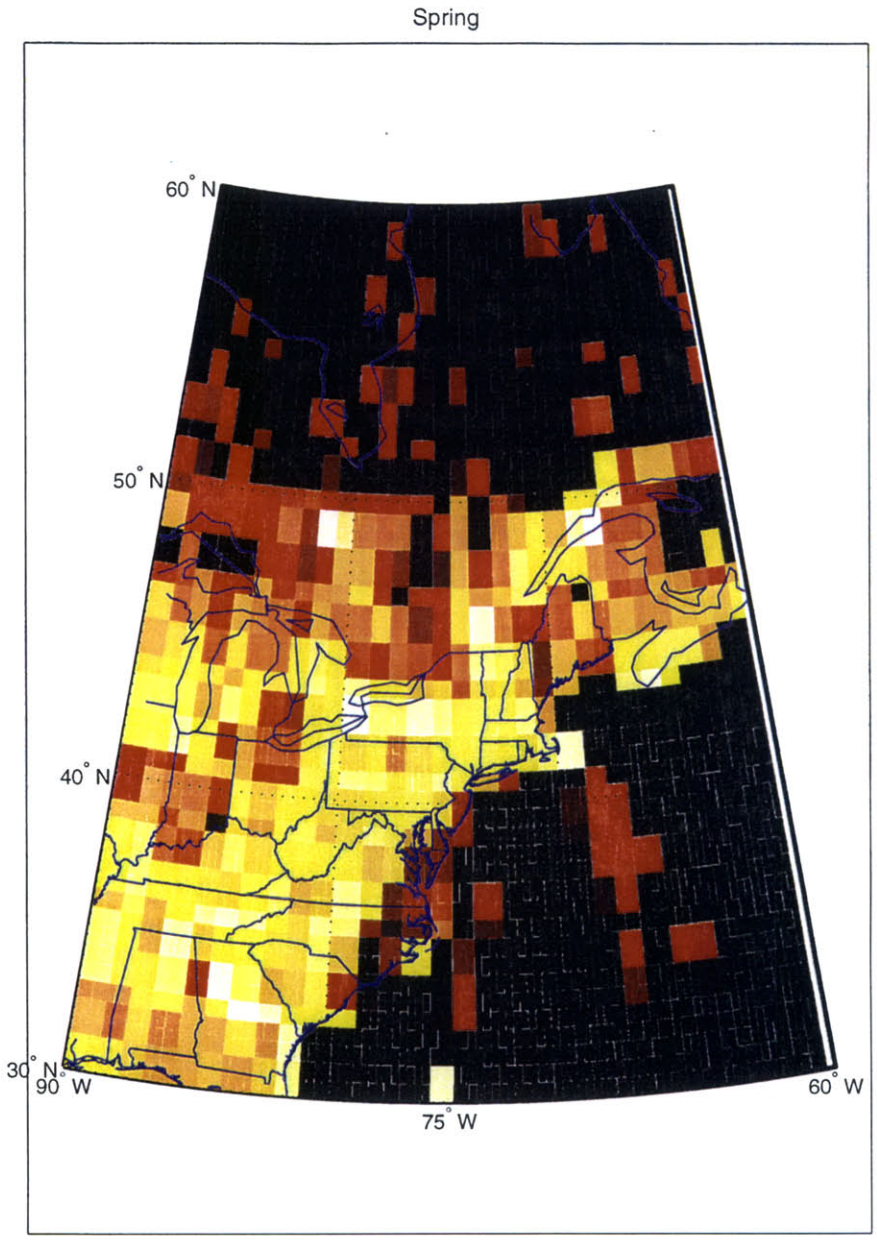

Figure 36. Distribution of Spring trichloroethene emissions based on our calculated Spring corrections (Figure 32) to the Reactive Chlorine Emissions Inventory estimates shown in Figure 7. Units are ppt/hr as described in the caption for Figure 7. If fewer than 10 trajectories passed over a grid cell, no correction was calculated and the RCEI estimate was left unchanged.

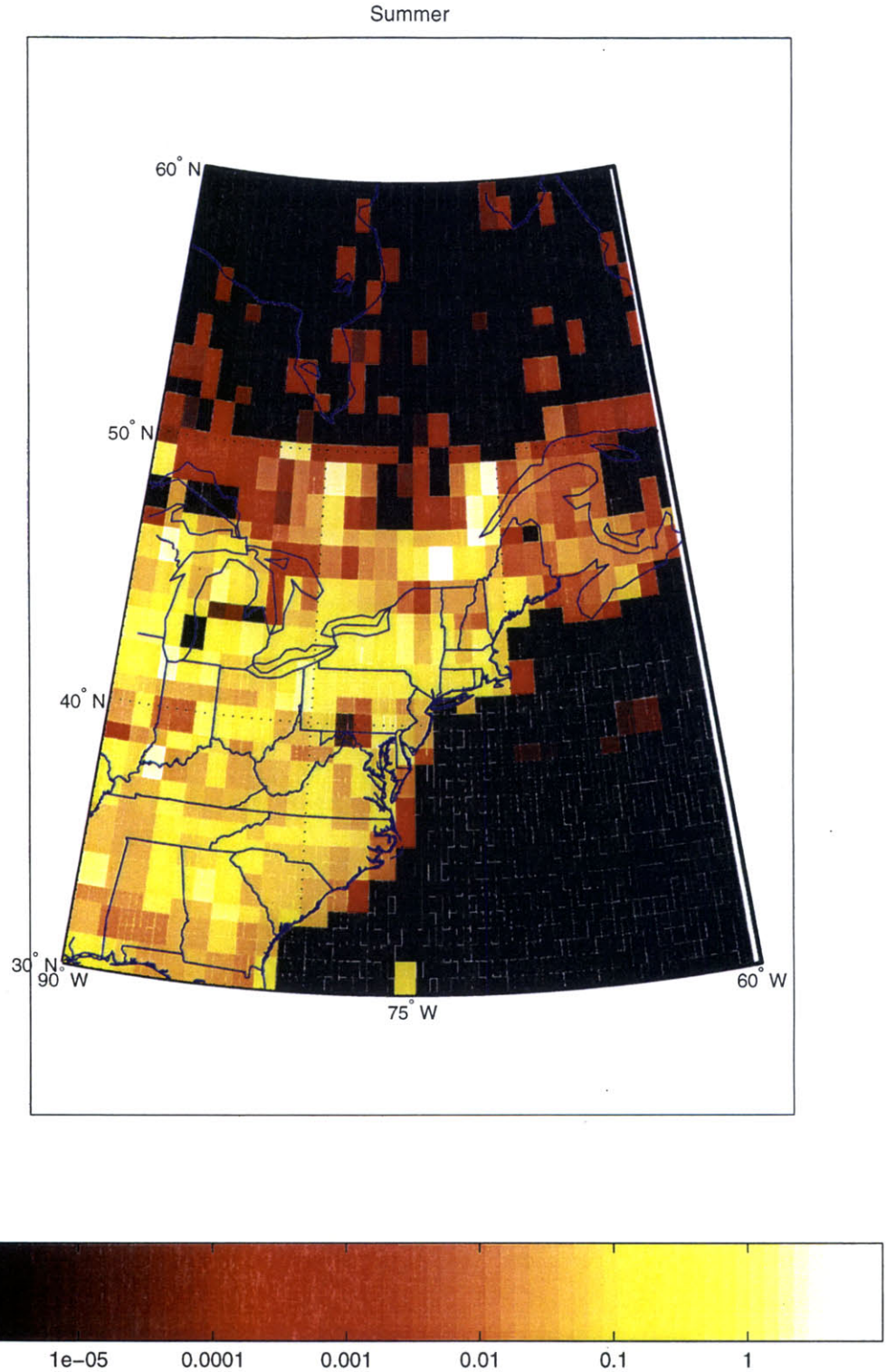

Figure 37. Distribution of Summer trichloroethene emissions based on our calculated Summer corrections (Figure 33) to the Reactive Chlorine Emissions Inventory estimates shown in Figure 7. Units are ppt/hr as described in the caption for Figure 7. If fewer than 10 trajectories passed over a grid cell, no correction was calculated and the RCEI estimate was left unchanged.

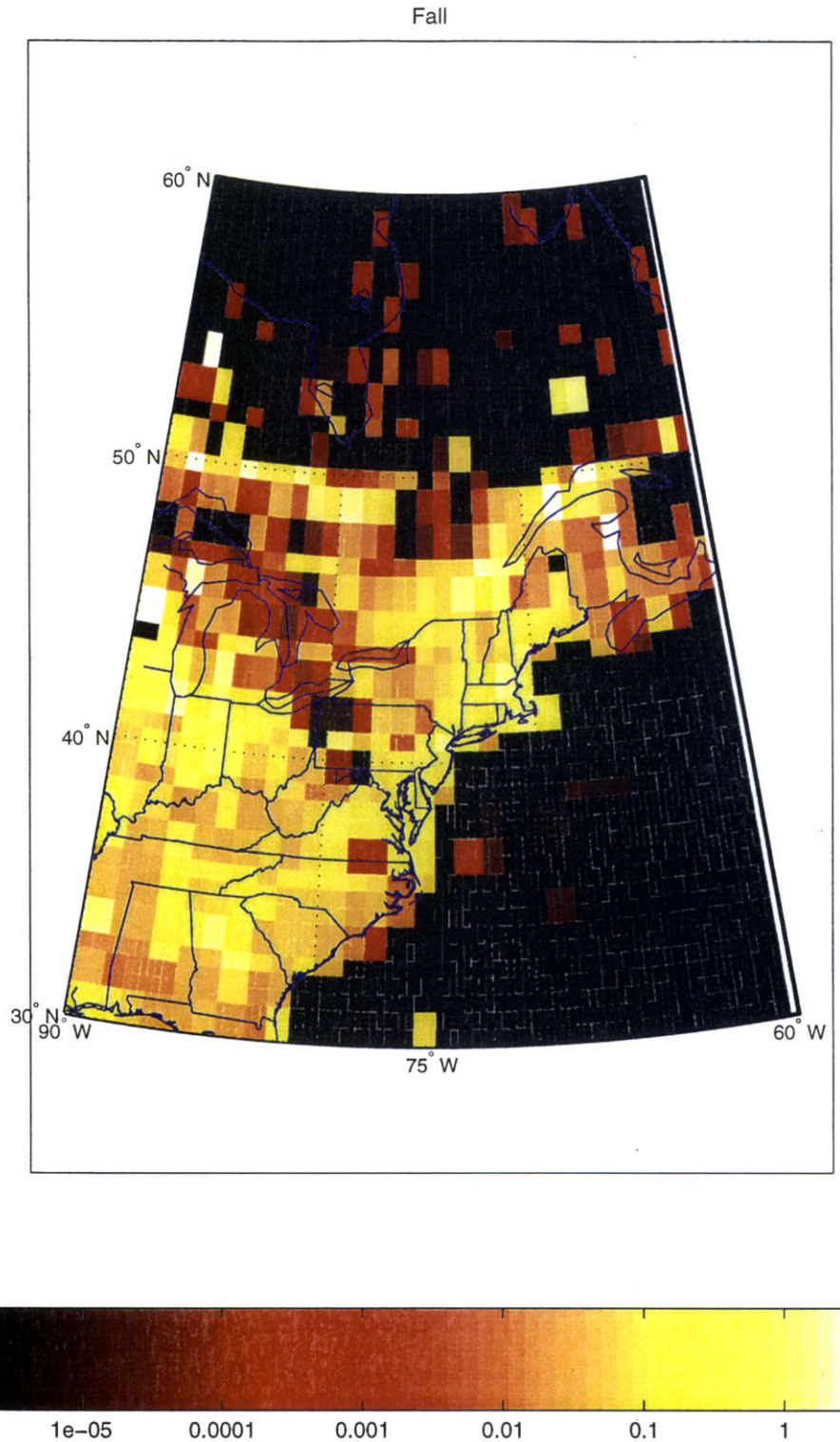

Figure 38. Distribution of Fall trichloroethene emissions based on our calculated Fall corrections (Figure 34) to the Reactive Chlorine Emissions Inventory estimates shown in Figure 7. Units are ppt/hr as described in the caption for Figure 7. If fewer than 10 trajectories passed over a grid cell, no correction was calculated and the RCEI estimate was left unchanged.

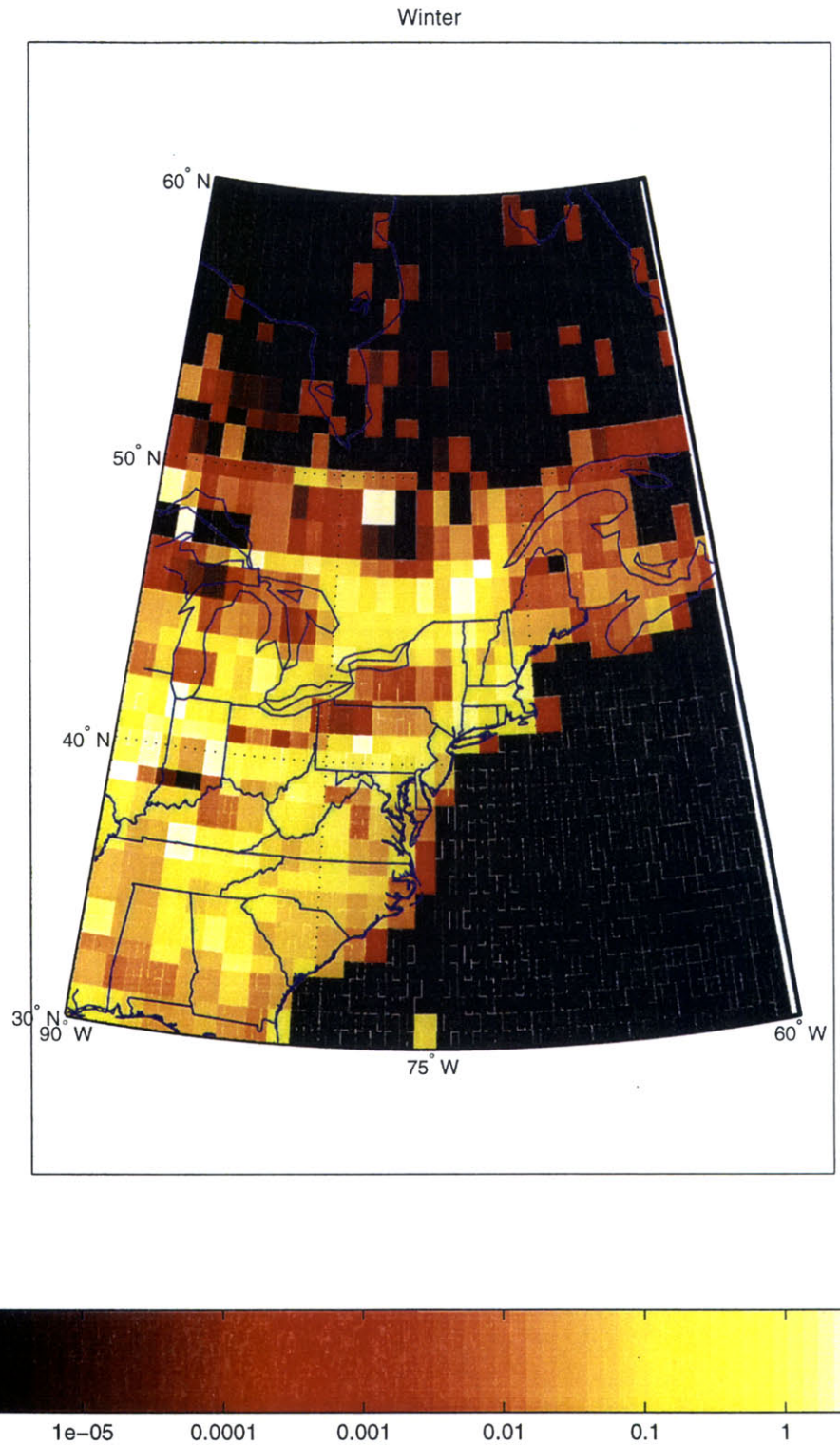

Figure 39. Distribution of Winter trichloroethene emissions based on our calculated Winter corrections (Figure 35) to the Reactive Chlorine Emissions Inventory estimates shown in Figure 7. Units are ppt/hr as described in the caption for Figure 7. If fewer than 10 trajectories passed over a grid cell, no correction was calculated and the RCEI estimate was left unchanged.

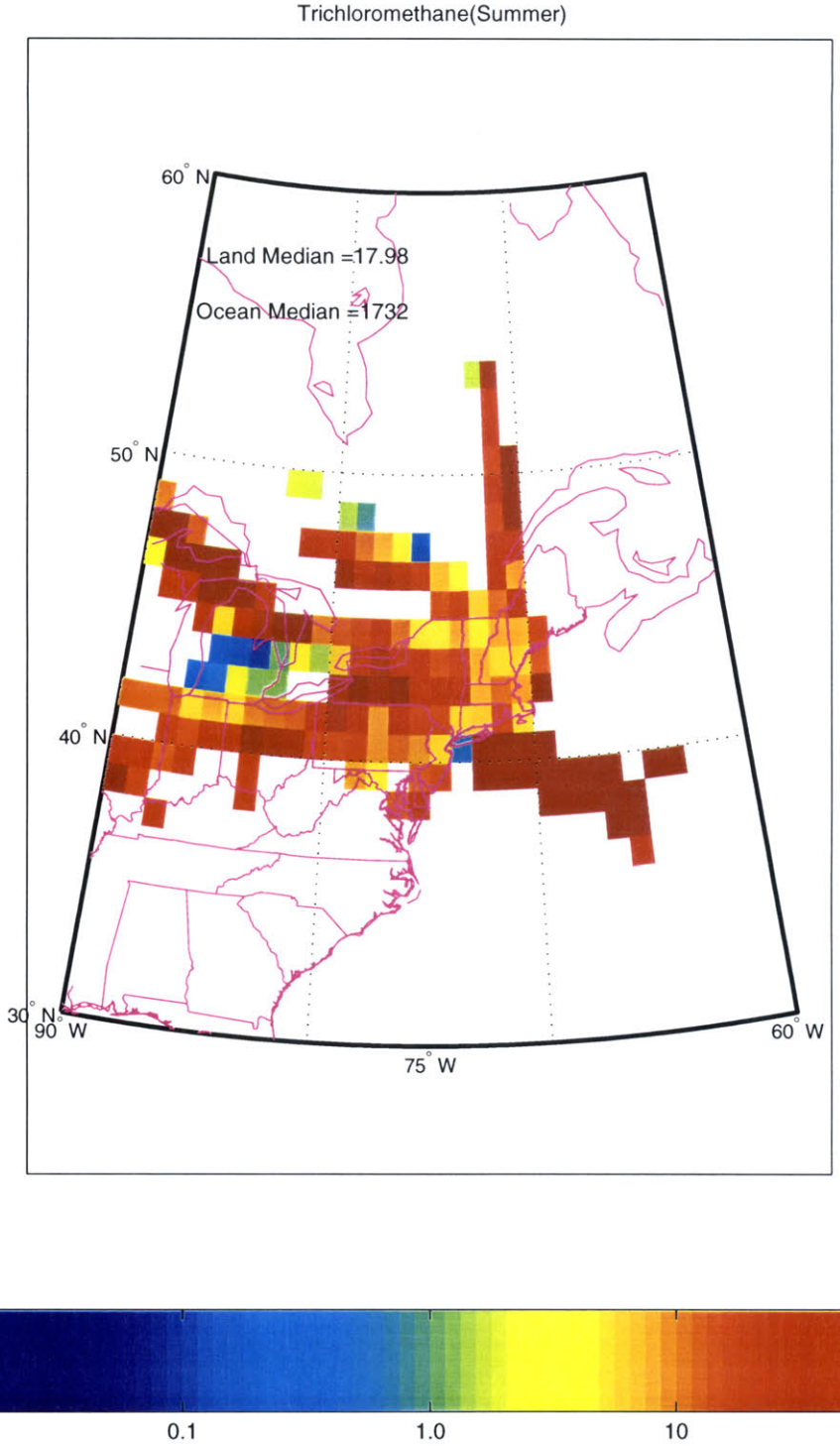

Figure 41. Trichloromethane correction factors α obtained after the tenth iteration of the Kalman filter for each grid cell within the domain (30-60N, 60-90W) which had at least 10 trajectories pass through them during Summer, 1998. Note that there were no Spring trichloromethane observations.

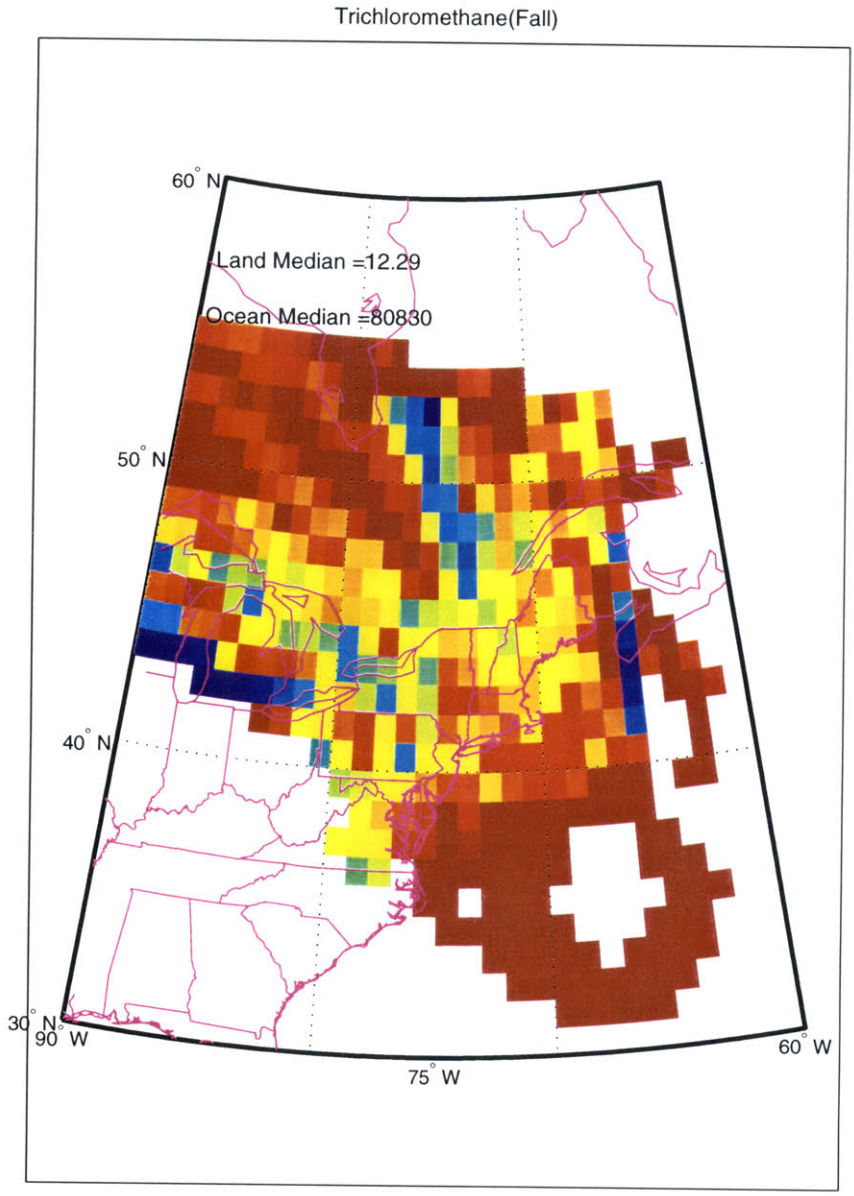

Figure 42. Trichloromethane correction factors α obtained after the tenth iteration of the Kalman filter for each grid cell within the domain (30-60N, 60-90W) which had at least 10 trajectories pass through them during Fall, 1998.

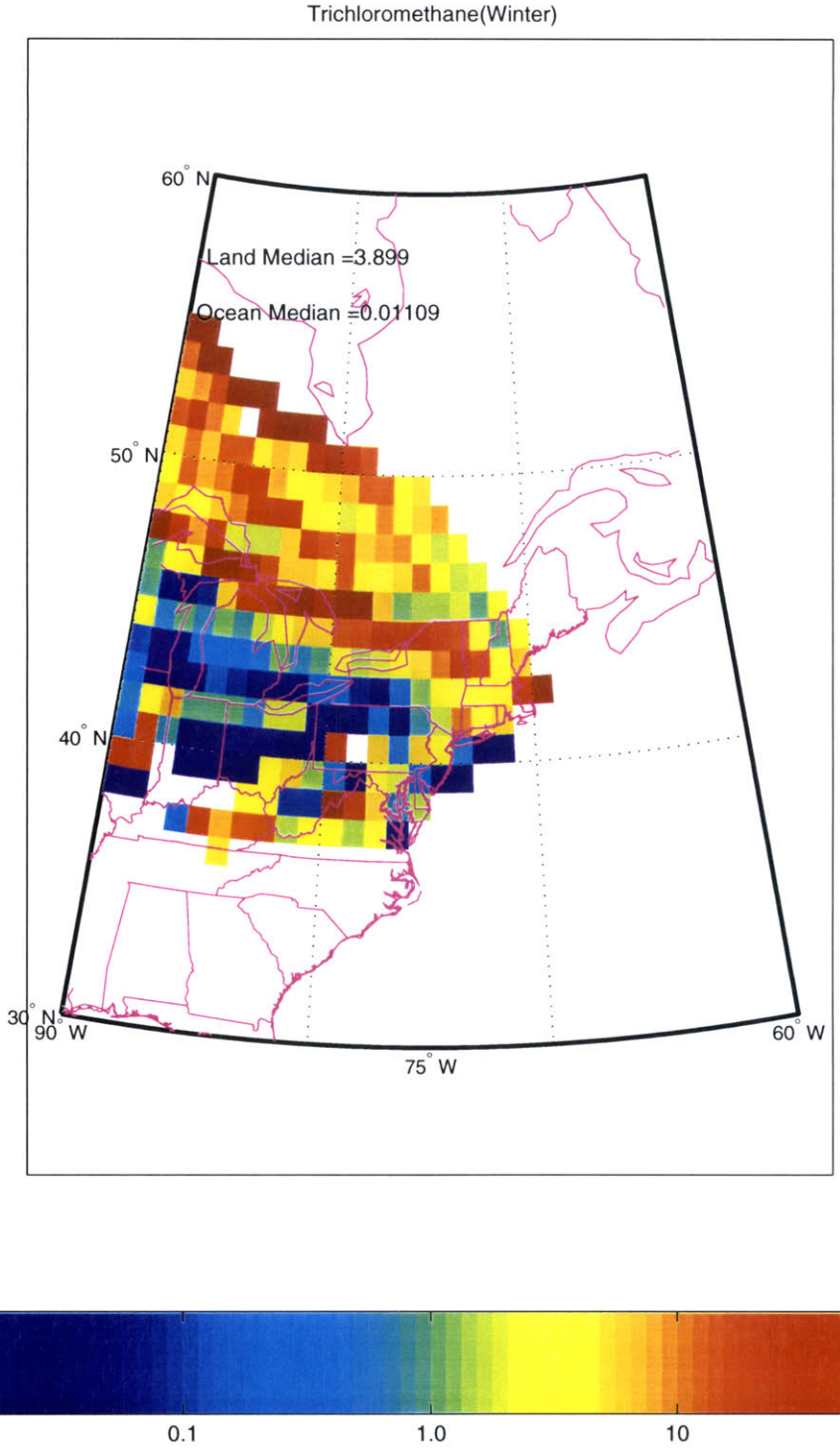

Figure 43. Trichloromethane correction factors α obtained after the tenth iteration of the Kalman filter for each grid cell within the domain (30-60N, 60-90W) which had at least 10 trajectories pass through them during Winter, 1998-99.

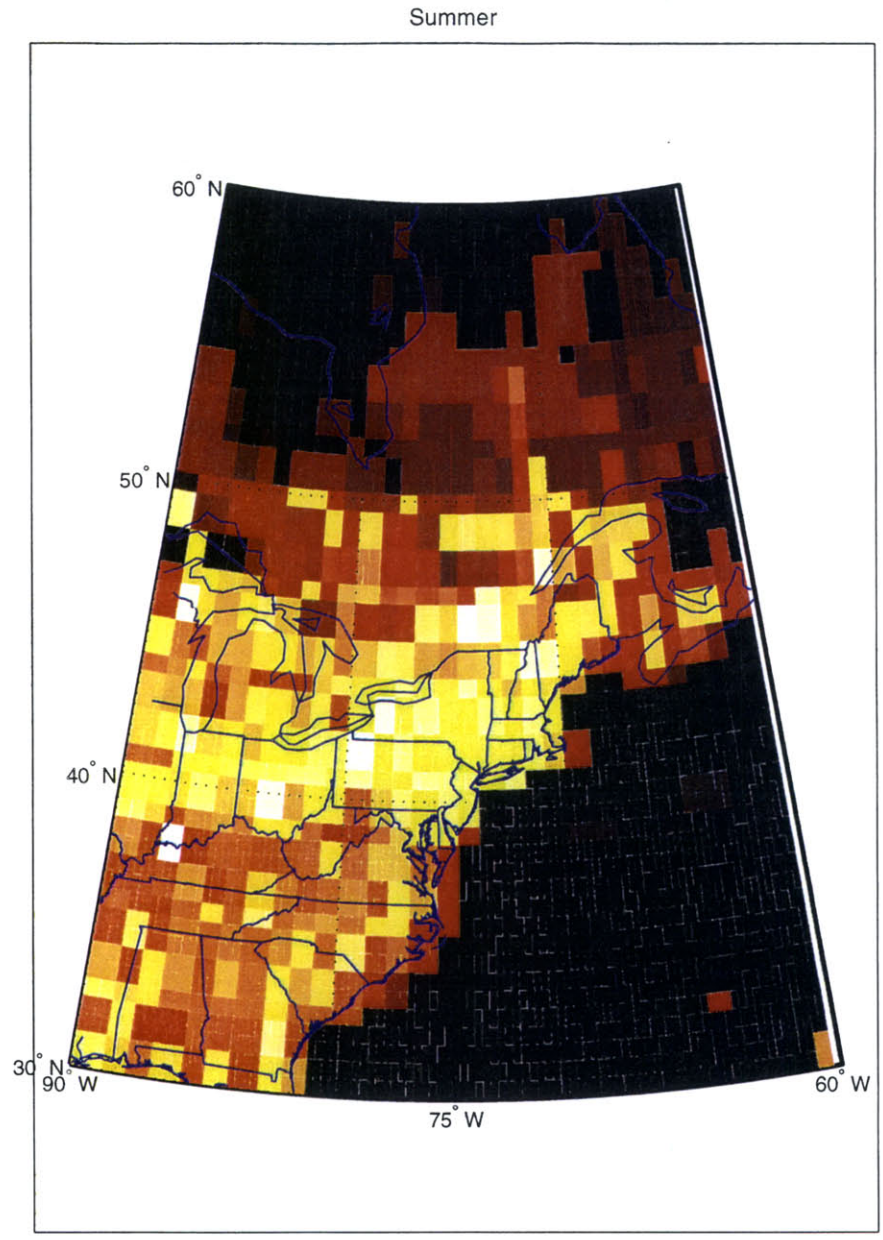

Figure 44. Distribution of Summer trichloromethane emissions based on our calculated Summer corrections (Figure 41) to the Reactive Chlorine Emissions Inventory estimates shown in Figure 9. Units are ppt/hr as described in the caption for Figure 9. If fewer than 10 trajectories passed over a grid cell, no correction was calculated and the RCEI estimate was left unchanged.

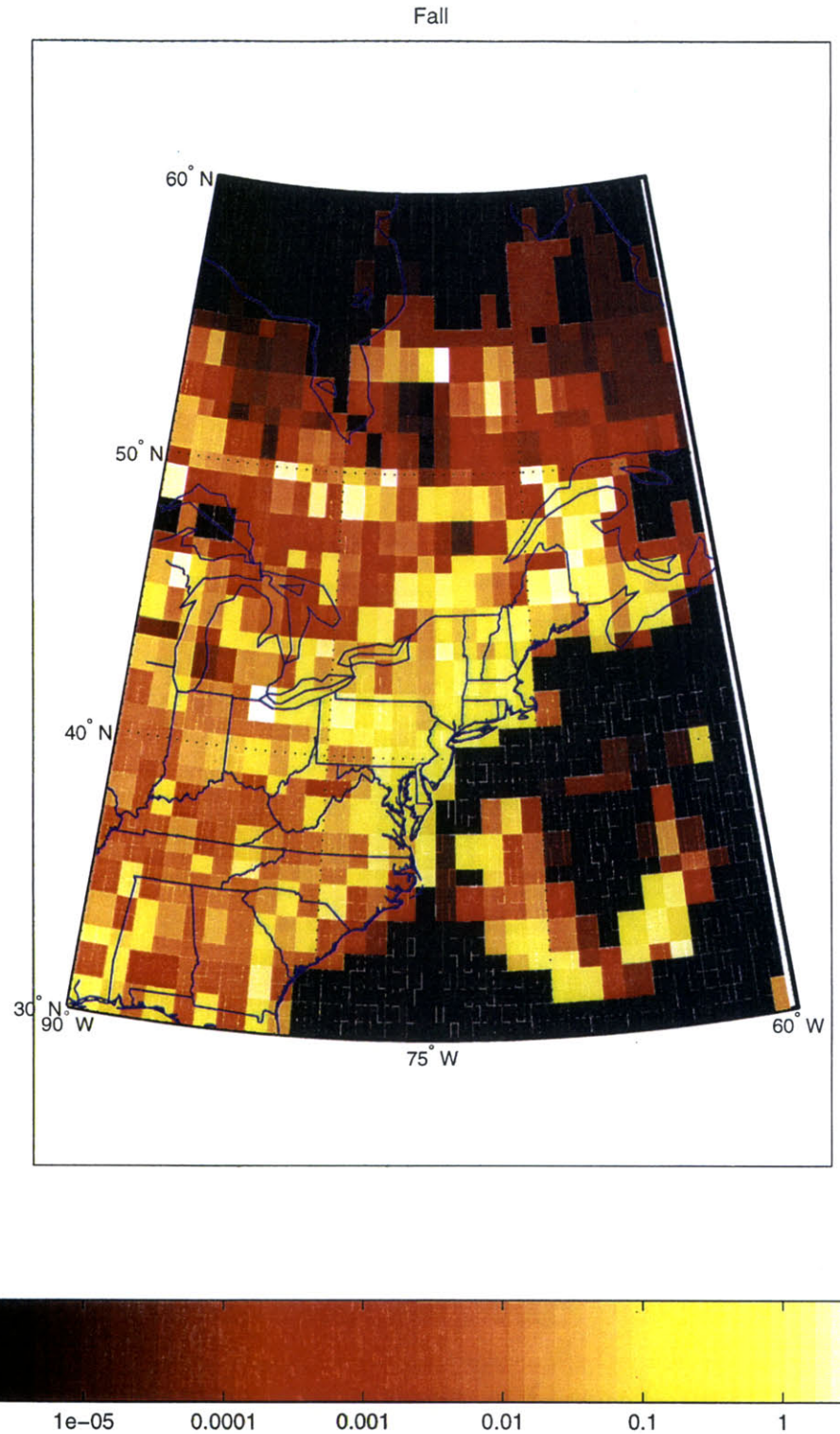

Figure 45. Distribution of Fall trichloromethane emissions based on our calculated Fall corrections (Figure 42) to the Reactive Chlorine Emissions Inventory estimates shown in Figure 9. Units are ppt/hr as described in the caption for Figure 9. If fewer than 10 trajectories passed over a grid cell, no correction was calculated and the RCEI estimate was left unchanged.

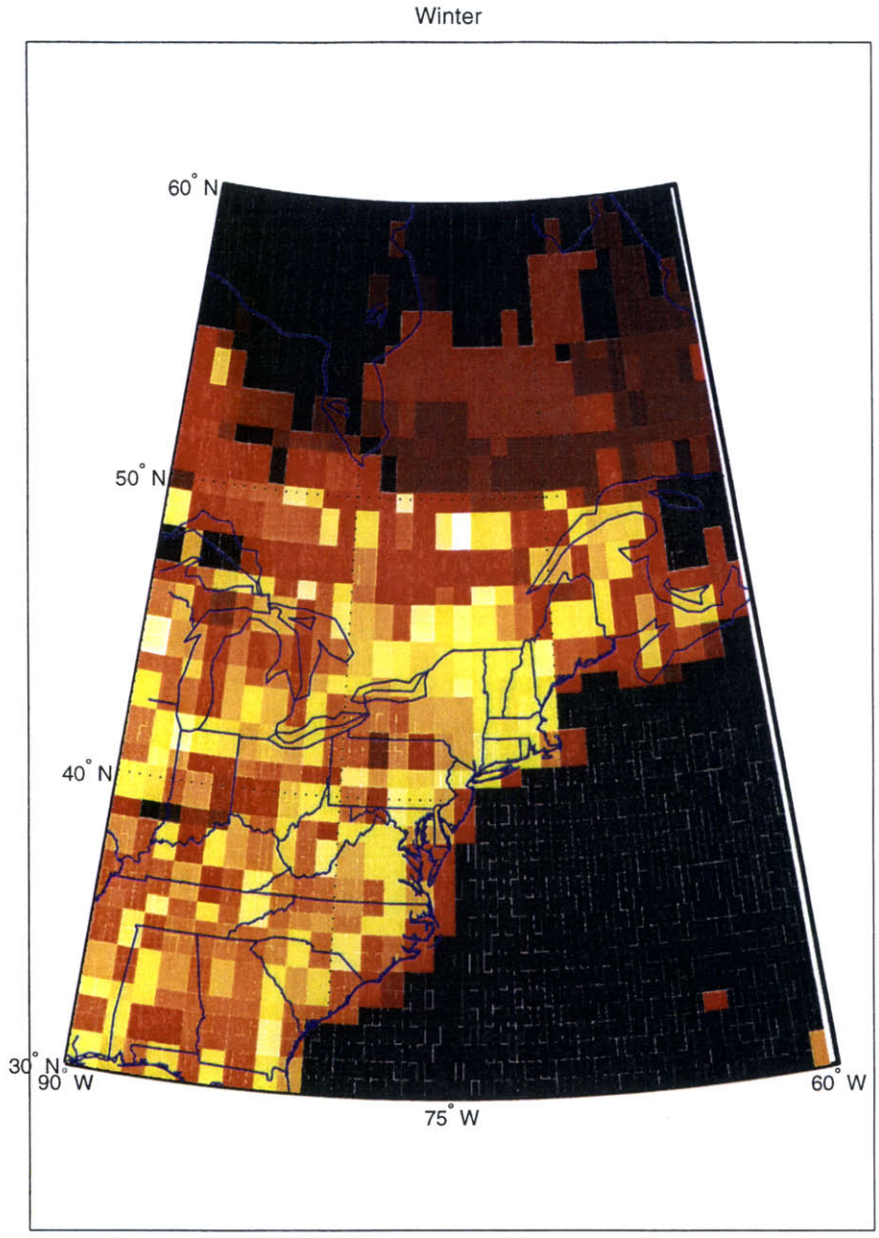

Figure 46. Distribution of Winter trichloromethane emissions based on our calculated Winter corrections (Figure 43) to the Reactive Chlorine Emissions Inventory estimates shown in Figure 9. Units are ppt/hr as described in the caption for Figure 9. If fewer than 10 trajectories passed over a grid cell, no correction was calculated and the RCEI estimate was left unchanged.

Emissions Uncertainty

Here, we review the sources of error which enter into our calculation of the emissions correction factor, α^*, which is applied to the RCEI emissions to obtain our best estimate of emissions according to the observations (see equations 3.4 and 3.6).

In the Kalman filter, it is assumed that the gain scalar, g, is calculated exactly (Table 7, equation 3.14). Hence the error incurred by our state update equation (3.13)(which is used to calculate α and α^*) comes from the difference z^{obs}-z^{est}. As shown in equation 3.3 of Table 7, this is simply the quantity ε. We have already discussed the theoretical sources of this error in Chapter 3 (i.e. instrumental precision, trajectory model error, time variation of emissions sources) and quantified them when possible. We see however in Figure 16 (seasonal runs of the 10th iteration of the Kalman filter for the grid cell containing Montreal) that inclusion of all quantified sources of error is not sufficient to account for all of the variations in the residual, ε. Hence we often observe the successive updates of our estimate of our state parameter, α, to lie outside the bounds of uncertainty associated with previous estimates.

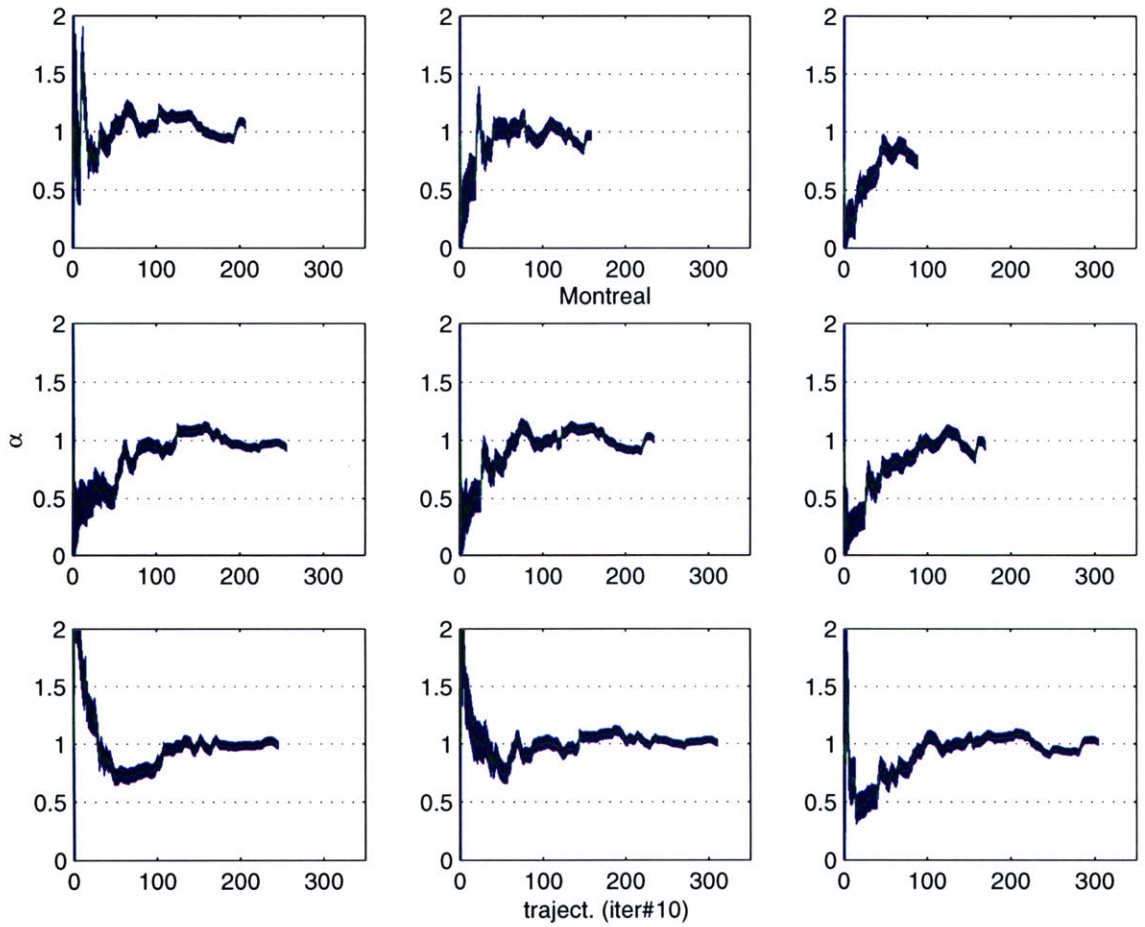

Figure 47. Fall runs of the final (tenth) iteration of the Kalman filter for 9 grid cells near the city of Montreal, Canada. The Montreal grid cell is located in the center. The grid cell centered just North, South, East and West of Montreal are shown above, below, to the right and to the left of the central figure respectively.

While Figure 16 shows us that all error is not included in the estimate of uncertainty used for these filter runs, it can also be used as a guide to assess the magnitude of the variations of the filter response. After 10 iterations of the application of the Kalman filter to every grid cell in the domain, we see variations of no more than ±15% after a significant portion of the data has been incorporated into the filter (e.g. after trajectory #50 for the Fall). To insure that this grid cell is representative of the region, we can look at the results of the filter runs for several other grid cells. Figure 47 shows the filter runs for 9 grid cells located in direct proximity to Montreal (Montreal and the 8 adjacent grid cells, North, Northeast, East, etc.). In this figure it is clear that during the Fall, when we had over 1,000 observations and corresponding trajectories to use in the filter, variations of no more than ±15% are observed for each of these grid cells.

We have examined similar plots for each of the other seasons and other chemicals to make comparable estimates of uncertainty for each of the other seasons. Differences in uncertainty estimates for each season largely reflect the number of measurements obtained for each season. There are some differences between chemicals as well, but the largest differences in accuracy are due to a grid cells distance from our observing site. Due to the increase in trajectory error and the decrease in the total trajectory density (total number of trajectories that pass through a particular grid cell) with distance from the observing site, we expect greater accuracy in our correction factor estimates (α) for nearby grid cells. Those grid cells which lie farthest away will have estimates based on (in general) fewer measurements and thus are more likely to be affected by a single erroneous measurement (e.g. local pollution event) or synoptic event (e.g. trajectory calculated with high vertical shear). We therefore have a range of accuracies from 15% for grid cells located a few hundred kilometers from our observing site up to 50% for those grid cells located thousands of kilometers from our observing site. We therefore take 15-50% as our, albeit subjective, estimate for the uncertainty in the correction factor ($\delta\alpha$). This error ($\delta\alpha$=*15-50%*) incorporates possible errors due to unmodelled time variations in emissions as well as trajectory and instrumental errors discussed earlier.

We are reminded from equation 3.6 that α and α^* are linearly related by the factor:

$$F = \frac{\alpha^*}{\alpha} = \frac{h - h^2/2H}{h_s - h_s^2/2H} \tag{4.1}$$

where h_s is taken to be 1.5 km and H is the scale height of the atmosphere (≈8km). To insure a reasonable estimate of the uncertainty in h, we can examine the statistics of trajectory heights for a set of representative trajectories. We calculate the average trajectory height and standard deviation for the set of Fall trajectories which appear in Figure 11. For these trajectories, we find an average height of 850 meters with an average standard deviation of 415 meters (that is the average of the standard deviations calculated for each of these trajectories). This implies very little time spent outside of our assumed mixed layer of 1500 meters; however, there is significant uncertainty in our chosen value

of h_s. If we assume that the mixed layer height varies between 750m and 2,250m ($\delta h \approx 50\%$), we can use standard error propagation techniques to calculate the uncertainty in F (Taylor, 1982). We estimate $\delta F \approx 45\%$ (the uncertainty in the difference in the numerator of equation 4.1 is somewhat smaller than the uncertainty in h alone since the two terms will vary together). The error in α^* is therefore given by adding δF and $\delta\alpha$ in quadrature. The overall uncertainty for our emissions correction factors α^* is therefore given by:

$$\delta\alpha^* = \sqrt{\delta\alpha^2 + \delta F^2} \approx 47 - 67\% . \qquad (4.2)$$

Chapter 5: Conclusions

We set out in this thesis to provide an observation-based estimate of regional emissions for three tropospherically active chlorocarbon molecules. To achieve these goals, a measurement campaign of these species has yielded over 12,000 new measurements of 4 trace gases. These measurements span 11 months between March 1998 and January 1999. The development of an automated cryogenic pre-concentration system allowed the continuous collection and analysis of samples resulting in a dataset containing periods of prolonged hourly temporal resolution. Instrumental precisions have been established at ±5% by looking at the variation of repeated measurements of a standard gas. Absolute accuracy has been established at ±10% through separate intercomparisons with colleagues at the Scripps Institution of Oceanography and the National Center for Atmospheric Research. These experiments involved the production of two samples which were sent to each laboratory where they were analyzed and calibrated and returned to MIT with a subsequent comparison of results. All observations are presented in Appendix B using the average of the calibration scales of SIO/NCAR which had scale factors agreeing within analytic uncertainty for the compounds which were measured in common by the two laboratories.

Measurements of the three most reactive compounds (trichloromethane, tetrachloroethene, and trichloroethene) have been used in conjunction with a Lagrangian trajectory model (HYSPLIT) developed at the NOAA Air Resources Laboratory and an optimal linear Kalman filter to estimate correction factors to emissions inventories published as part of the IGAC/GEIA Reactive Chlorine Emissions Inventory. A geographical domain between 30°N and 60°N latitude between 60°W and 90°W longitude was chosen and backtrajectories were calculated for each observation for between 48 and 72 hours prior to the time of observation. The trajectories are used initially in conjunction with the RCEI emissions inventory and subsequently with the corrected version of this inventory to calculate the total integrated emissions along the length of each trajectory. The RCEI emissions inventory presents 1990 annual average emissions for each of the three species studied based on industrial and manufacturing sources, bio-mass burning, and natural sources. Only trichloromethane has significant natural sources, and because only about 11% of total estimated emissions were anthropogenic and available in a gridded inventory for this compound, we expected and obtained major corrections to the initial inventory of emissions for this species.

To take turbulent mixing into account along each trajectory, average values of horizontal velocity and horizontal velocity deformation were taken from the HYSPLIT model and used with an analytical solution to the continuity equation to numerically estimate the strength of atmospheric convergence along each trajectory. This convergence rarely exceeded 10% of the impact due to the emissions on the estimated mole fraction at the observing site.

A simplified version of the Kalman filter was chosen which essentially calculates a recursive weighted least-squares average of the correction factors for each trajectory that passes over a particular grid cell. This factor is required to bring the integrated emissions

along the trajectory into better agreement with the observation and is updated with each new observation and corresponding trajectory. The results of the ten iterations of the Kalman filter runs for each chemical in each season (along with annual averages) are presented in Table 11.

Table 11 - Median Correction Factors over Land and Ocean

tetrachloroethene

	a*(h=2250m)			a*(h=1500m)			a*(h=750m)	
Season	land	ocean	Season	land	ocean	Season	land	ocean
Spring	3.1	1.2E+02	Spring	2.2	8.5E+01	Spring	1.2	4.5E+01
Summer	2.0	3.6E-01	Summer	1.4	2.5E-01	Summer	0.7	1.3E-01
Fall	2.6	7.0E+01	Fall	1.8	4.9E+01	Fall	0.9	2.6E+01
Winter	1.4	1.4E-03	Winter	1.0	1.0E-03	Winter	0.5	5.3E-04
annual av.	2.3	4.8E+01	annual av.	1.6	3.4E+01	annual av.	0.8	1.8E+01

trichloroethene

	a*(h=2250m)			a*(h=1500m)			a*(h=750m)	
Season	land	ocean	Season	land	ocean	Season	land	ocean
Spring	5.0	1.4E+02	Spring	3.5	1.0E+02	Spring	1.8	5.3E+01
Summer	2.3	6.5E+03	Summer	1.6	4.6E+03	Summer	0.8	2.4E+03
Fall	5.0	1.4E+00	Fall	3.5	1.0E+00	Fall	1.8	5.3E-01
Winter	2.7	4.1E-01	Winter	1.9	2.9E-01	Winter	1.0	1.5E-01
annual av.	3.7	1.7E+03	annual av.	2.6	1.2E+03	annual av.	1.4	6.2E+02

trichloromethane

	a*(h=2250m)			a*(h=1500m)			a*(h=750m)	
Season	land	ocean	Season	land	ocean	Season	land	ocean
Summer	28.4	2.8E+03	Summer	20.0	2.0E+03	Summer	10.5	1.1E+03
Fall	21.3	1.0E+05	Fall	15.0	7.2E+04	Fall	7.9	3.8E+04
Winter	6.2	3.6E-01	Winter	4.4	2.5E-01	Winter	2.3	1.3E-01
annual av.	18.6	3.5E+04	annual av.	13.1	2.5E+04	annual av.	6.9	1.3E+04

trichloromethane(less 5ppt)

	a*(h=2250m)			a*(h=1500m)			a*(h=750m)	
Season	land	ocean	Season	land	ocean	Season	land	ocean
Summer	25.6	2.4E+03	Summer	18.0	1.7E+03	Summer	9.5	8.9E+02
Fall	17.0	1.1E+05	Fall	12.0	8.0E+04	Fall	6.3	4.2E+04
Winter	5.5	1.4E-02	Winter	3.9	1.0E-02	Winter	2.0	5.3E-03
annual av.	16.0	3.9E+04	annual av.	11.3	2.7E+04	annual av.	5.9	1.4E+04

The effect of emissions on mole fractions varies inversely with mixed layer height, assumed here to be 1500±750 m. Thus our estimates of emissions correction factors must be scaled with a factor which is a function of mixed layer height. The significant uncertainty (in our correction factors) associated with our estimate of mixed layer height (±45%) along with the uncertainty of our correction factor estimates themselves (±50%) lead to an overall uncertainty of ±47-67% in our final estimate of RCEI inventory corrections. These uncertainties are likely to be largest for grid cells which are farthest from the observing site, as that is where backtrajectories will have the most error and

where the trajectory density will be lowest (resulting in estimates based on fewer measurements).

We find that within these large uncertainties, our land-based estimates of emissions are larger than but still statistically consistent with the trichloroethene and tetrachloroethene emissions estimates produced by RCEI for our standard mixed layer height of 1500 m. If the mixed layer height is only 750 m to 1000m, we find better agreement. Here, we gauge agreement by the annual average of the median correction factor for all land based grid cells. Because RCEI had near zero emissions listed for the oceans, the corrections factors calculated for these grid cells are sometimes extremely large, while still yielding very small resultant emissions. This is true for many grid cells in central Canada as well, and thus very high values here will skew the mean value. The median value of the land-based correction factor appears to give a reasonable estimate of the overall tendency to either overestimate of underestimate emissions for land-based grid cells. The annual average of these medians is included in Table 11 because for each season we have different meteorology and thus different grid cells have been included in the analysis. But if an overall tendency for overestimation or underestimation exists, we expect it to persist throughout the year as we expect no large seasonal cycle in the emissions for these two solvents.

For trichloromethane, we are comparing our final estimates to an initial inventory consisting of only industrial and bio-mass burning emissions from the RCEI inventory. As already noted, these emissions represent only 11% of the global total, and if we assume that emissions from our geographic domain will scale linearly to the global emissions, then we expect that only 11% of the regional trichloromethane emissions are captured by the initial gridded inventory. Hence to find good agreement with the known trichloromethane sources reported by the RCEI, we expect correction factors to the initial inventory of about 9. Again we find that within the 47-67% uncertainty associated with our estimates, we have statistically consistent agreement for mixed layer heights between 750 and 1,500 meters with 1000 meters giving estimates closest to 9. Here we may expect some seasonality of the emissions with a significant fraction of the emissions resulting from natural biogeochemical cycles in soils and the ocean. The median land-based correction factors in Table 11 imply that the land-based natural sources are strongest during the Summer months. Strong soil sources are consistent with the observed latitudinal distribution of trichloromethane observations (Khalil et al., 1999).

We note that over the oceans, where the RCEI inventory has zero emissions gridded, we do expect small emissions for tetrachloroethene and trichloroethene and significant emissions for trichloromethane. In fact, from our filter we estimate large emissions for trichloromethane and some small emissions for tetrachloroethene. The magnitude of these sources are consistent with estimates which were known but not included in the gridded emissions fields produced by RCEI and used as the initial guess for this work adding to the credibility of these results.

To improve this technique for deducing emissions on a regional basis, a method for eliminating (or properly weighting) trajectories that are most subject to errors is

important. The trajectory model has been validated with an estimated uncertainty of 10-20% of total trajectory distance during typical meteorological conditions. However, during times of high vertical shear or significant horizontal dispersion the uncertainty in the trajectory rises significantly. In principle, one could scrutinize each trajectory and reject all those during times during any unique meteorological conditions that degrade the ability of a Lagrangian trajectory model to accurately simulate the path taken by an observed air mass, but this is tremendously time consuming. These trajectories would either be rejected, or assigned a low weighting so as not to carry the same significance of trajectories which are likely to be highly accurate.

Increased observations would be an improvement as occasional unrecognized local pollution events would have less weight on the final estimate. Some local pollution events which are easily identifiable (sudden rapid increase and subsequent decrease in concentrations inconsistent with mixing over regional transport scales) have been removed from the dataset prior to the use of the Kalman filter. However, some high measurements remain which are likely to have resulted from local emissions which we are unable to resolve with 1 degree horizontal resolution. These will have an undesired effect on the filter to the extent that they do not represent the integrated emissions from the length of the trajectory, but rather represent one nearby point source. As we have more measurements to incorporate into the filter, the effects of a few possibly erroneous measurements should have less of an impact on the final result. In addition, if we had enough measurements (more observations with associated trajectories), we would be able to estimate a separate correction factor for each grid cell passed through by a trajectory, rather than a single correction factor for the integrated emissions of all grid cells passed through which is applied equally to each.

While much work remains to be done to utilize this technique with higher accuracy, the measurements and their analysis presented here have yielded observation-based emissions estimates which are an important new contribution to our growing body of knowledge regarding reactive chlorine species in the lower atmosphere.

References

Aucott, M. L., A. McCulloch, T. E. Graedel, G. Kleiman, P. Midgley, and Yi-Fan Li, "Anthropogenic Emissions of Trichloromethane (Chloroform, $CHCl_3$) and Chlorodifluoromethane (HCFC-22): Reactive Chlorine Emissions Inventory", *Journal of Geophysical Research*, **104**, pg. 8,405-8,415, 1999.

Bakwin, P. S., D. F. Hurst, P. P. Tans and J. W. Elkins, "Anthropogenic sources of halocarbons, sulfur hexafluoride, carbon monoxide, and methane in the southeastern United States", *Journal of Geophysical Research*, **102**, pg. 15,915-15,925, 1997.

Ballschmiter, K. "Persistent, ecotoxic, and bioaccumulative compounds and their possible environmental effects." *Pure and Applied Chemistry*, **68**, pg. 1771-1780, 1996.

Colborn, T., F. S. vom Saal, and A. M. Soto. "Developmental effects of endocrine-disrupting chemicals in wildlife and humans." *Env. Health Perspectives.* **101**, pg. 378-384, October, 1993.

Colborn, T., J. Peterson Myers, D. Dumanoski. *Our Stolen Future*. Dutton Books, New York, NY. 1996.

Cunnold, D.M., R.F. Weiss, R.G. Prinn, D.E. Hartley, P.G. Simmonds, P.J. Fraser, B.R. Miller, F.N. Alyea, and L. Porter, GAGE/AGAGE measurements indicating reductions in global emissions of CCl3F and CCl2F2 in 1992-94, *Journal of Geophysical Research*, **102**, pg. 1259-1269, 1997.

Currie, L.A., *Analytical Chemistry*, **40**, pg. 586-593, 1968.

DeMore, W.B., S.P. Sander, D.M. Golden, R. F. Hampson, M.J. Kurylo, C.J. Howard, A.R. Ravishankara, C.E. Kolb, M.J. Molina, *Chemical Kinetics and Photochemical Data for use in Stratospheric Modeling*, JPL publication 97-4, Jet Propulsion Laboratory, Pasadena, California, 1997.

Draxler, R.D., "The accuracy of trajectories during ANATEX calculated using dynamic model analyses versus rawinsonde observations.", *Journal of Applied Meteorology*, **30**, pg. 1446-1467, 1991.

Draxler, R.D., "Trajectory Optimization for Balloon Flight Planning", *Weather Forecasting*, **11**, pg. 111-114, 1996.

Draxler, R.D., and G.D. Hess, "Description of the HYSPLIT-4 Modelling System", *NOAA Technical Memorandum ERL, ARL-224*, Air Resources Laboratory, Silver Springs, Maryland, 1997.

Draxler, R.D., and G.D. Hess, "An Overview of the HYSPLIT-4 Modelling System for Trajectories, Dispersion, and Deposition", *Australian Meteorological Magazine*, **47**, pg. 295-308, 1998.

Elkins, J.W., J.H. Butler, D. F. Hurst, S.A. Montzka, F.L. Moore, and T.M. Thompson, Nitrous Oxide and Halocompounds Group/Climate Monitoring and Diagnostics Laboratory (NOAA/CMDL) web site (http://www.cmdl.noaa.gov/noah/), Boulder, CO, updated data available on anonymous ftp site (file://ftp.cmdl.noaa.gov/noah), 1998.

Fauvarque, J. "The chlorine industry." *Pure and Applied Chemistry*, **68**, pg. 1713-1720, 1996.

Fay, J. and J. Rosenzweig, "An analytical diffusion model for long distance transport of air pollution", *Atmospheric Environment*, **14**, pg. 355-365, 1980.

Frank, H., W. Frank, and H. J. C. Neves, "Airborne C1- and C2-halocarbons at four representative sites in Europe", *Atmospheric Environment*, **25**A(2), pg.257-261, 1991.

Frank, W., H. J. C. Neves, and H. Frank, "Levels of airborne halocarbons at urban and mountain forest sites in Germany and at the Atlantic coast.", *Chemosphere*, **23**(5), pg.609-626, 1991.

Galal-Gorchev, H. "Chlorine in water disinfection." *Pure and Applied Chemistry*, **68**, pg. 1731-1735, 1996.

Gay, B.W., P.L. Hanst, J.J. Bufalini, and R.C. Noonan. "Atmospheric Oxidation of Chlorinated Ethylenes", *Environmental Science and Technology*, **10**, pg. 58, 1976.

Gelb, A., J.F. Kasper, Jr., R.A. Nash, Jr., C.F. Price, and A.A. Sutherland, Jr., Applied Optimal Estimation, M.I.T. Press, Massachusetts Institute of Technology, Cambridge, Massachusetts, 13th Printing, 1994.

Graedel, T.E. and W.C. Keene. "The budget and cycle of Earth's natural chlorine." *Pure and Applied Chemistry*, **68**, pg. 1689-1697, 1996.

Graedel, T.E. and William C. Keene. "Preface: The Reactive Chlorine Emissions Inventory." *Journal of Geophysical Research*, **104**, pg. 8,331-8,332, 1999.

Graff, G. "The chlorine controversy." *Technology Review*, January 1995.

Harkov, R., B. Kebbekus, J. W. Bozzelli, and P. J. Lioy, "Measurement of selected volatile organic compounds at three locations in New Jersey during the summer season", *Journal of the Air Pollution Control Association*, **33**, pg. 1177-1183, 1983.

Hartley, D.E., and R.G. Prinn, "On the feasibility of determining surface emissions of trace gases using an inverse method in a three-dimensional chemical transport model", *Journal of Geophysical Research*, **98**, pg. 5183-5198, 1993.

Hartwell, T. D., E. D. Pellizzari, R. L. Perritt, R. W. Whitmore, H. S. Zelon, L. S. Sheldon, and C. M. Sparacino, "Results from the total exposure assessment methodology

(TEAM) study in selected communities in Northern and Southern California", *Atmospheric Environment*, **21**, pg. 1995-2004, 1987.

Hecht, B., Th. Class, and K. Ballschmiter, "Chemistry of organic traces in air X. Variations of volatile halocarbons in ambient air in Southern Germany.", *Fresenius Z Analytical Chemistry*, **327**, pg. 45-46, 1987

Hileman, B. "Concerns broaden over chlorine and chlorinated hydrocarbons.", *Chem. & Eng. News*, pg. 11-20, April, 1993.

Hurst, D. F., P. S. Bakwin, R.C. Myers and J. W. Elkins, "Behavior of trace gas mole fractions on a very tall tower in North Carolina", *Journal of Geophysical Research*, **102**, pg. 8825-8835,1997.

Keene, W.C., M. Aslam K. Khalil, David J. Erickson, III, Archie McCulloch, Thomas E. Graedel, Jurgen M. Lobert, Michael L. Aucott, Sun Ling Gong, David B. Harper, Gary Kleiman, Valentin Koropolov, Pauline Midgley, Robert M. Moore, Christophe Seuzaret, William T. Sturges, Leonard A. Barrie, Jennifer A. Logan and Yi Fan Li, "Composite Global Emissions of Reactive Chlorine from Anthropogenic and Natural Sources: Reactive Chlorine Emissions Inventory", *Journal of Geophysical Research*, **104**, pg. 8,429-8,440, 1999.

Kessel, M. and K. Bachmann, "Long term nonmethane hydrocarbon and halogenated hydrocarbon measurements at three West German sampling sites.", *Fresenius Z Analytical Chemistry*, **339**, pg. 754-756, 1991.

Khalil, M. A. K., R.M. Moore, , D.B. Harper, J.M. Lobert, D.J. Erickson, III, V. Koropolov, , W.T. Sturges, and W.C. Keene, "Natural emissions of chlorine-containing gases: Reactive Chlorine Emissions Inventory", *Journal of Geophysical Research*, **104**, pg. 8,333-8,346, 1999.

Kirchmer, C.J., "Estimation of Detection Limits for Environmental Analytical Procedures", *Detection in Analytical chemistry*, Lloyd A. Currie, Ed., ACS Symposium series: **361**, American Chemical Society, 1988.

Lillian, D., H.B. Singh, A. Appleby, L. Lobban, R. Arnts, R. Gumpert, R. Hauge, J. Toomey, J. Kazazis, M. Antell, D. Hansen and B. Scott, "Atmospheric fates of halogenated compounds.", Environmental Science and Technology, **9**, pg. 1042-1048, 1975.

Lobert, Jurgen M., William C. Keene, Jennifer A. Logan and Rosmarie Yevich, "Global chlorine emissions from biomass burning: Reactive Chlorine Emissions Inventory", *Journal of Geophysical Research*, **104**, pg. 8,373-8,389, 1999.

Mahowald, N.M., R.G. Prinn, and P.J. Rasch, "Deducing CCl_3F emissions using an inverse method and chemical transport models with assimilated winds", *Journal of Geophysical Research*, **102**, pg. 28,153-28,168, 1997.

Makide, Y., A. Yokihata, Y. Kubo, and T. Tominaga, "Atmospheric concentrations of halocarbons in Japan in 1979-1986", *The Bulletin of the Chemical Society of Japan*, **60**, pg. 571-574, 1987.

McCulloch, Archie, Michael L. Aucott, Thomas E. Graedel, Gary Kleiman, Pauline M. Midgley and Yi-Fan Li, "Industrial emissions of trichloroethene, tetrachloroethene, and dichloromethane: Reactive Chlorine Emissions Inventory", *Journal of Geophysical Research*, **104**, pg. 8,417-8,427, 1999.

Molina, M. J., and F. S. Rowland. "Stratospheric sink for chlorofluoromethanes: Chlorine atom catalyzed destruction of ozone." *Nature*, **249**, pg. 810-812, 1974.

Montzka, S.A., J.H. Butler, R.C. Myers, T.M. Thompson, T.H. Swanson, A.D. Clarke, L.T. Lock, and J.W. Elkins. "Decline in the Tropospheric Abundance of Halogen from Halocarbons: Implications for Stratospheric Ozone Depletion", Science, **272**, pg. 1318, 1996.

Pellizari, E. D., "Analysis for organic vapor emissions near industrial and chemical waste disposal sites", Environmental Science and Technology, **16**, pg. 781-785, 1982.

Prinn, R. G., R. F. Weiss, B. Miller, J. Huang, F. N. Alyea, D. M. Cunnold, P. J. Fraser, D. E. Hartley, and P. G. Simmonds. "Atmospheric Trends and Lifetime of CH3CCl3 and Global OH Concentrations." *Science*, **269**, pg. 187-192, 1995.

Prinn, R. G., R. F. Weiss, P. J. Fraser, P. G. Simmonds, D. M. Cunnold, F. N. Alyea, S. O'Doherty, P. Salameh, B. Miller, J. Huang, D. E. Hartley, C. Harth, P. Steele, and P. Midgley. "A History of Chemically and Radiatively Important Gases in Air deduced from ALE/GAGE/AGAGE." Journal of Geophysical Research, (submitted, 1999a).

Prinn, R., "Measurement Equation for Trace Chemicals in Fluids and Solution of its Inverse", in *Inverse Methods in Biogeochemical Cycles*, Eds. P. Kashibhatla et al., Geophysical Monographs, American Geophysical Union, (in press, 1999b).

Prinn, R.G., R. Zander, D.M. Cunnold, J.W. Elkins, A. Engel, P.J. Fraser, M.R. Gunson, M.K.W. Ko, E. Mahieu, P.M. Midgley, J.M. Russell III, C.M. Volk, R.F. Weiss et al., Long-Lived Ozone-Related Compounds, Chapter 1, In *Scientific Assessment of Ozone Depletion: 1998*, World Meteorological Organization Global Ozone Research and Monitoring Project, Geneva, Report 44, pg. 1.1-1.54, 1999c.

Putnam, S. W. and J. D. Graham. "Chemicals versus microbials in drinking water: A decision sciences perspective." *Journal of American Waste and Water Association.* March, 1993.

Singh, H. B., L. J. Salas, A. J. Smith and H. Shigeishi, "Measurement of some potentially hazardous organic chemicals in urban environments", *Atmospheric Environment*, **15**, pg. 601-612, 1981.

Singh, H. B., L. J. Salas, and R. E. Stiles, "Distribution of selected gaseous organic mutagens and suspect carcinogens in ambient air.", *Environmental Science and Technology*, **16**, pg. 872-880, 1982.

Singh, H. B., L. J. Salas, and R. E. Stiles, "Selected man-made halogenated chemicals in the air and oceanic environment.", *Journal of Geophysical Research*, **88**, pg. 3675-3683, 1983.

Singh, H. B., A. N. Thakur, Y. E. Chen, and M. Kanakidou, "Tetrachloroethylene as an indicator of low Cl atom concentrations in the troposphere.", *Geophysical Research Letters*, **23**, pg. 1529-1532, 1996.

Sprengnether, M.M., *An Active Titration Method for the Local Measurement of Tropospheric Hydroxyl Radical*, Ph.D. Thesis, Massachusetts Institute of Technology, Center for Global Change Science Report No. 16, Pg.156-169, 1992.

Stunder, B.J.B., "An Assessment of the Quality of Forecast Trajectories", *Journal of Applied Meteorology*, **35**, (1996).

Taylor, J.R., *An Introduction to Error Analysis*, University Science Books, Mill Valley, CA, pg. 62, 1982.

Urano, K., K. Kawamoto, Y. Abi, M. Otake, "Chlorinated organic compounds in urban air in Japan.", *The Science of the Total Environment*, **74**, pg. 121-131, 1988.

Warneck, P. *Chemistry of the Natural Atmosphere*, Academic Press, San Diego, CA. pg. 178-194 , 1988.

Wiedmann, T. O., B. Guthner, T. J. Class, and K. Ballschmiter, "Global distribution of Tetrachloroethene in the Troposphere: Measurements and Modeling", *Environmental Science and Technology*, **28**, pg. 2321-2329, 1994.

Appendix A. *Images of Halocarbon Detection System at Nahant, Massachusetts*

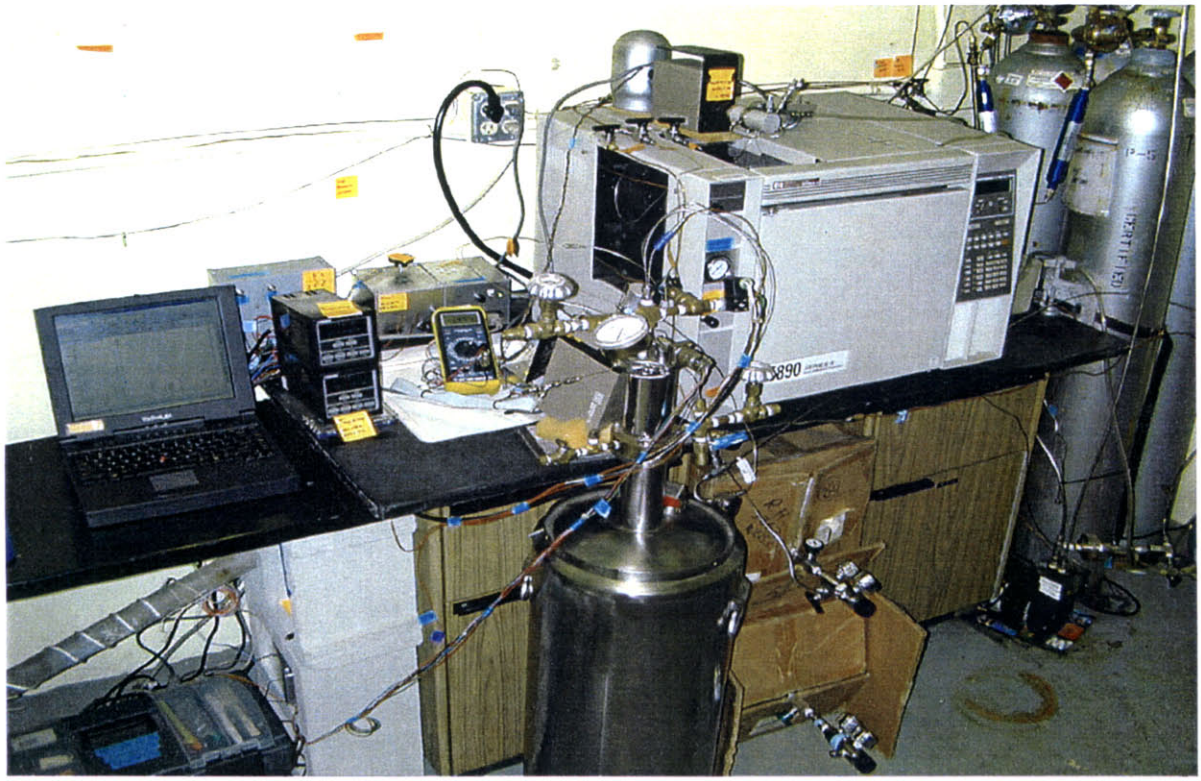

Halocarbon Detection System at Nahant, MA. Instrumentation includes automated cryogenic collection system (in the foreground) coupled with a Hewlett-Packard Series II Gas Chromatograph with Electron Capture Detector (on the bench).

East Point, Nahant, Massachusetts. Northeastern University's Marine Science Center can be seen on the right and the John B. Murphy bunker can be seen in the center of the frame.

Air inlet on the roof of the bunker. 1/4" stainless steel tubing extends from the laboratory up through a ventilation shaft to this meteorological instrument tower. Our air inlet can be seen extending out to the left just over halfway up the tower. A teflon funnel is inverted at the end of the stainless steel tube to prevent water from being sucked into the tube.

Appendix B. *Ambient Halocarbon Mole Fractions at Nahant, Massachusetts*

We present the entire set of ambient mole fraction measurements for four of the chlorocarbon species measured at the Nahant field site. Instrumentation used to obtain these measurements is described in Chapter 2 and shown in Appendix A. In all plots, measurements have been calibrated against the National Center for Atmospheric Research (NCAR) or Scripps Institution of Oceanography (SIO) absolute calibration scale (or an average of the two for compounds measured in comon) as described in Chapter 2. Measurements are shown as blue diamonds. Open blue diamonds represent observations which were measured below the limit of detection (LOD) as defined by Currie (1968). Red diamonds represent measurements which were not used for the emission estimation procedures described in this thesis. These measurements which were observed to contain very high levels of the compounds of interest, but of short duration, were deemed inconsistent with regional scale pollution as described in Chapter 4.

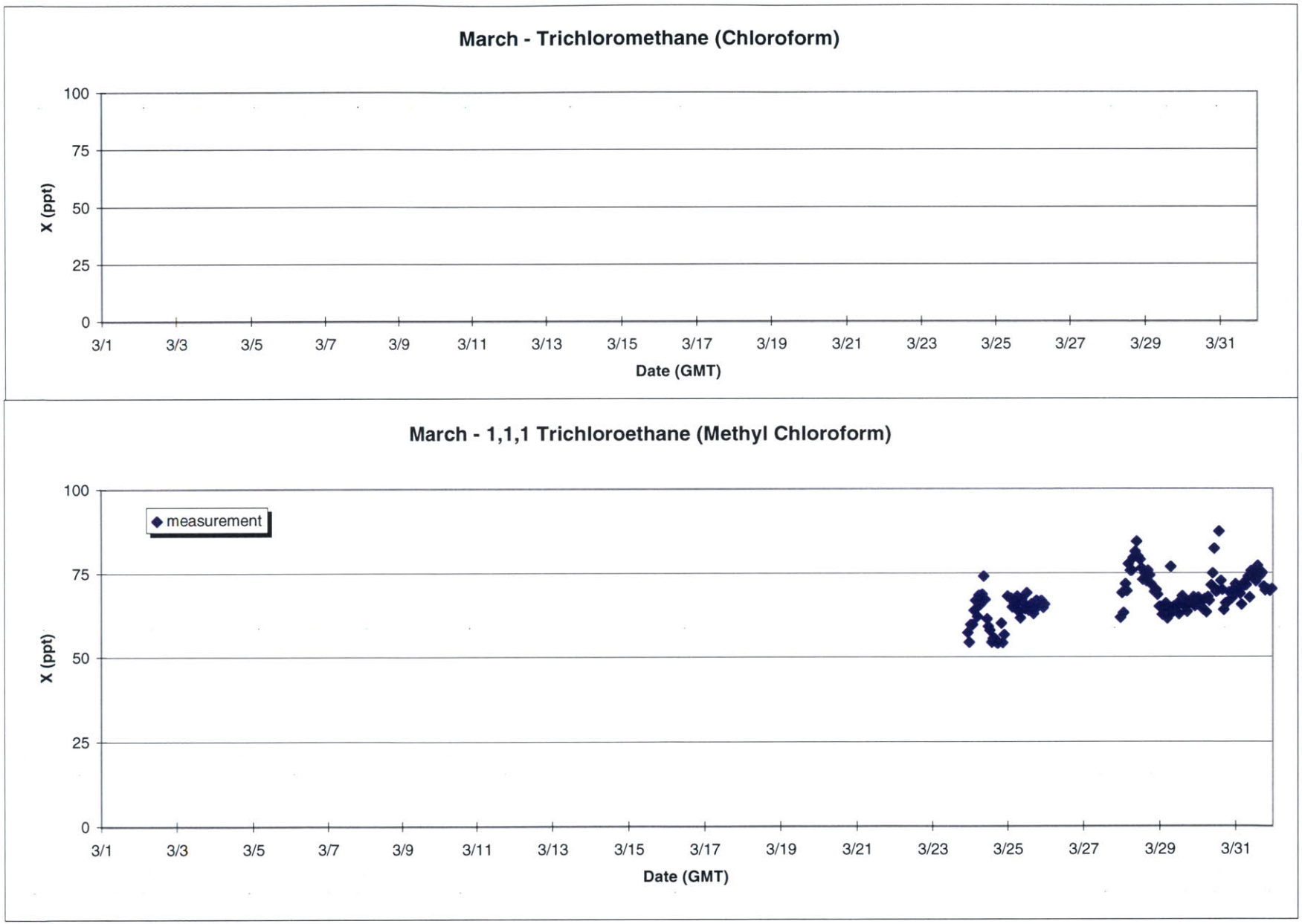
March - Trichloromethane (Chloroform)
100
75
50
25
0
X (ppt)
3/1
3/3
3/5
3/7
3/9
3/11
3/13
3/15
3/17
3/19
3/21
3/23
3/25
3/27
3/29
3/31
Date (GMT)
March - 1,1,1 Trichloroethane (Methyl Chloroform)
measurement
100
75
50
25
0
X (ppt)
3/1
3/3
3/5
3/7
3/9
3/11
3/13
3/15
3/17
3/19
3/21
3/23
3/25
3/27
3/29
3/31
Date (GMT)

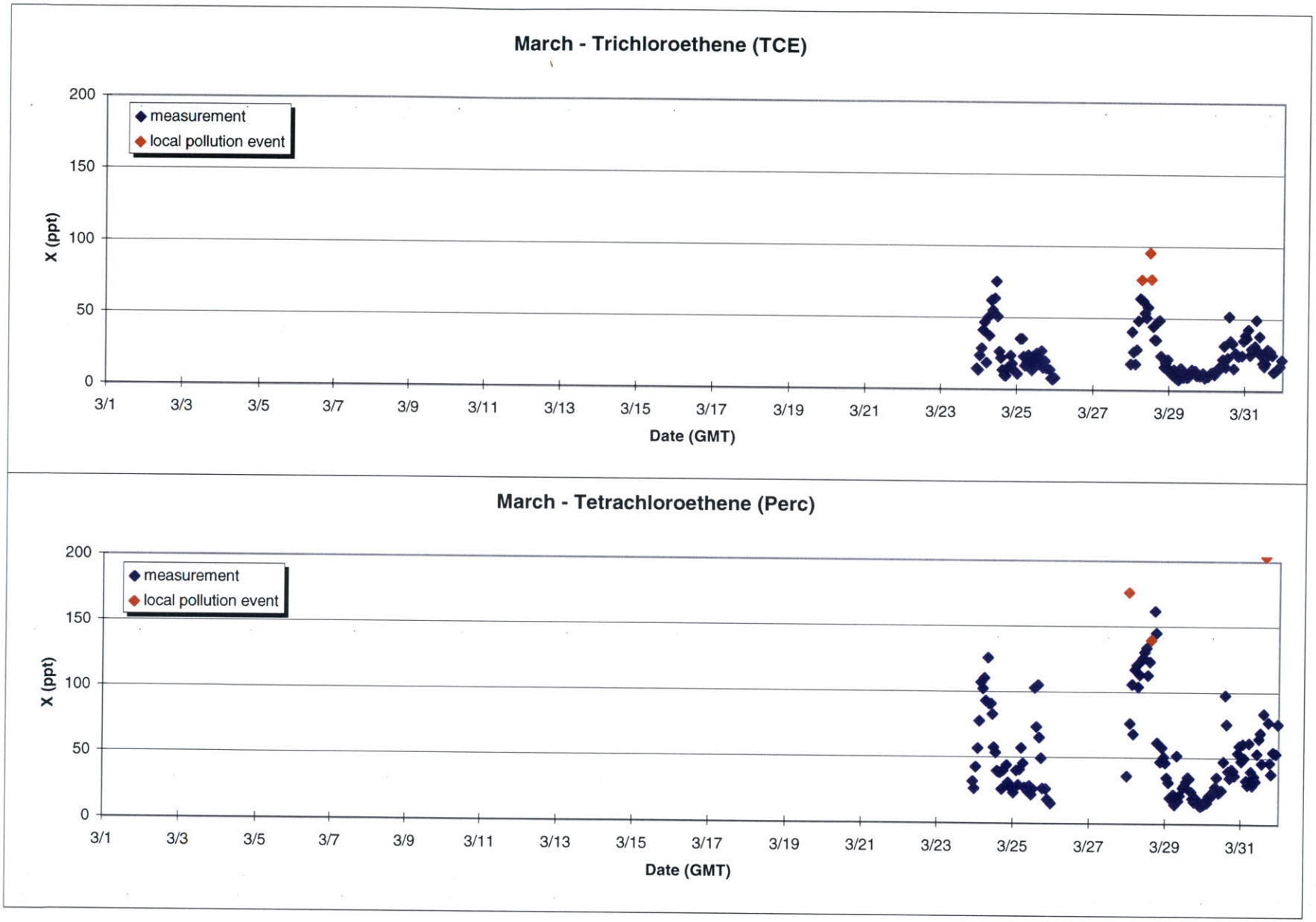
March - Trichloroethene (TCE)
measurement
local pollution event
X (ppt)
200
150
100
50
0
3/1
3/3
3/5
3/7
3/9
3/11
3/13
3/15
3/17
3/19
3/21
3/23
3/25
3/27
3/29
3/31
Date (GMT)
March - Tetrachloroethene (Perc)
measurement
local pollution event
X (ppt)
200
150
100
50
0
3/1
3/3
3/5
3/7
3/9
3/11
3/13
3/15
3/17
3/19
3/21
3/23
3/25
3/27
3/29
3/31
Date (GMT)

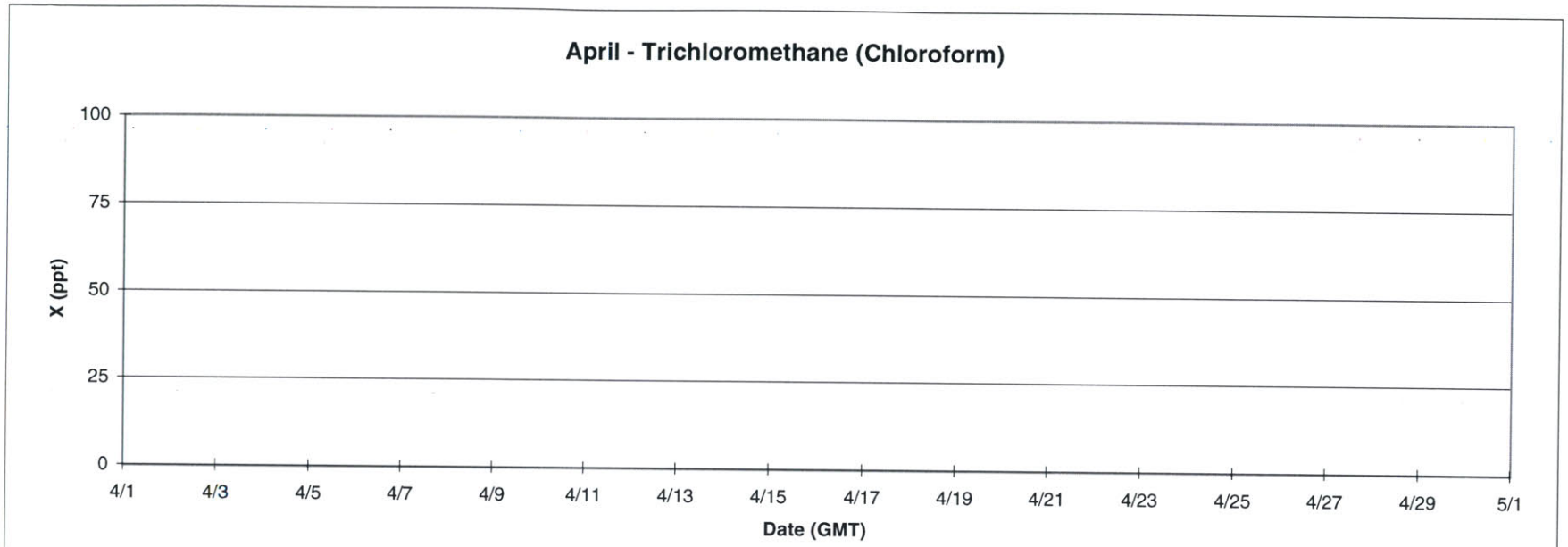
April - Trichloromethane (Chloroform)
100
75
50
25
0
X (ppt)
4/1
4/3
4/5
4/7
4/9
4/11
4/13
4/15
4/17
4/19
4/21
4/23
4/25
4/27
4/29
5/1
Date (GMT)

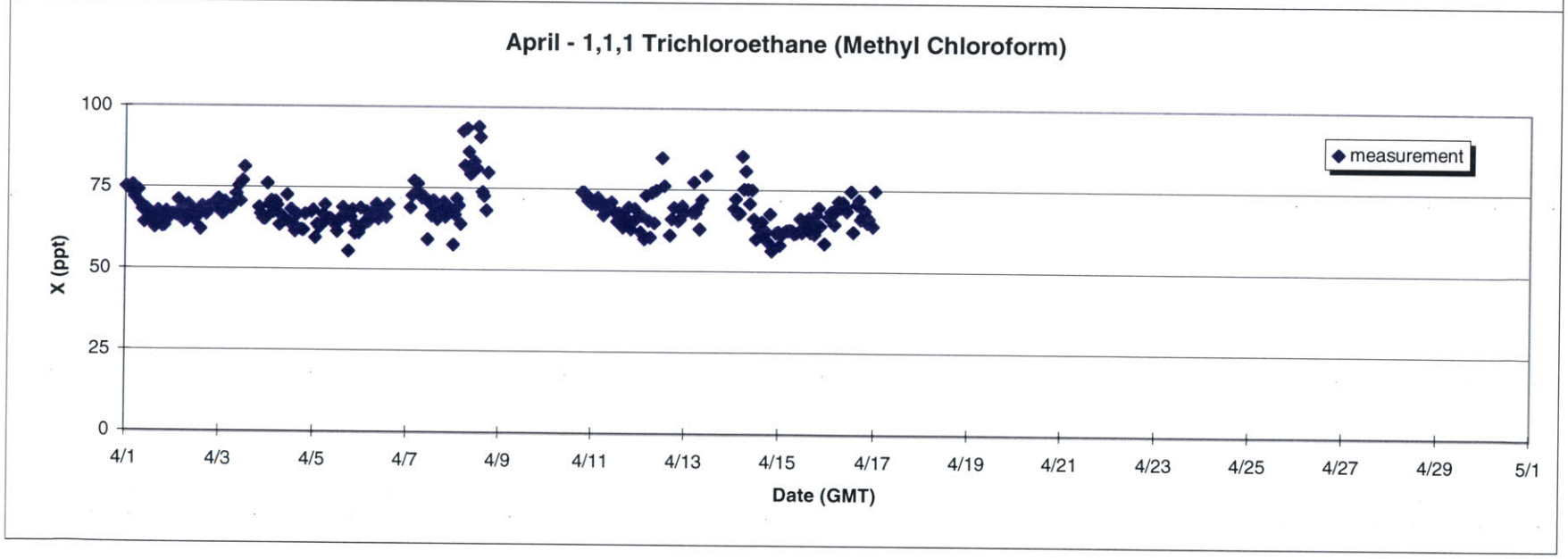
April - 1,1,1 Trichloroethane (Methyl Chloroform)
100
75
50
25
0
X (ppt)
measurement
4/1
4/3
4/5
4/7
4/9
4/11
4/13
4/15
4/17
4/19
4/21
4/23
4/25
4/27
4/29
5/1
Date (GMT)

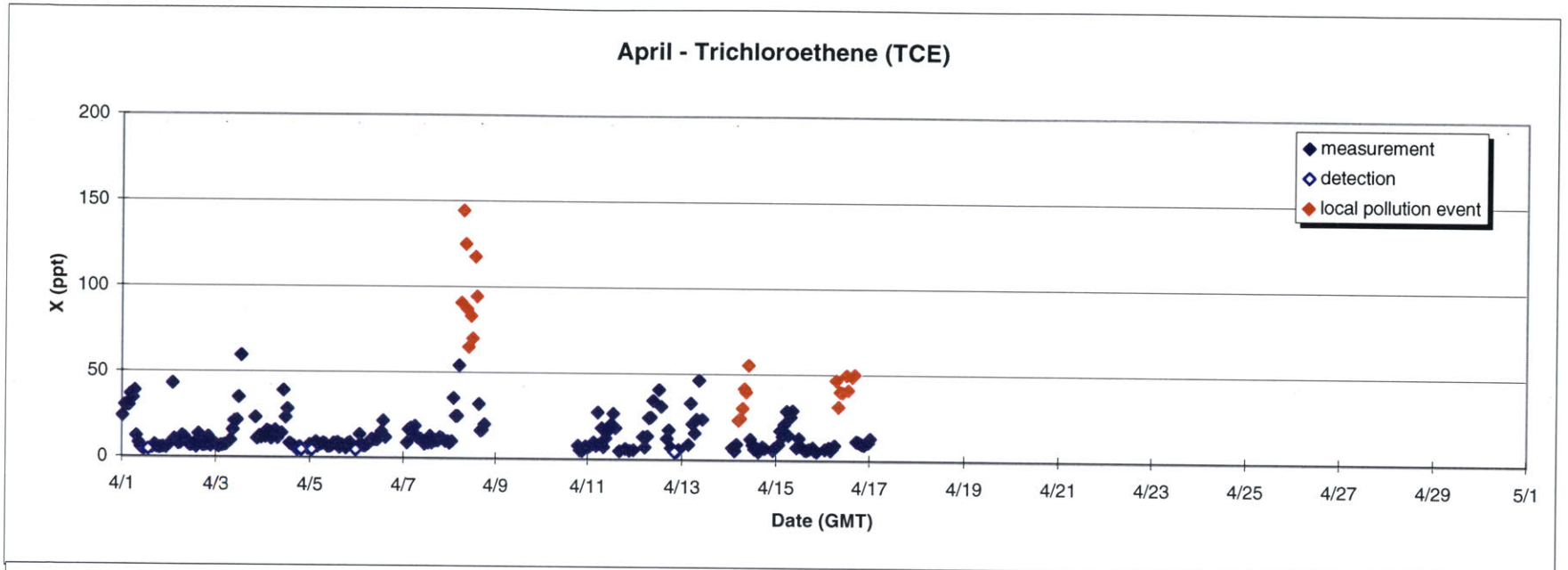
April - Trichloroethene (TCE)
200
150
100
50
0
X (ppt)
measurement
detection
local pollution event
4/1
4/3
4/5
4/7
4/9
4/11
4/13
4/15
4/17
4/19
4/21
4/23
4/25
4/27
4/29
5/1
Date (GMT)

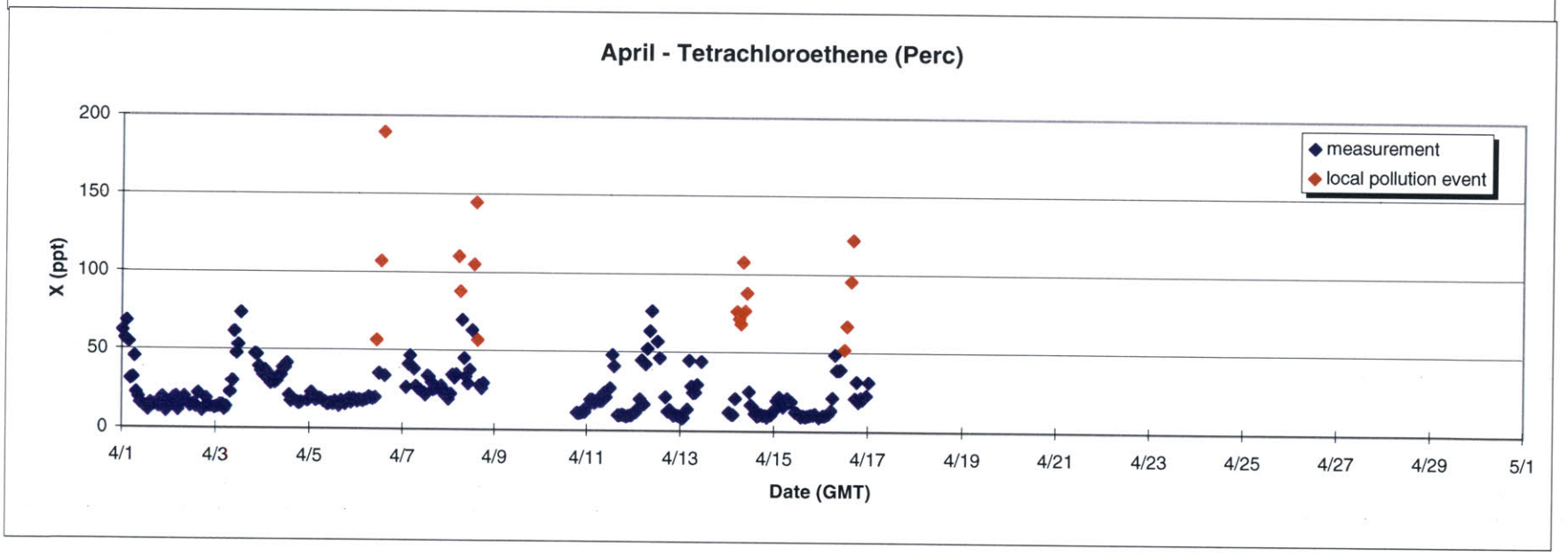
April - Tetrachloroethene (Perc)
200
150
100
50
0
X (ppt)
measurement
local pollution event
4/1
4/3
4/5
4/7
4/9
4/11
4/13
4/15
4/17
4/19
4/21
4/23
4/25
4/27
4/29
5/1
Date (GMT)

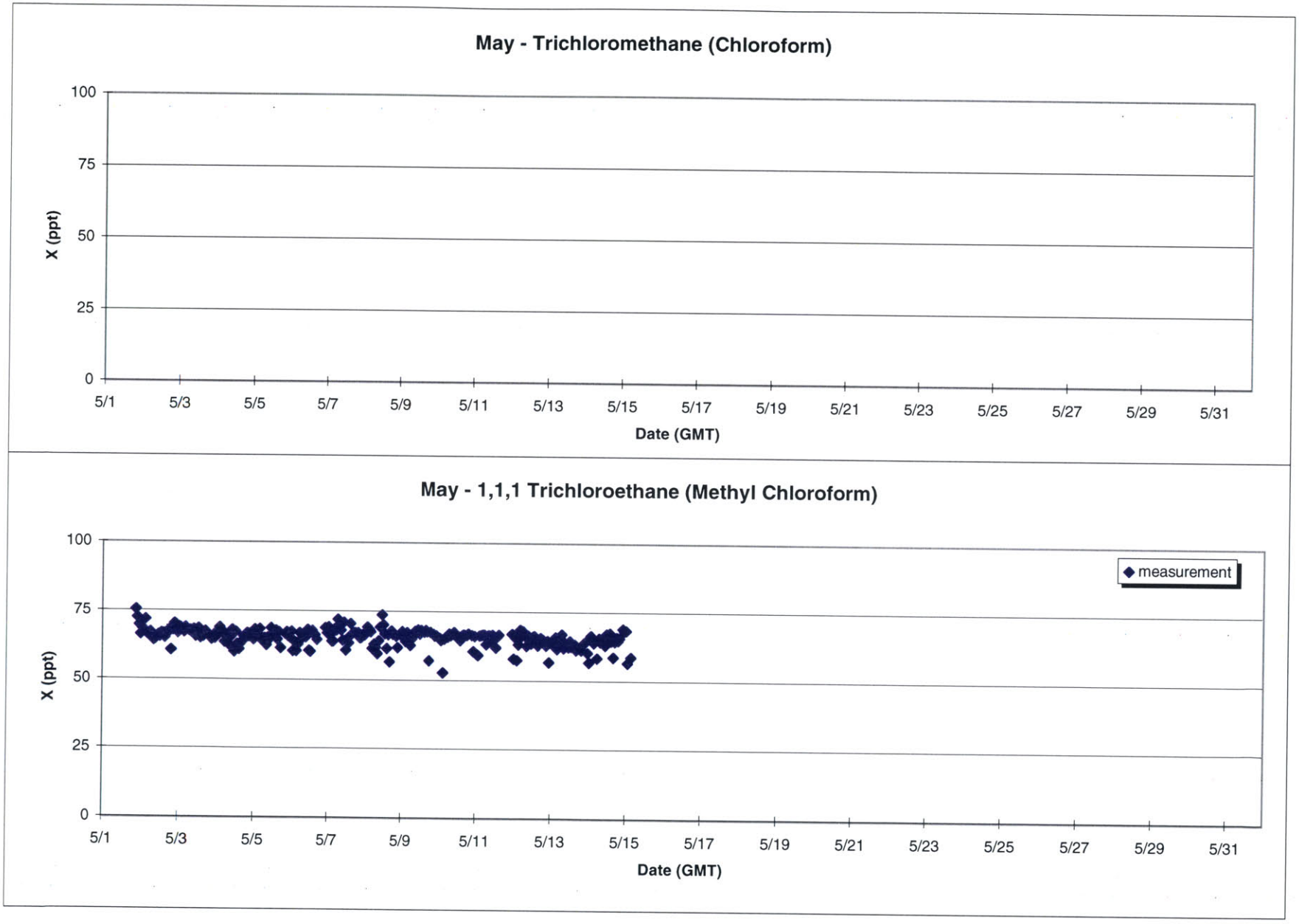
May - Trichloromethane (Chloroform)
100
75
50
25
0
X (ppt)
5/1
5/3
5/5
5/7
5/9
5/11
5/13
5/15
5/17
5/19
5/21
5/23
5/25
5/27
5/29
5/31
Date (GMT)
May - 1,1,1 Trichloroethane (Methyl Chloroform)
100
75
50
25
0
X (ppt)
measurement
5/1
5/3
5/5
5/7
5/9
5/11
5/13
5/15
5/17
5/19
5/21
5/23
5/25
5/27
5/29
5/31
Date (GMT)

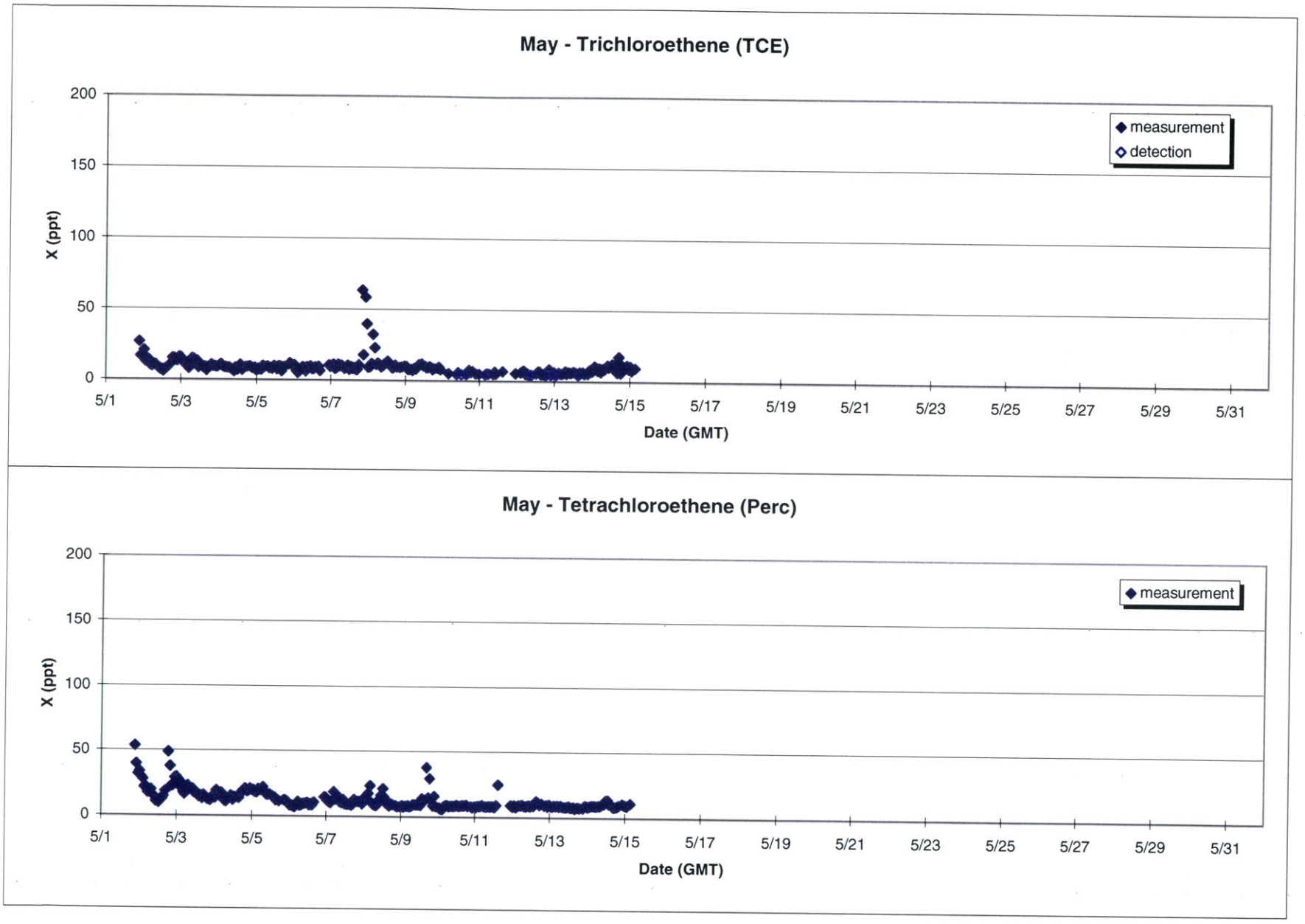
May - Trichloroethene (TCE)
200
150
100
50
0
X (ppt)
measurement
detection
5/1
5/3
5/5
5/7
5/9
5/11
5/13
5/15
5/17
5/19
5/21
5/23
5/25
5/27
5/29
5/31
Date (GMT)
May - Tetrachloroethene (Perc)
200
150
100
50
0
X (ppt)
measurement
5/1
5/3
5/5
5/7
5/9
5/11
5/13
5/15
5/17
5/19
5/21
5/23
5/25
5/27
5/29
5/31
Date (GMT)

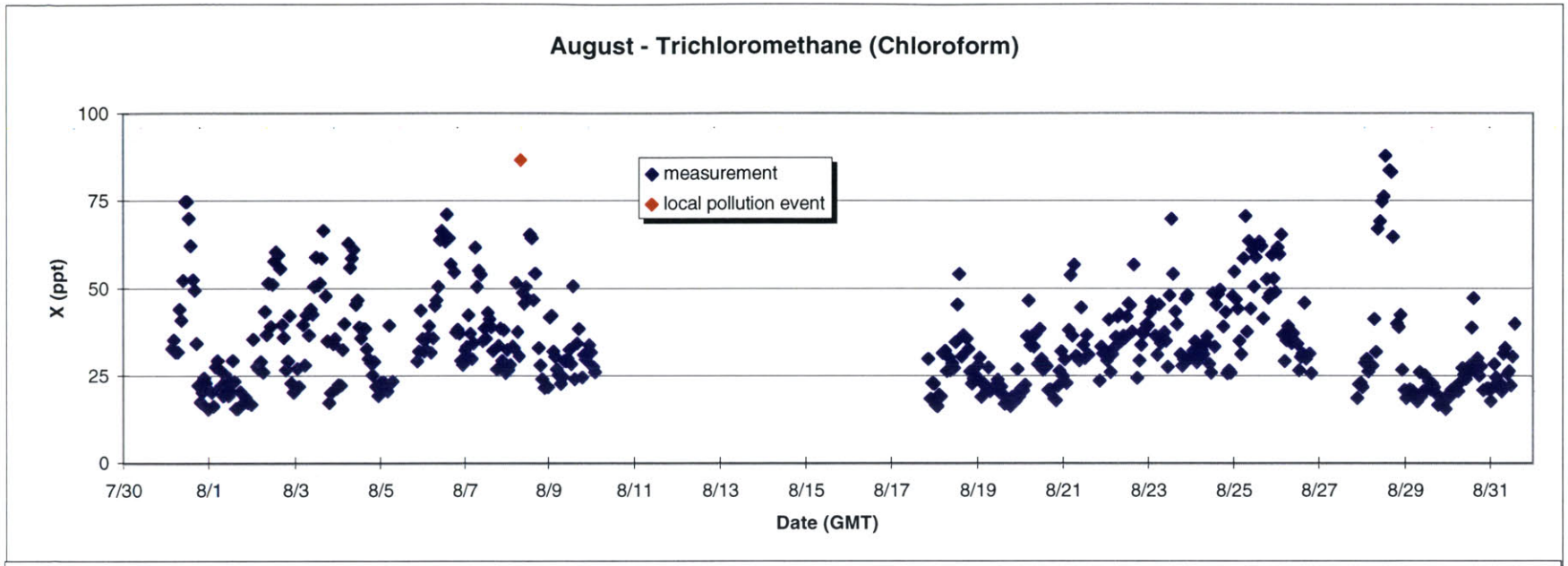
August - Trichloromethane (Chloroform)
100
75
50
25
0
X (ppt)
measurement
local pollution event
7/30
8/1
8/3
8/5
8/7
8/9
8/11
8/13
8/15
8/17
8/19
8/21
8/23
8/25
8/27
8/29
8/31
Date (GMT)

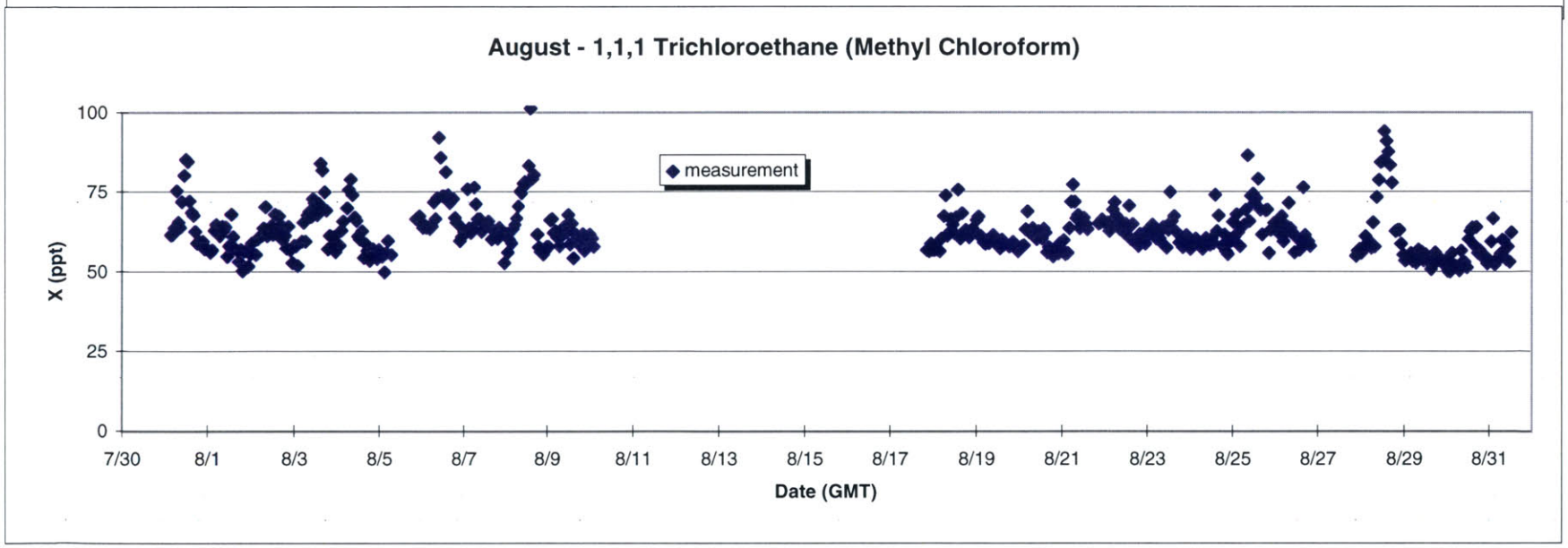
August - 1,1,1 Trichloroethane (Methyl Chloroform)
100
75
50
25
0
X (ppt)
measurement
7/30
8/1
8/3
8/5
8/7
8/9
8/11
8/13
8/15
8/17
8/19
8/21
8/23
8/25
8/27
8/29
8/31
Date (GMT)

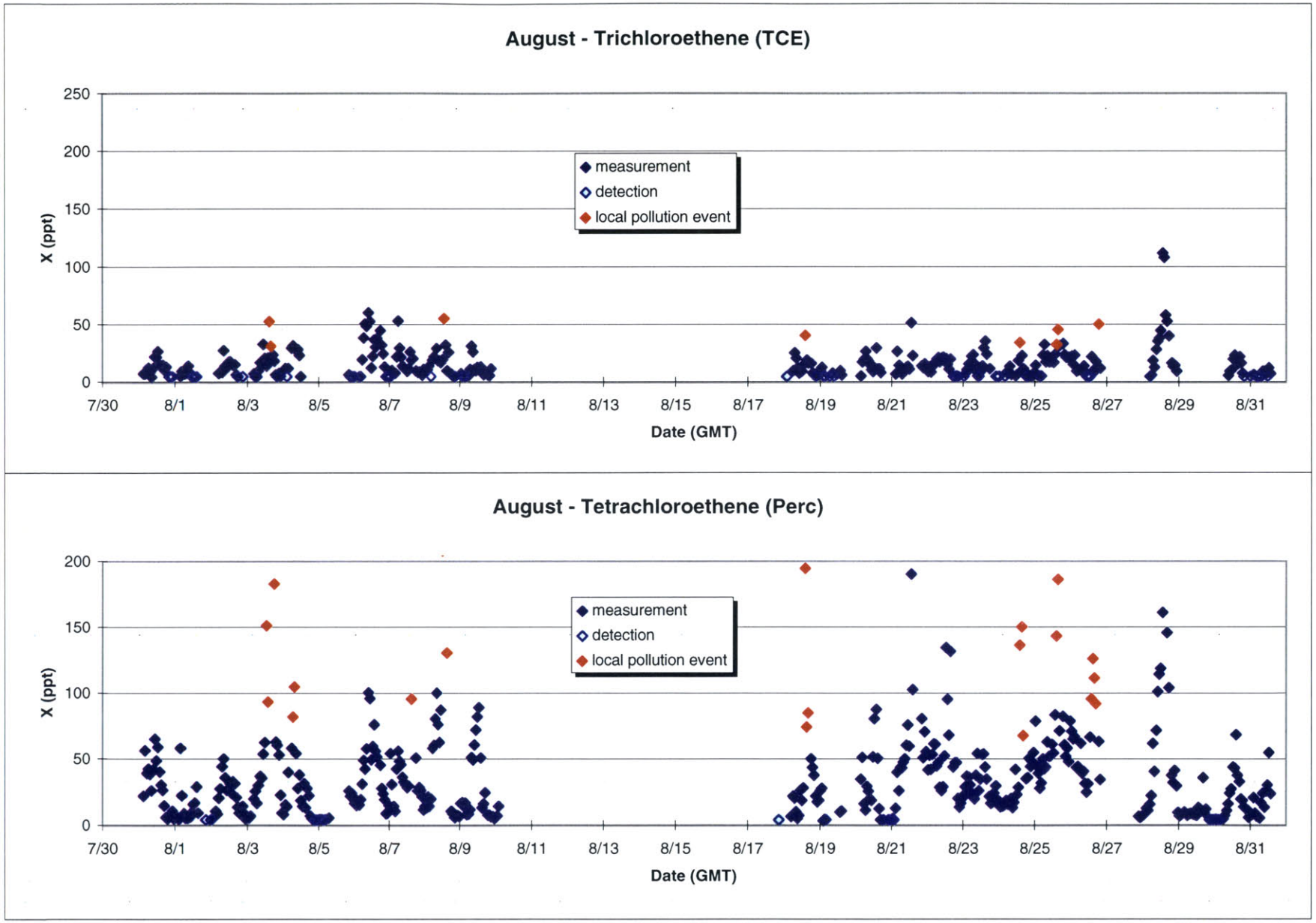
August - Trichloroethene (TCE)
250
200
150
100
50
0
X (ppt)
measurement
detection
local pollution event
7/30
8/1
8/3
8/5
8/7
8/9
8/11
8/13
8/15
8/17
8/19
8/21
8/23
8/25
8/27
8/29
8/31
Date (GMT)
August - Tetrachloroethene (Perc)
200
150
100
50
0
X (ppt)
measurement
detection
local pollution event
7/30
8/1
8/3
8/5
8/7
8/9
8/11
8/13
8/15
8/17
8/19
8/21
8/23
8/25
8/27
8/29
8/31
Date (GMT)

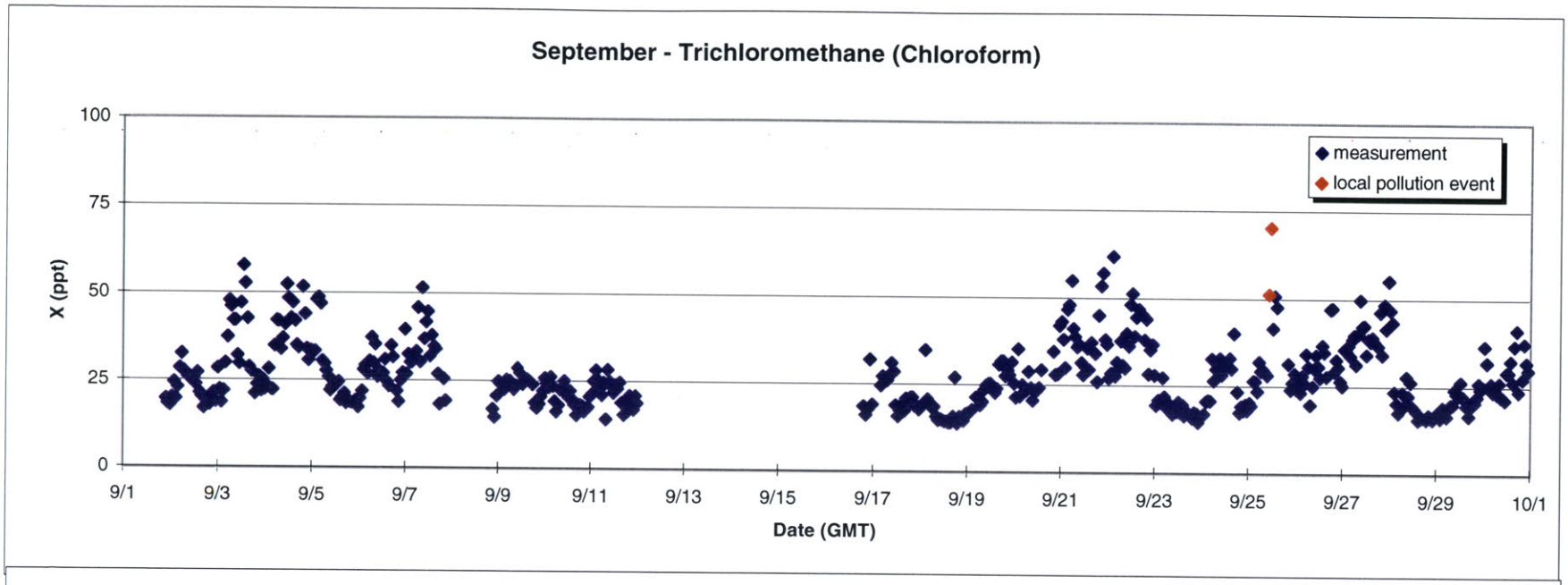
September - Trichloromethane (Chloroform)
100
75
50
25
0
X (ppt)
measurement
local pollution event
9/1
9/3
9/5
9/7
9/9
9/11
9/13
9/15
9/17
9/19
9/21
9/23
9/25
9/27
9/29
10/1
Date (GMT)

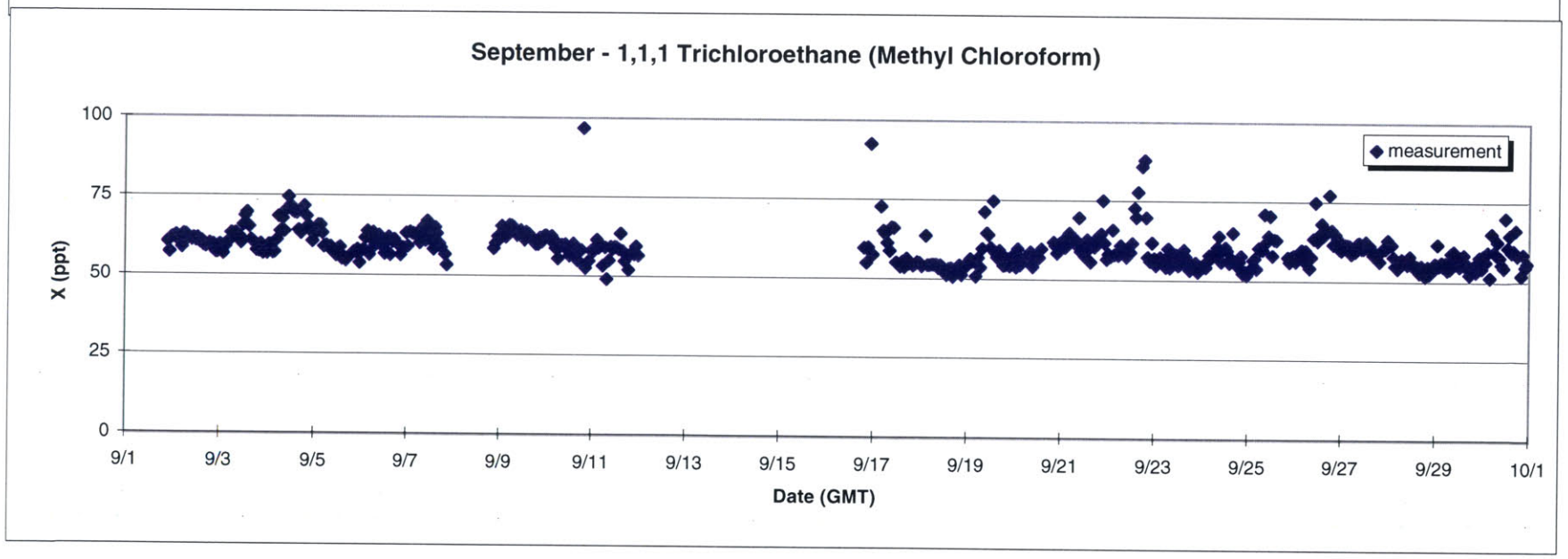
September - 1,1,1 Trichloroethane (Methyl Chloroform)
100
75
50
25
0
X (ppt)
measurement
9/1
9/3
9/5
9/7
9/9
9/11
9/13
9/15
9/17
9/19
9/21
9/23
9/25
9/27
9/29
10/1
Date (GMT)

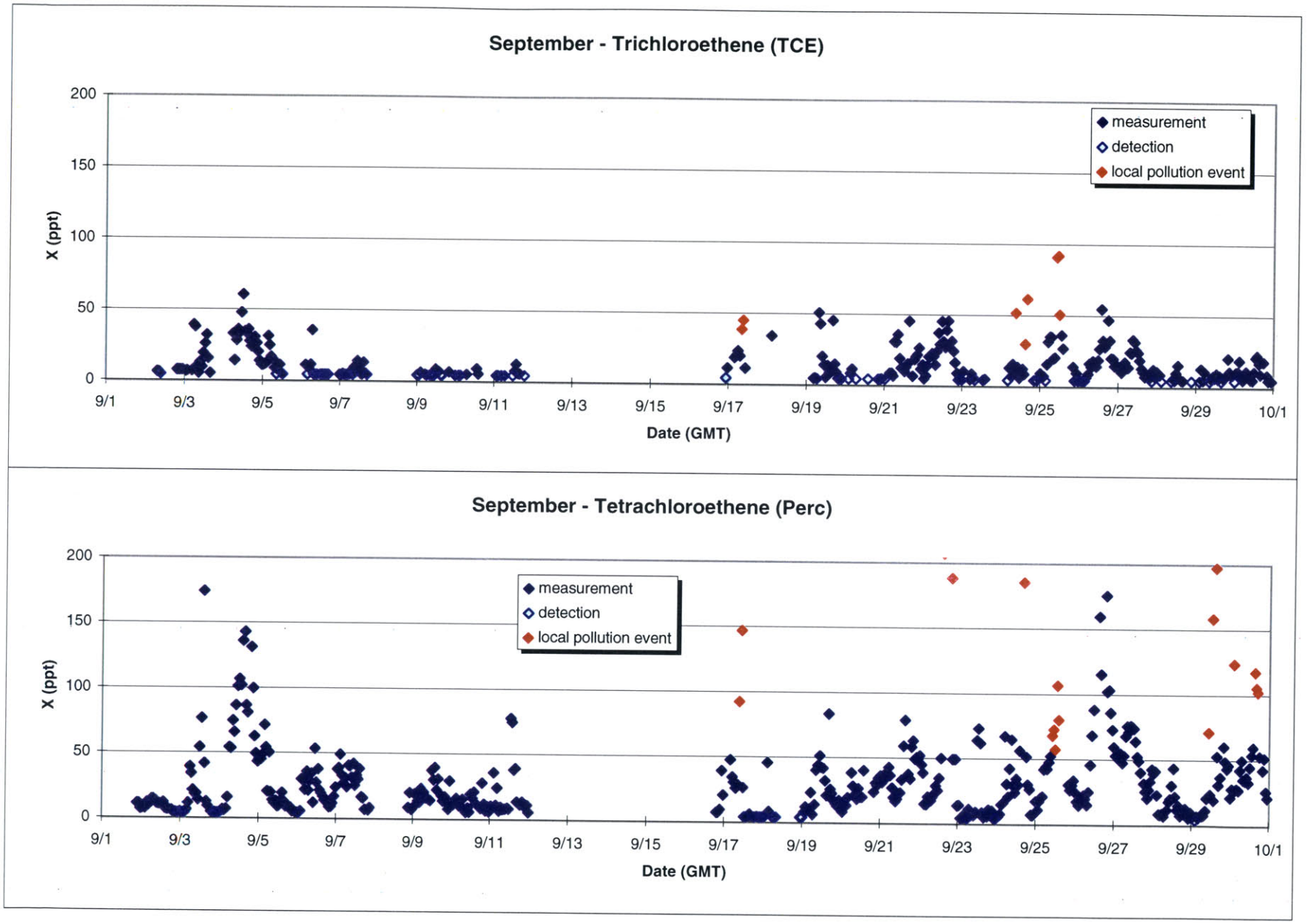
September - Trichloroethene (TCE)
200
150
100
50
0
X (ppt)
measurement
detection
local pollution event
9/1
9/3
9/5
9/7
9/9
9/11
9/13
9/15
9/17
9/19
9/21
9/23
9/25
9/27
9/29
10/1
Date (GMT)
September - Tetrachloroethene (Perc)
200
150
100
50
0
X (ppt)
measurement
detection
local pollution event
9/1
9/3
9/5
9/7
9/9
9/11
9/13
9/15
9/17
9/19
9/21
9/23
9/25
9/27
9/29
10/1
Date (GMT)

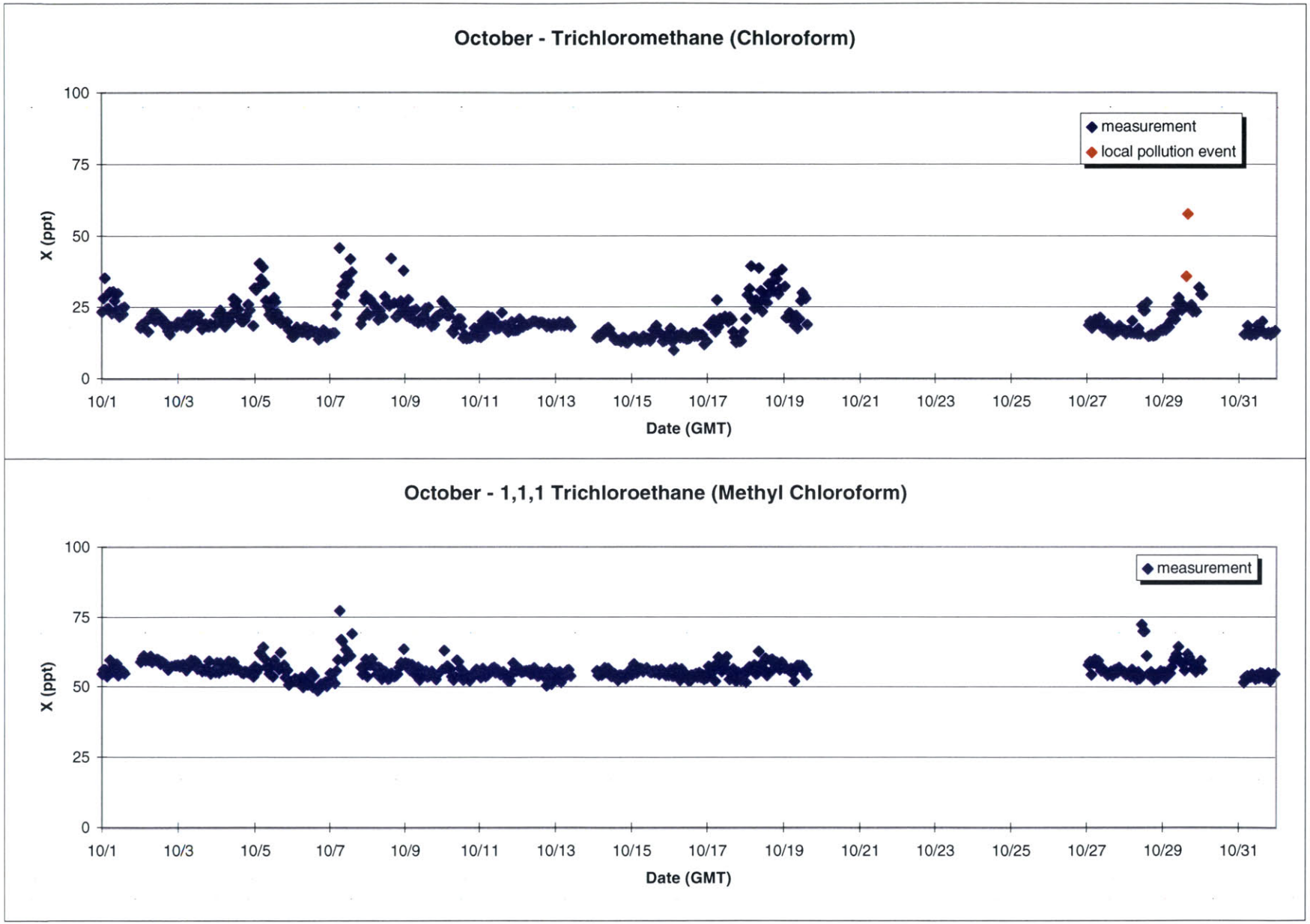
October - Trichloromethane (Chloroform)
100
75
50
25
0
X (ppt)
measurement
local pollution event
10/1
10/3
10/5
10/7
10/9
10/11
10/13
10/15
10/17
10/19
10/21
10/23
10/25
10/27
10/29
10/31
Date (GMT)
October - 1,1,1 Trichloroethane (Methyl Chloroform)
100
75
50
25
0
X (ppt)
measurement
10/1
10/3
10/5
10/7
10/9
10/11
10/13
10/15
10/17
10/19
10/21
10/23
10/25
10/27
10/29
10/31
Date (GMT)

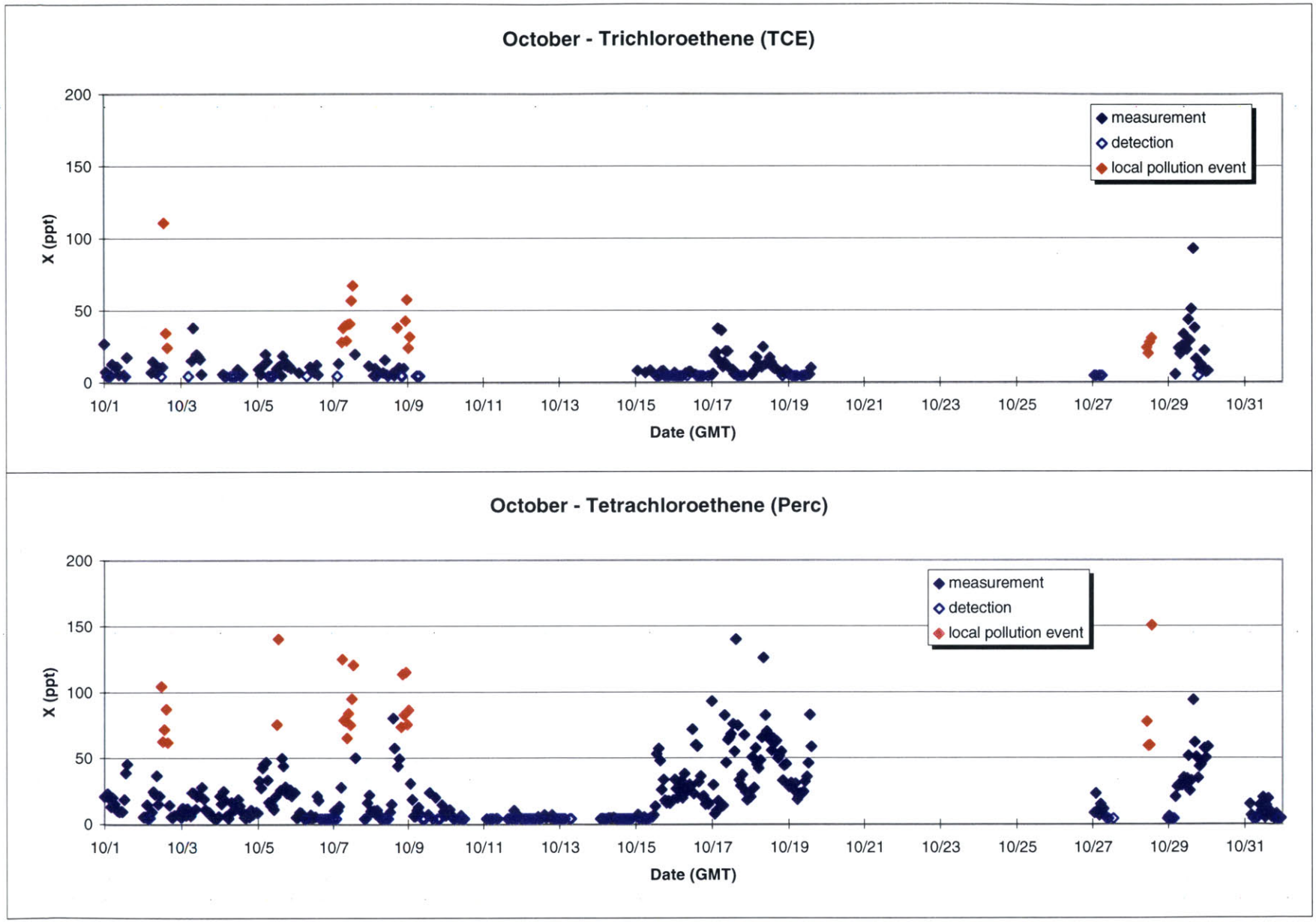
October - Trichloroethene (TCE)
200
150
100
50
0
X (ppt)
measurement
detection
local pollution event
10/1
10/3
10/5
10/7
10/9
10/11
10/13
10/15
10/17
10/19
10/21
10/23
10/25
10/27
10/29
10/31
Date (GMT)
October - Tetrachloroethene (Perc)
200
150
100
50
0
X (ppt)
measurement
detection
local pollution event
10/1
10/3
10/5
10/7
10/9
10/11
10/13
10/15
10/17
10/19
10/21
10/23
10/25
10/27
10/29
10/31
Date (GMT)

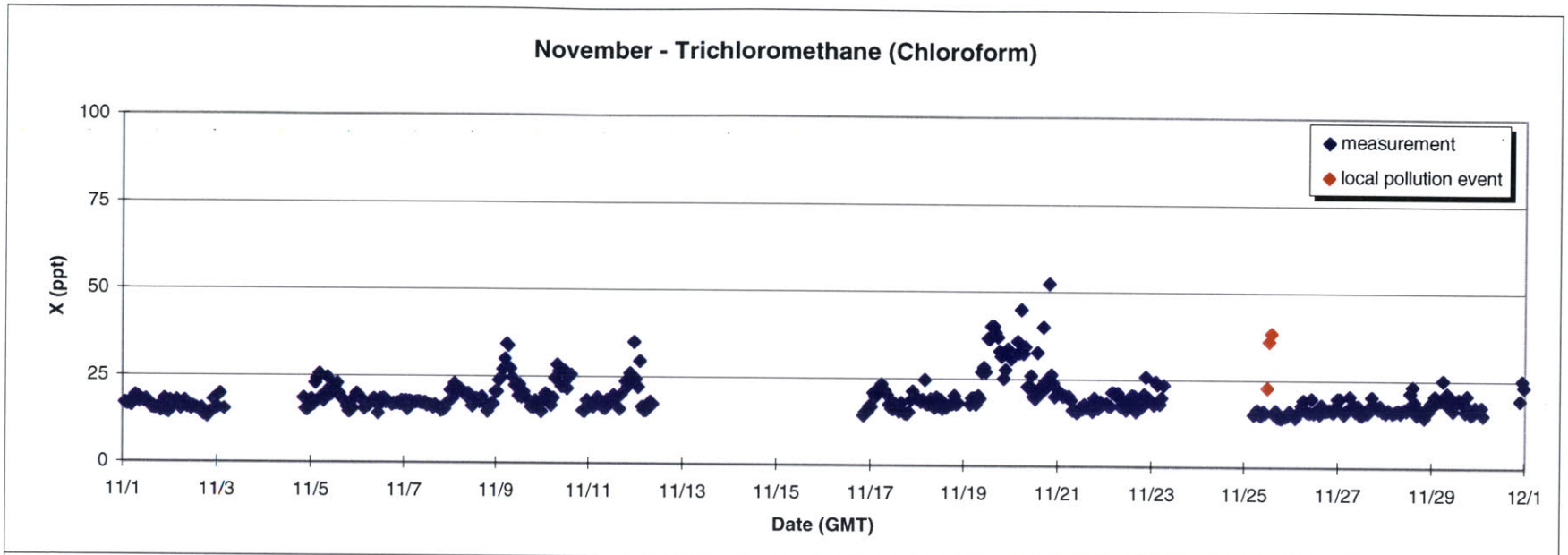
November - Trichloromethane (Chloroform)
100
75
50
25
0
X (ppt)
measurement
local pollution event
11/1
11/3
11/5
11/7
11/9
11/11
11/13
11/15
11/17
11/19
11/21
11/23
11/25
11/27
11/29
12/1
Date (GMT)

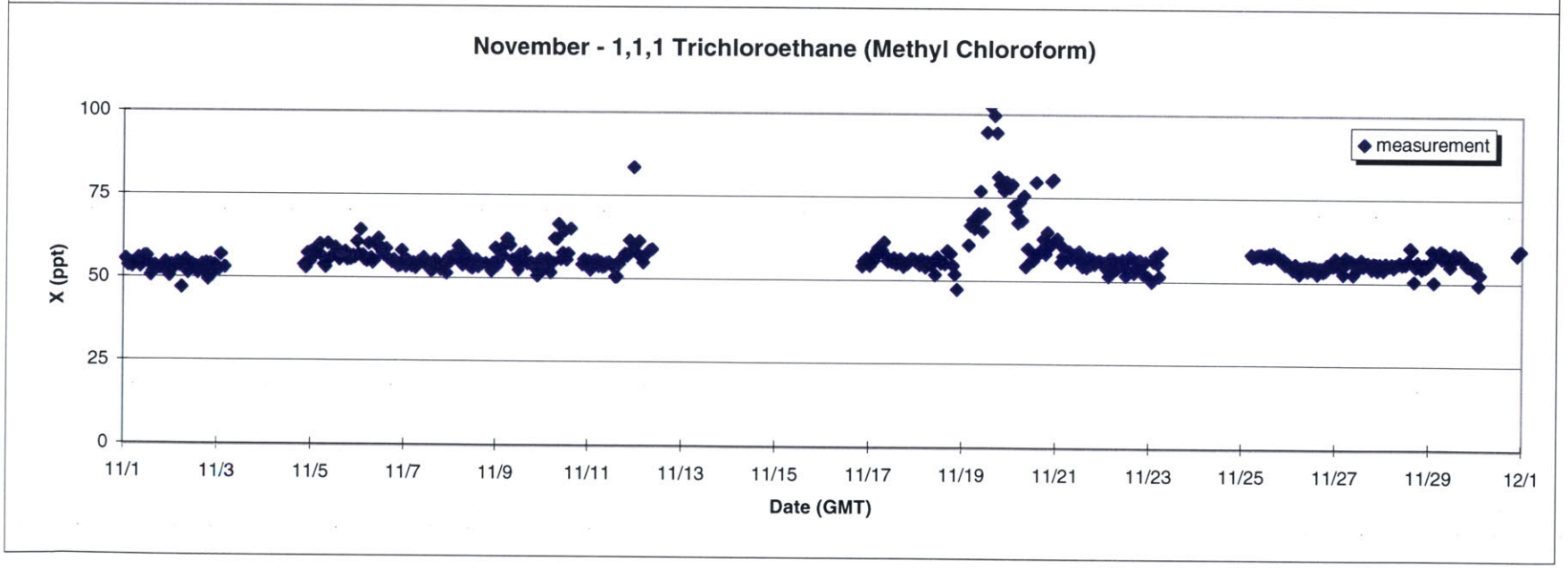
November - 1,1,1 Trichloroethane (Methyl Chloroform)
100
75
50
25
0
X (ppt)
measurement
11/1
11/3
11/5
11/7
11/9
11/11
11/13
11/15
11/17
11/19
11/21
11/23
11/25
11/27
11/29
12/1
Date (GMT)

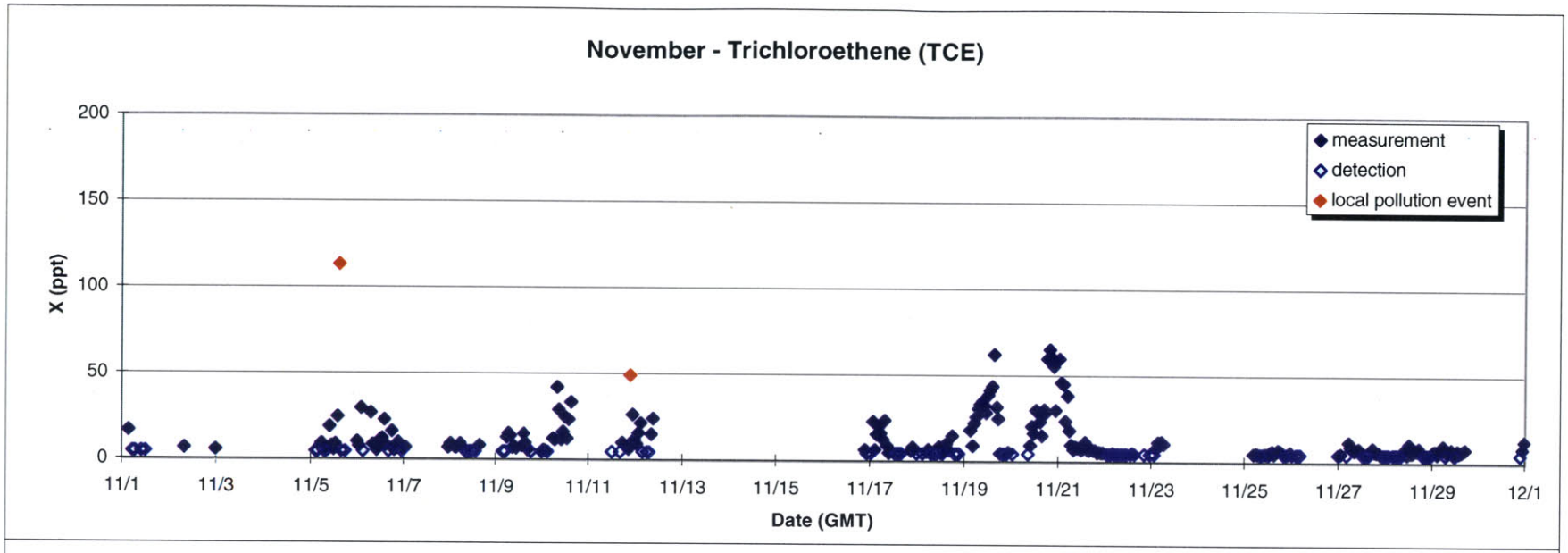
November - Trichloroethene (TCE)
200
150
100
50
0
X (ppt)
measurement
detection
local pollution event
11/1
11/3
11/5
11/7
11/9
11/11
11/13
11/15
11/17
11/19
11/21
11/23
11/25
11/27
11/29
12/1
Date (GMT)

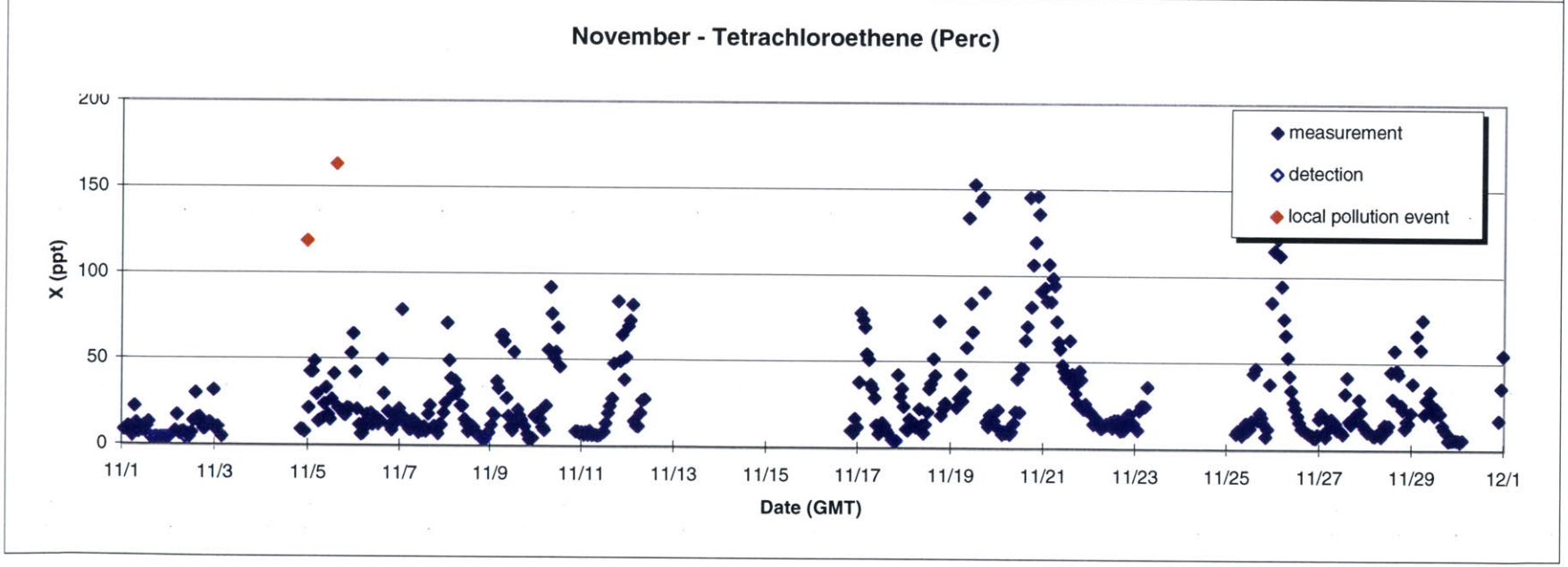
November - Tetrachloroethene (Perc)
200
150
100
50
0
X (ppt)
measurement
detection
local pollution event
11/1
11/3
11/5
11/7
11/9
11/11
11/13
11/15
11/17
11/19
11/21
11/23
11/25
11/27
11/29
12/1
Date (GMT)

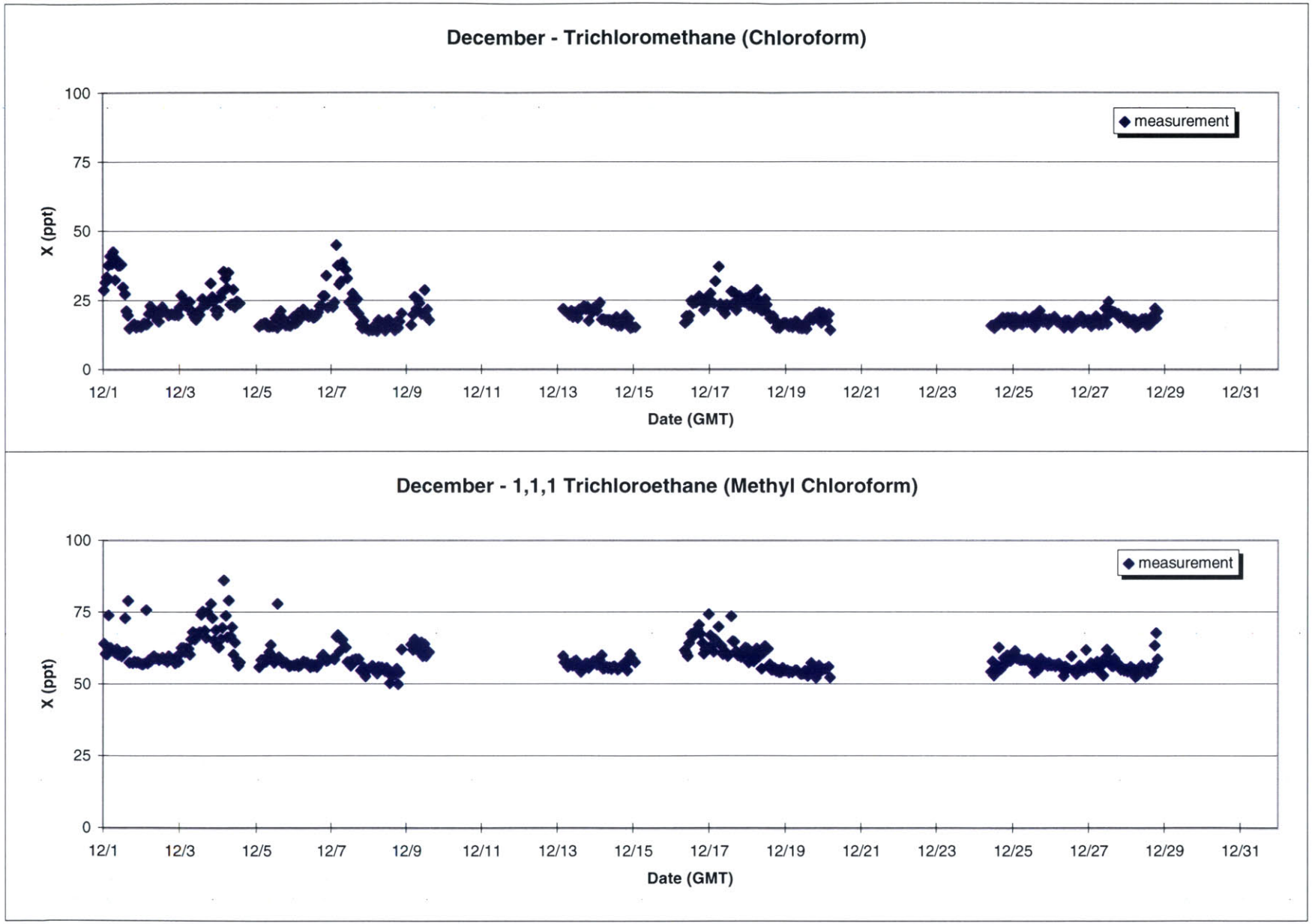
December - Trichloromethane (Chloroform)
100
75
50
25
0
X (ppt)
measurement
12/1
12/3
12/5
12/7
12/9
12/11
12/13
12/15
12/17
12/19
12/21
12/23
12/25
12/27
12/29
12/31
Date (GMT)
December - 1,1,1 Trichloroethane (Methyl Chloroform)
100
75
50
25
0
X (ppt)
measurement
12/1
12/3
12/5
12/7
12/9
12/11
12/13
12/15
12/17
12/19
12/21
12/23
12/25
12/27
12/29
12/31
Date (GMT)

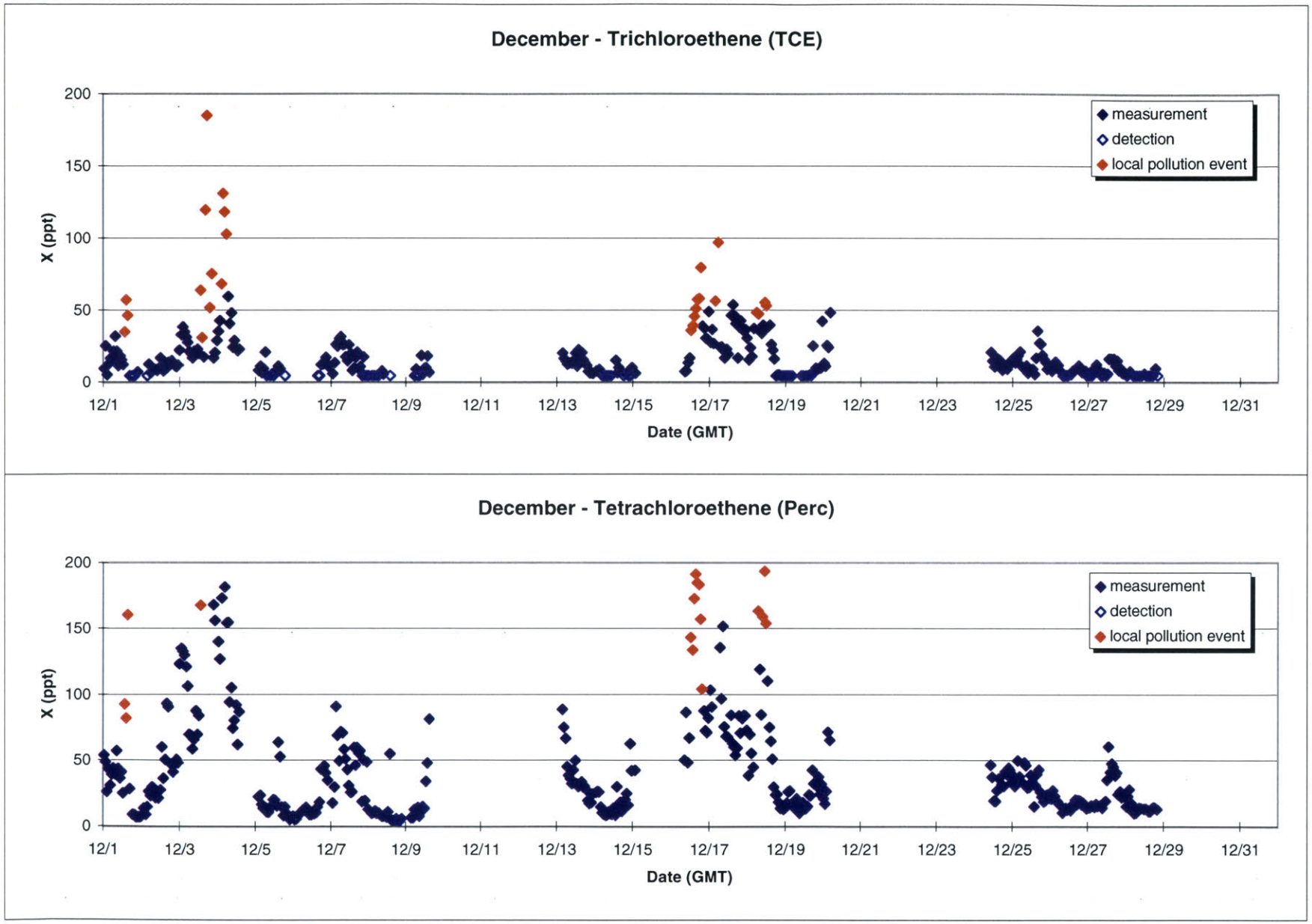
December - Trichloroethene (TCE)
200
150
100
50
0
X (ppt)
12/1
12/3
12/5
12/7
12/9
12/11
12/13
12/15
12/17
12/19
12/21
12/23
12/25
12/27
12/29
12/31
Date (GMT)
measurement
detection
local pollution event
December - Tetrachloroethene (Perc)
200
150
100
50
0
X (ppt)
12/1
12/3
12/5
12/7
12/9
12/11
12/13
12/15
12/17
12/19
12/21
12/23
12/25
12/27
12/29
12/31
Date (GMT)
measurement
detection
local pollution event

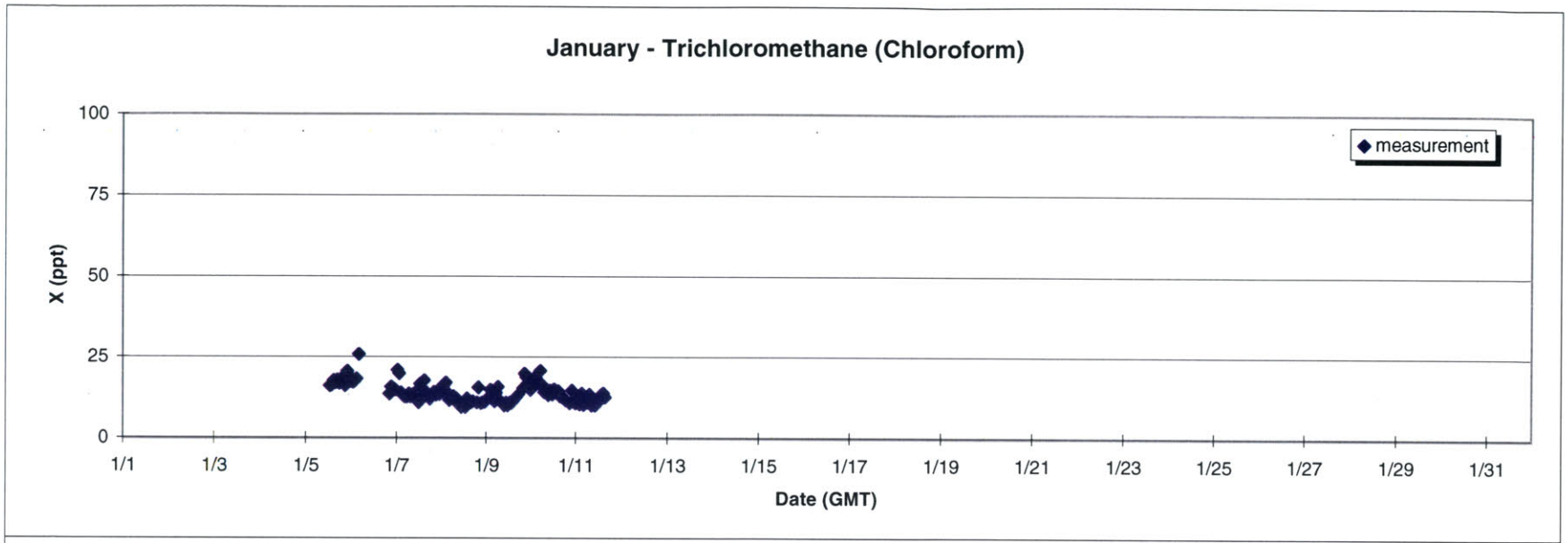
January - Trichloromethane (Chloroform)
100
75
50
25
0
X (ppt)
measurement
1/1
1/3
1/5
1/7
1/9
1/11
1/13
1/15
1/17
1/19
1/21
1/23
1/25
1/27
1/29
1/31
Date (GMT)

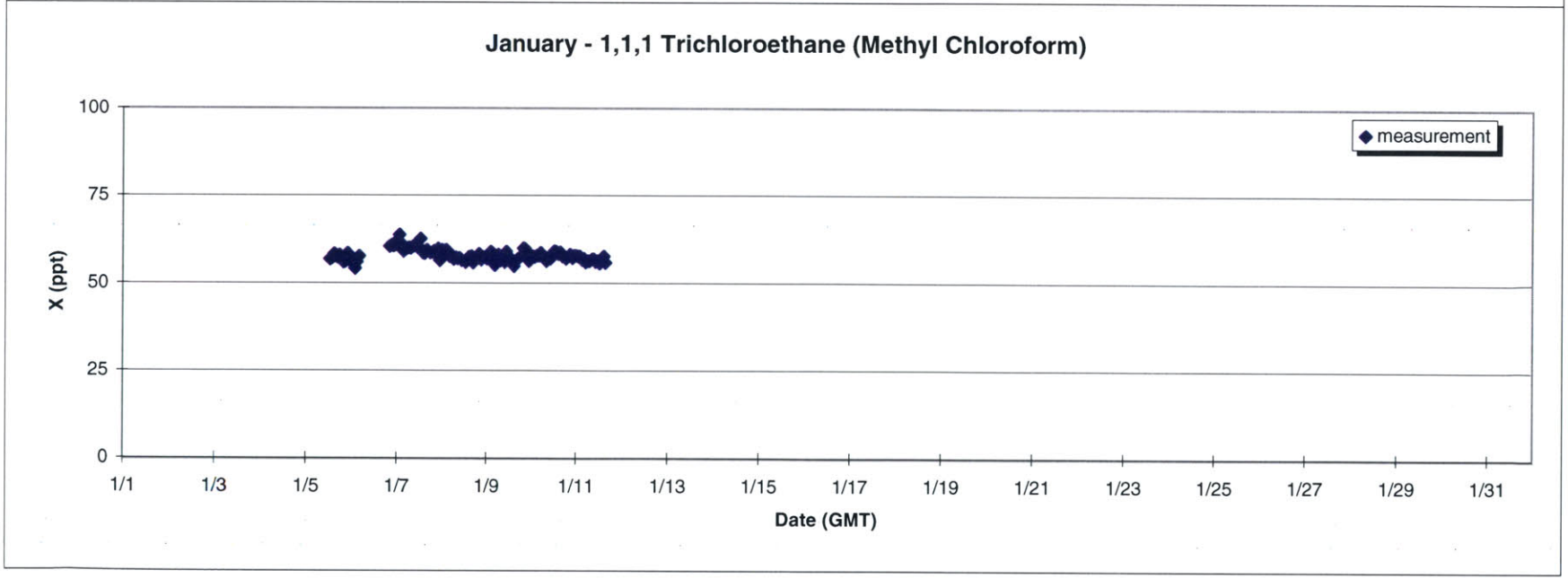
January - 1,1,1 Trichloroethane (Methyl Chloroform)
100
75
50
25
0
X (ppt)
measurement
1/1
1/3
1/5
1/7
1/9
1/11
1/13
1/15
1/17
1/19
1/21
1/23
1/25
1/27
1/29
1/31
Date (GMT)

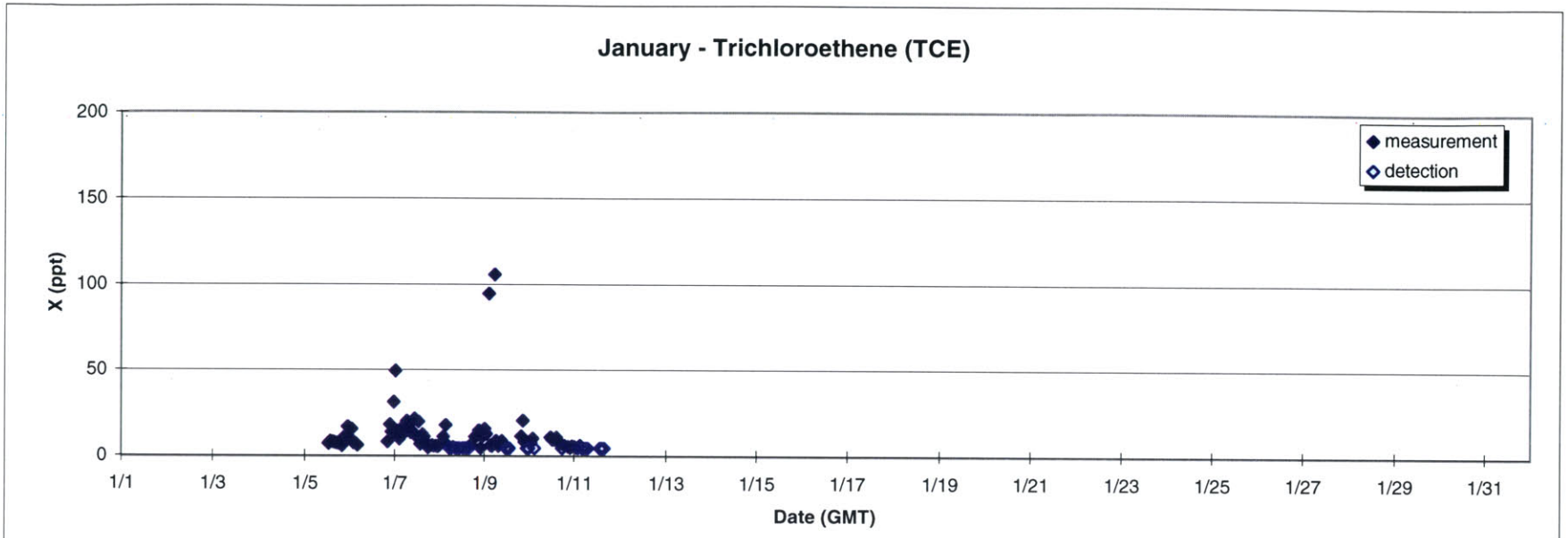
January - Trichloroethene (TCE)
200
150
100
50
0
X (ppt)
measurement
detection
1/1
1/3
1/5
1/7
1/9
1/11
1/13
1/15
1/17
1/19
1/21
1/23
1/25
1/27
1/29
1/31
Date (GMT)

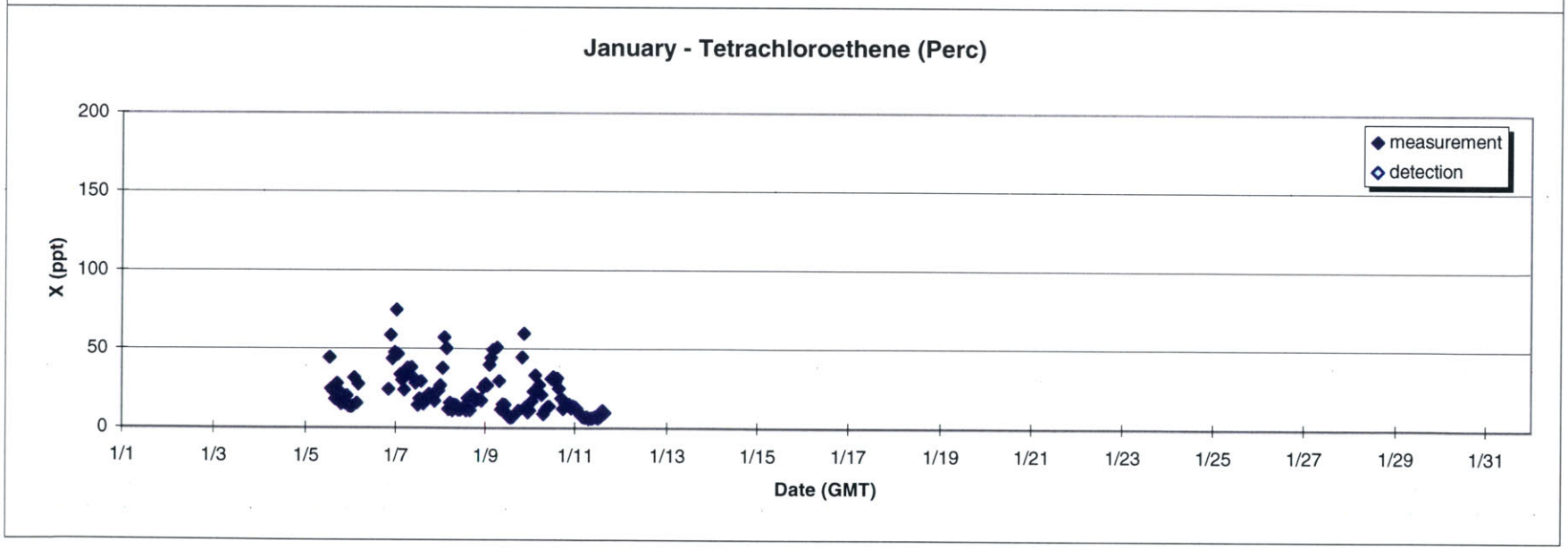
January - Tetrachloroethene (Perc)
200
150
100
50
0
X (ppt)
measurement
detection
1/1
1/3
1/5
1/7
1/9
1/11
1/13
1/15
1/17
1/19
1/21
1/23
1/25
1/27
1/29
1/31
Date (GMT)